Over-The-Air (OTA) Measurement Method for MIMO-enabled Mobile Terminals

Von der Fakultät für Ingenieurwissenschaften,
Abteilung Elektrotechnik und Informationstechnik
der Universität Duisburg-Essen

zur Erlangung des akademischen Grades

Doktor der Ingenieurwissenschaften

genehmigte Dissertation

von

Yifei Feng
aus
Changsha, China

Datum der Einreichung:
20/09/2012

Tag der mündlichen Prüfung:
07/05/2013

Gutachter: Prof. Dr.-Ing. Thomas Kaiser
Gutachter: Prof. Dr.-Ing. Werner L. Schroeder

DEDICATION

To my grandfather whom I drew courage and inspiration from.

To my parents, grandmother and other family members for their unconditional love and support.

To all my friends and colleagues whose encouragements and banter made this long journey enjoyable and kept me going.

ACKNOWLEDGEMENTS

This dissertation would not be possible without the support and guidance from many individuals. I would like to express my sincerest gratitude to Prof. Dr.-Ing. Schroeder who is both a mentor and a friend. He was always there to support me patiently with his encouragements and his incredibly deep knowledge. I would like to thank my supervisor Prof. Dr.-Ing. Kaiser for his generous guidance. I would also like to thank my colleague and good friend Aleksander Krewski. His contribution to my work is significant and insightful.

The help and support from our industrial partners should never be unaccounted-for. Many thanks to Dr.-Ing. von Gagern and Dr.-Ing. Tankielun of Rohde & Schwarz for their gracious support of equipment and ideas. Many thanks to Mr. Acharkaoui of CETECOM for his eagerness in helping us organizing measurements. I am also grateful to our students Mr. Jonas and Mr. Krini for their help in the measurement campaigns.

Last but not the least, I would like to express my appreciation to Bundesministerium für Bildung und Forschung (BMBF) for funding the research project.

Abstract

Over-The-Air (OTA) test methods for performance evaluation play an important role in the certification process of commercial User Equipment (UE) and for admission of UE to cellular networks. Novel OTA test methods and metrics are required for state-of-the-art mobile communication standards such as 3rd Generation Partnership Project (3GPP) Long Term Evolution (LTE) due to the extensive use of Multiple Input – Multiple Output (MIMO) transmission techniques. The variety of different MIMO operating modes and the almost unlimited choice of possible multi-path channel conditions under which UE performance may be evaluated is not accounted for by established Single Input – Single Output (SISO) OTA performance metrics like Total Isotropic Sensitivity (TIS) and Total Radiated Power (TRP). As pointed out in this dissertation, meaningful metrics and cost effective, low complexity measurement methods can nevertheless be derived by focusing on characterization of the physical attributes of UE and by adopting statistical metrics.

Starting from an overview of existing OTA measurement methods for SISO devices, extensions which are necessary to evaluate UE performance in the different MIMO operating modes which are foreseen in the 3GPP LTE standard are discussed. Relations between UE implementation attributes and the UE performance which is observed in different MIMO operating modes are derived using generic antenna and propagation models. Based on these models existing proposals for OTA test methods are reviewed. Their suitability and the relevance of different implementation aspects therein are discussed.

The main result of this dissertation is a novel MIMO OTA test plan which focuses on the characterization of relevant UE attributes and meets the goals of low complexity and high reproducibility. Two complementary metrics and corresponding measurement procedures for evaluation of MIMO OTA performance are developed in order to address the diversity of possible propagation scenarios. The theoretical results are supported by extensive measurements using preliminary implementations of the proposed method. These include results from an international round-robin measurement campaign for High-Speed

Packet Access (HSPA) devices and results from a variety of measurements on LTE devices which were performed at different test sites. Additional validation and investigation of specific aspects is addressed by simulation.

Zusammenfassung

Over-The-Air (OTA) Testverfahren für die Bewertung der Qualität von kommerziellen Endgeräten (*User Equipment (UE)*) sind von großer Bedeutung im Rahmen der Zertifizierung von UE und der Zulassung zu Mobilfunknetzwerken. Im Zusammenhang mit den aktuellen mobilen Kommunikationsstandards, wie etwa dem *3rd Generation Partnership Project (3GPP)* Standard *Long Term Evolution (LTE)*, sind, aufgrund der Verwendung von *Multiple Input – Multiple Output (MIMO)* Übertragungstechniken neuartige Metriken und Messverfahren erforderlich. Die Vielfalt der verschiedenen MIMO Betriebsarten und die fast unbegrenzte Auswahl möglicher Kanalbedingungen (Mehrwegeausbreitung), unter denen die Qualität von UE bewertet werden kann, wird von den etablierten *Single Input – Single Output (SISO)* OTA Metriken *Total Isotropic Sensitivity (TIS)* und *Total Radiated Power (TRP)* nicht abgedeckt. Wie in dieser Arbeit gezeigt wird, lassen sich durch Fokussierung auf die Charakterisierung der maßgeblichen physikalischen Eigenschaften des UE sowie Einführung statistischer Metriken dennoch aussagekräftige Metriken und kostengünstige Messmethoden geringer Komplexität gewinnen.

Ausgehend von einem Überblick existierender OTA Testverfahren für SISO Endgeräte werden die Erweiterungen diskutiert, die notwendig sind, um die Qualität von Endgeräten unter den verschiedenen MIMO Betriebsarten, die der Standard 3GPP LTE vorsieht, bewerten zu können. Unter Verwendung generischer Modelle für Antennen und Ausbreitungsszenarien werden Beziehungen zwischen den Eigenschaften von UE und der in den verschiedenen MIMO Betriebsarten zu beobachtenden Emfangsqualität abgeleitet. Darauf aufbauend werden existierende Vorschläge für OTA Testverfahren untersucht. Deren Eignung und die Relevanz der verschiedener Aspekte in ihrer Implementierung werden diskutiert.

Das wesentliche Ergebnis dieser Arbeit ist ein neuartiges MIMO OTA Testkonzept, bei dem die Charakterisierung der relevanten UE Eigenschaften im Mittelpunkt steht und welches den Anforderungen geringer Komplexität und hoher Reproduzierbarkeit genügt. Es werden zwei einander ergänzende Metri-

ken definiert und die zugehörigen Testvorschriften vorgestellt, mit dem Ziel die Vielfalt der möglichen Übertragungszenarien abzudecken. Der theoretische Herleitungen werden durch umfangreiche Messungen mit vorläufigen Implementierungen des vorgeschlagenen Testkonzeptes unterstüzt. Dazu gehören Ergebnisse aus einer internationalen *Round-Robin*-Messkampagne für *High-Speed Packet Access (HSPA)*-Endgeräte und Ergebnisse aus zahlreichen Messungen an LTE Endgeräten, die in verschiedenen Laboren durchgeführt wurden. Eine Zusätzliche Validierung sowie die Untersuchung einiger spezifischer Aspekte erfolgt mit Hilfe von Simulationen.

Contents

1 Introduction

1.1 Motivation

In recent years, wireless communication services in forms of cellular and local area networks become an integral part of daily life. Users enjoy the convenience of cable-free communication and request the Mobile Network Operators (MNOs) to provide better services and faster network infrastructure. Better service in this context means wider coverage and always-stable connection to stay in contact with family and friends. Faster networks enable on-the-road entertainment which wired networks are not able to provide. Devices and standards are being rapidly replaced to fulfill ever-growing demand for faster wireless transmission. For the MNOs, a guideline to select reasonably performing mobile terminals is of the highest interest. In addition to conformance tests, standard test methodology to reliably predict in-the-field performance of a mobile terminal is highly demanded.

Traditionally, evaluation of mobile terminals was heavily based on conducted measurements. Baseband functionality and Radio Frequency (RF) circuits of the Device Under Test (DUT) are evaluated together via cables attached to its antenna ports. Antenna is separately tested in passive antenna measurements. However, some properties e.g. self-interference which are important in description of device performance cannot be properly evaluated in conducted measurements. Over-The-Air (OTA) test methods were first introduced when MNOs experienced that devices with comparable conducted performance expose significantly different in-the-field performance, including increased rates of dropped connections. OTA measurements evaluate the DUT end-to-end. The interaction between components of the DUT that were not able to be quantified separately in conducted measurements are then evaluated in a single OTA measurement. Conformance evaluation of baseband functionality that were served effectively by conducted measurements are still carried out conducted. Since most of the small form-factor terminals with single antenna have inherently omni-directional patterns, especially in the low frequency bands, the

focus of traditional OTA test is eventually on total antenna efficiency [1, 2].

State-of-the-art mobile communication standards such as 3rd Generation Partnership Project (3GPP) Long Term Evolution (LTE) bear the promise of significantly enhanced cell capacity and per-user throughput by exploiting multipath propagation through implementing Multiple Input – Multiple Output (MIMO) techniques. The existing OTA test methods are not sufficient to evaluate the performance of devices with multiple antennas. Whether the performance of commercial User Equipment (UE) holds up to the promise has become more intricate to predict because MIMO performance depends strongly on UE antenna properties. New OTA measurement methods and performance metrics are necessary to address the spatial aspects in MIMO transmission. A well designed DUT with MIMO antenna system needs to be appreciated in OTA measurements for its advantages comparing to traditional single antenna DUTs in terms of connection stability, achievable throughput etc. A DUT with badly implemented MIMO antenna system has to be clearly identified for its lack of MIMO performance in forms of diversity, spatial multiplexing, interference avoidance etc.

First LTE network was deployed in the year 2009. Since then, more and more LTE terminals are introduced to the market by the MNOs with the large-scale construction of networks global-wise. The evaluation and certification of LTE devices with MIMO antenna systems is now a highly demanded topic. After an initial request by 3GPP RAN4 to address this issue [3], directed to COST 2100 and CTIA, several OTA test method proposals have been made by participants of COST 2100, 3GPP RAN4 and CTIA. The proposals differ significantly in terms of measurement setup and equipment because each approach is trying to solve the issue from a different perspective. Some initial comparison between methods has been conducted in two large-scale Round-Robin Measurement Campaigns [4] and other smaller scale ones [5] without arriving at definite conclusions with respect to advantages and drawbacks of each method [6, 7]. Further measurement campaigns and comparison to simulation [8] and a decision on a suitable test methodology or several methodologies is planned in the near future [9, 10].

1.1.1 SISO and MIMO terminology of UE

It is necessary at this point to clarify the terminology used in description of the four different cases of radio link structure, namely SISO, SIMO, MISO and MIMO.

- Single Input – Single Output (SISO) transmission is the traditional radio link structure that is used with both transmitter and receiver having single antenna. Examples of this structure would be existing cellular standards e.g. Global System for Mobile Communications (GSM) and Universal Mobile Telecommunications System (UMTS). Only one spatial stream is transmitted.
- Multiple Input – Multiple Output (MIMO) transmission requires both transmitter and receiver to have multiple antennas. The important feature of MIMO transmission is it exploits the spatial aspects of the channel. Multiple spatial streams are transmitted in this case. In scatter-rich environment, multiple signal streams can be assigned to different spatial streams in order to achieve higher throughput, a.k.a. Spatial Multiplexing (SM).
- Single Input – Multiple Output (SIMO) and Multiple Input – Single Output (MISO) are degenerate cases of MIMO with transmitter or receiver (respectively) having only a single antenna. Although it is not possible in this case to transmit multiple signal streams, it is still possible to exploit the multi-path channel for better transmission reliability. In these cases, radio systems can implement different techniques to improve signal quality e.g. switching, selecting, combining and in MISO case, also Transmit Diversity (TD).

How a DUT should be tested hence depends on two factors:

- whether the operating standard supports MIMO transmission;
- how many antennas do exist in the DUT.

If a DUT has a single antenna and supports only standards with no MIMO modes implementation, it can be tested using traditional SISO OTA measurement methods. In all other cases, new methodologies and metrics are required to correctly characterize the DUT.

1.2 OTA measurements for terminals with a single antenna

For devices which support only SISO transmission, traditional OTA measurement focuses on the radiation efficiency of the antenna. Metrics to be re-

ported are Total Isotropic Sensitivity (TIS) for downlink and Total Radiated Power (TRP) for uplink transmission. TIS and TRP measurements can be completed in either anechoic chambers or reverberation chambers.

- TIS is defined as a discrete approximation of the reciprocal average of Equivalent Isotropic Sensitivity (EIS). For each Angle of Arrival (AOA), EIS is in turn defined as the power which would have been received by a terminal with a fictitious ideal isotropic antenna under the same test conditions where the criterion (Bit Error Rate (BER) or Block Error Rate (BLER)) by which sensitivity is defined is observed for the DUT.
- Conversely in the uplink, TRP is defined as the integral of radiated power density over the sphere of Angles of Departure (AOD).

Each measurement in the process represents a Line of Sight (LOS) scenario without fading. The Figure of Merit (FOM) (i.e. TIS and TRP) is under the assumption that the distribution of direction of transmission is isotropic (uniform two-dimensional Power Angular Spectrum (PAS)). The FOMs represent the evaluation of one major antenna radiation property – antenna efficiency. The two polarizations of the DUT are separately measured.

1.2.1 SISO OTA measurements in anechoic chambers

The anechoic chamber is mostly adopted as the environment for SISO OTA testing. Absorbers are placed on all interior surfaces of the chamber. The measurements are isolated from external sources and reflections inside of the chamber are absorbed. A two-axis rotation mechanism is necessary in this setup. The principle of the measurement is to record sensitivity and radiated power density of each orientation of the DUT taken from a finite sampling grid of the unit sphere. The measurement is repeated for all the points in the sampling grid.

There are two types of anechoic chamber structures defined in standard SISO OTA measurements [2]. One type (i.e. combined-axis chamber) has a dual polarized test antenna fixed in the chamber. The DUT is mounted on a two-axis positioner as illustrated in Fig. 1.1. The other type (i.e. distributed-axis chamber) has the dual polarized test antenna mounted on a one-axis boom positioner, making it possible to move along a vertical circle. The DUT is mounted on a platform which is capable of rotation around the Z-axis as given in Fig. 1.2. Both types of anechoic chambers are setups allow for the positioning of a test

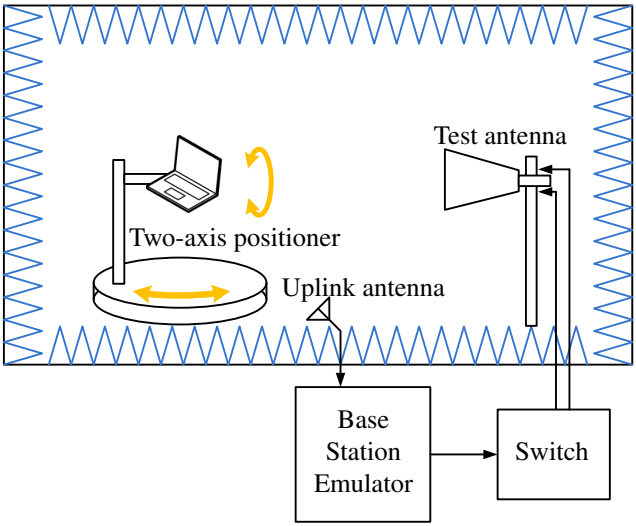

Figure 1.1: Standardized anechoic chamber with a combined-axis structure as introduced in [2].

antenna which moves freely on the surface of the unit sphere around the DUT in order to access all possible orientations of the DUT in the measurements.

The results drawn from the measurements in standardized chambers are highly repeatable. The measurement time of a SISO OTA testing in anechoic chambers depends on the resolution of the sampling grid. Commercial certificate requires 15° resolution for TRP measurements and 30° for TIS measurements. The measurement time of a complete SISO OTA measurement set covering European bands in UMTS is in the level of days. To test UE with consideration of near-field impairments caused by user, head or hand phantoms are also included as separate measurements. Measurement time in this case is multiplied by the number of cases to be tested.

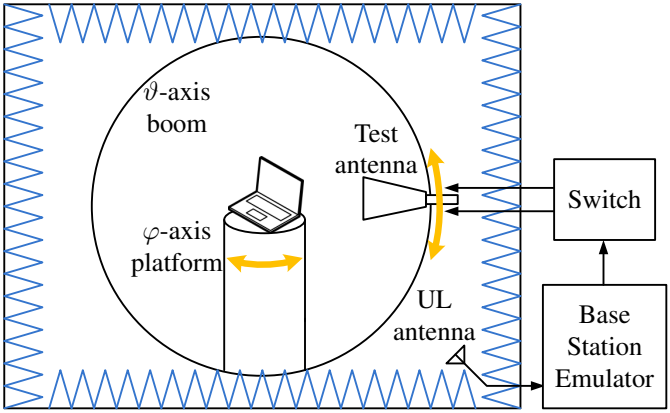

Figure 1.2: Standardized anechoic chamber with a distributed-axis structure as introduced in [2].

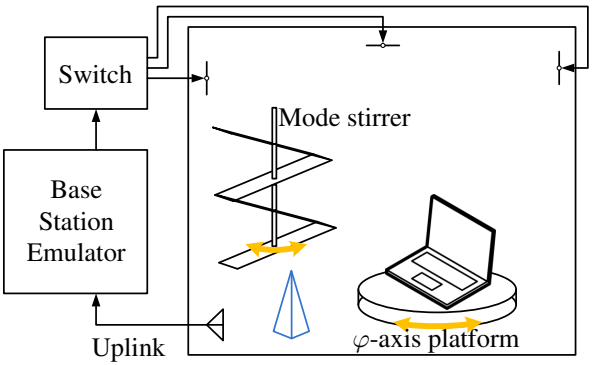

Figure 1.3: Structure of a typical reverberation chamber.

1.2.2 SISO OTA measurements in reverberation chambers

Reverberation chamber was first introduced in Electromagnetic Compatibility (EMC) testing [11]. Mechanical mode stirrers are used in a metallic enclosure to generate a statistically isotropic channel environment. The purpose of reverberation chamber was to eliminate necessity of rotating DUT e.g. vehicles in the EMC tests.

The introduction of reverberation chamber to SISO OTA measurements is to exploit the isotropic channel environment in order to simplify the measurement procedures [12, 13, 14, 15]. Rotation of a small DUT is an additional option here to emulate a statistically isotropic environment. The cost of constructing a reverberation chamber used for OTA testing is significantly lower than anechoic chambers because of its small size.

In reverberation chambers, efficiency related metrics like TRP or TIS can be measured quickly utilizing the isotropy of the channel. The accuracy of the measurement results is in theory comparable to what is obtained in anechoic chambers using procedures briefly discussed in the last subsection.

1.3 Challenges in OTA testing for MIMO-enabled terminals

UE with multiple antennas can benefit from the multi-path propagation in MIMO transmission modes. SISO OTA measurements are insufficient to quantify this aspect without implementation of spatial diversity in the measurement setup. Although the antennas of a MIMO-enabled terminal can also be evaluated individually, similar to what is done in a SISO OTA test, the relations between their patterns would be dismissed. MIMO antenna systems in electrically small terminals expose strong coupling between ports and cannot be treated as a collection of separate antennas (e.g. antenna array).

With many MIMO transmission modes in the play, the goal of a MIMO OTA measurement is to evaluate UE with respect to in-the-field performance for various MIMO transmission modes and an almost infinite choice of multipath channel conditions. An agreed test method should nevertheless clearly discriminate between “good” and “bad” devices without footnotes stating “under certain conditions”. Excellent reproducibility of results is mandatory. Consistent results should be obtained by every test lab.

A further important requirement is low complexity because tests are to be performed for large number of E-UTRA frequency bands and for a variety of different near-field conditions (e.g. with head or hand phantoms), a fact which increases test time substantially [16]. The time required for each measurement should not exceed typical measurement time for established SISO OTA measurement procedures like TIS and TRP (matter of days). Additional cost for the certification process would have to be transferred to the end-user.

2 Characteristics of UE with a MIMO antenna system

2.1 Physical antenna attributes

This chapter covers the discussion of properties of UE with MIMO antenna system. Among these properties, physical antenna attributes are good starting points of investigating characteristics of UE that contribute to the difference in performance.

2.1.1 Compound polarimetric pattern

A passive N-port antenna can be fully characterized by its *compound polarimetric pattern*, the $N \times 2$ complex matrix function

$$\mathbf{T}(\Omega) = \begin{pmatrix} \boldsymbol{T}_1(\Omega) \\ \vdots \\ \boldsymbol{T}_N(\Omega) \end{pmatrix} = \begin{pmatrix} T_{\vartheta,1}(\Omega) & T_{\varphi,1}(\Omega) \\ \vdots & \vdots \\ T_{\vartheta,N}(\Omega) & T_{\varphi,N}(\Omega) \end{pmatrix}, \tag{2.1}$$

with $\Omega = (\theta, \phi)$, and its *scattering matrix* $\mathbf{S}$. Subscripts ϑ and φ denote two orthogonal polarizations. With $\boldsymbol{a}$ and $\boldsymbol{b}$ denoting the vectors of incoming (TX $\rightarrow$ antenna) and outgoing (antenna $\rightarrow$ RX) wave quantities at the N ports, the receive mode is described by

$$\boldsymbol{b}(\Omega) = \mathbf{S}\boldsymbol{a} + \boldsymbol{b}_0(\Omega)\,, \quad \boldsymbol{b}_0(\Omega) = \frac{\lambda_0}{\sqrt{4\pi Z_0}} \mathbf{T}(\Omega)\boldsymbol{E}(\Omega) \tag{2.2}$$

and the transmit mode by

$$\boldsymbol{E}(\Omega, r) = \mathrm{j}\sqrt{\frac{Z_0}{4\pi}} \frac{\mathrm{e}^{-\mathrm{j}\,k_0 r}}{r} \mathbf{T}(\Omega)^{\top} \boldsymbol{a} \quad \text{and} \quad \boldsymbol{b} = \mathbf{S}\boldsymbol{a} \tag{2.3}$$

where $\boldsymbol{E}$ gives the E-field, λ_0 denotes the wavelength in free space, r presents the radius, k_0 the wavenumber in free space and Z_0 the free space impedance.

Radiated power can be written as

$$P_{\mathrm{rad}} = \frac{1}{2}\boldsymbol{a}^{\dagger}\mathbf{R}\boldsymbol{a} \tag{2.4}$$

where

$$\mathbf{R} = \frac{1}{4\pi}\oiint_{\Omega} \mathbf{T}(\Omega)^{*}\mathbf{T}(\Omega)^{\top}\,\mathrm{d}\Omega \tag{2.5}$$

is referred to as the *radiation matrix*. Superscripts $(\cdot)^{\top}$, $(\cdot)^{*}$ and $(\cdot)^{\dagger}$ denote transposed, conjugate and Hermitian transposed, respectively.

2.1.2 Per-port antenna efficiency

A closer inspection of the radiation matrix is mandatory because it contains all relevant information about the performance of the antenna system in a statistically isotropic environment. Although the isotropic scattering environment is of rare occurrence, the concept takes its justification from the fact that the orientation of UE in space may be random. We shall see that the radiation matrix is one of the UE attributes to be characterized.

To understand its meaning consider the case that only port n is fed, i.e. $\boldsymbol{a} = (0,\ldots,0,a_n,0,\ldots,0)^{\top}$. Available power is then given by $P_{\mathrm{avail},n} = \frac{1}{2}a_n^{*}a_n$ and radiated power by $P_{\mathrm{rad},n} = \frac{1}{2}a_n^{*}R_{nn}a_n$ with

$$R_{nn} = \frac{1}{4\pi}\int_{\Omega}\left(|T_{\vartheta,n}(\Omega)|^2 + |T_{\varphi,n}(\Omega)|^2\right)\,\mathrm{d}\Omega, \tag{2.6}$$

the norm of the n-th pattern. Obviously the diagonal element R_{nn} is equal to the ratio of radiated over available power from port n, i.e. to per-port (total) efficiency,

$$\eta_{\mathrm{tot},n}^{\mathrm{port}} = \frac{P_{\mathrm{rad},n}}{P_{\mathrm{avail},n}} = R_{nn}. \tag{2.7}$$

Different per-port efficiencies correspond to the different expectation values of received power in a statistically isotropic environment and are therefore linked to the concept of *antenna imbalance*. But we shall see below that a deeper look into this concept is necessary.

2.1.3 Antenna correlation

The off-diagonal elements of the radiation matrix $\mathbf{R}$ contain the scalar products between patterns associated with different ports,

$$R_{mn} = \frac{1}{4\pi} \int_{\Omega} \left(T_{\vartheta,m}(\Omega)^* T_{\vartheta,n}(\Omega) + T_{\varphi,m}(\Omega)^* T_{\varphi,n}(\Omega) \right) \mathrm{d}\Omega, \tag{2.8}$$

from which the traditional pattern correlation coefficient is obtained as

$$\rho_{mn} = \frac{R_{mn}}{\sqrt{R_{mm} R_{nn}}}. \tag{2.9}$$

The correlation corresponds to the expectation value of the observed Complex Envelope Correlation Coefficient (CECC) at the antenna ports in a statistically isotropic environment.

However, "antenna correlation" defined as CECC with respect to different port patterns does not convey useful information. It is noted in passing that antenna correlation is anyway always small if the antenna system is properly matched (Hermitian match with respect to impedance matrix) and if dissipative losses are small [17]. For a lossless antenna system (no dissipation) power balance in fact implies that radiated power is equal to power incident at the ports minus power scattered back from the ports, i.e.

$$\mathbf{R} = \mathbf{I} - \mathbf{S}^\dagger \mathbf{S}. \tag{2.10}$$

If a multi-port antenna is correctly matched (at a given frequency) then all elements of the scattering matrix $\mathbf{S}$ are small in magnitude. The off-diagonal elements of the radiation matrix $\mathbf{R}$ (corresponding to pattern correlation) are then obviously also small. This statement applies irrespective of the spatial separation between different antenna elements. The latter may have an influence on the bandwidth over which a good multi-port match is attainable but is otherwise not directly related to pattern correlation. Generalization to lossy antennas is straightforward by adding a loss matrix term to the power balance relation.

2.1.4 Modal efficiency

The introduction of radiation matrix provides more insight into the antenna property than familiar parameters like per-port efficiencies and correlation be-

tween per-port patterns. It is important to understand that the traditional parameters "antenna imbalance" and "antenna correlation" which are defined as per-port parameters are actually meaningless for MIMO transmission if considered separately.

This conclusion can be explained using a simple example. Consider an N-port antenna which receives N uncorrelated paths of equal power coming in with different AOAs and isotropic PAS. The received signal vector $\boldsymbol{b}_0$ will contain components with different amplitudes and some correlation between the components will be observed. The noise contributions in each component may be considered uncorrelated and of equal power because they are dominated by receiver noise figure. The MIMO detector now basically applies an approximate inverse of the channel matrix to the received signal vector in order to recover the transmitted signal vector, i.e. to remove the correlation. The quality of this approximation depends on the condition number of the channel matrix and to certain extend, noise power. In the present setting the expectation value of the channel matrix is just the radiation matrix of the antenna. Consequently, the relevant property of the radiation matrix is the attainable rank which in fact is the number of eigenvalues (assumedly ordered in sequence of decreasing magnitude) for which the ratio of largest to smallest magnitude does not exceed some threshold.

Moreover, in case of Closed-loop Spatial Multiplexing (CL-SM), the evolved Node-B (eNB)'s pre-coder and the UE's MIMO detector make a joint attempt to diagonalize the channel matrix. In either case unitary transforms are applied to the channel matrix. Hence only those properties of the radiation matrix which are invariant under unitary transforms are relevant: the eigenvalues of $\mathbf{R}$. The radiation matrix is Hermitian and hence has real eigenvalues which correspond to the *modal efficiencies* of the N orthogonal radiation modes which are supported by the antenna system. The discussion can be summarized as follows:

(a) The MIMO performance of an N-port antenna in a statistically isotropic environment is described by the N modal efficiencies $\eta_1 \geq \eta_2, \ldots, \geq \eta_n$, the eigenvalues of the radiation matrix.

(b) *Total antenna system efficiency* is described by the invariant property

$$\overline{\eta_{\mathrm{tot}}} = \frac{1}{N} \operatorname{tr}(\mathbf{R}). \tag{2.11}$$

This figure is equal to the ratio of transmitted over available power in

case that the total available power is evenly distributed over N uncorrelated feed port signals [18].

2.1.5 Modal imbalance

Modal imbalance is a relevant parameter whereas conventional per-port "antenna imbalance" is not. The attainable rank of MIMO transmission is restricted by the number of modal efficiencies with value η_n not less than a given (power and noise power dependent) fraction of η_1. An *imbalance figure* can be introduced as the ratio of the arithmetic over the geometric mean of modal efficiencies

$$\beta = \frac{\overline{\eta_{\mathrm{tot}}}}{\sqrt[N]{\eta_1 \eta_2 \cdots \eta_n}}. \tag{2.12}$$

A perfectly balanced antenna system with $\eta_1 = \eta_2 = \cdots = \eta_n = \overline{\eta_{\mathrm{tot}}}$ will have $\beta = 1$. An antenna system with higher modal imbalance has larger β.

After having identified the eigenvalues of the radiation matrix, i.e. the efficiencies of the N orthogonal radiation modes supported by the antenna system as the relevant parameters, a brief look into their physical behaviour is indicated.

Each radiation mode (orthogonal pattern) comes with an individual *radiation quality factor* defined as the ratio of average reactive energy stored in its near field over radiated energy per period. As opposed to what the term "quality" suggests, a high radiation quality factor is detrimental. It corresponds to narrow matching bandwidth and high dissipation, i.e. the modal efficiency of the respective mode is acceptable only over a small bandwidth and may be still poor even there. Reduction of radiation quality factors is the goal of antenna design but unfortunately subject to fundamental physical limits. When adding further antennas to small form factor devices the radiation quality factors of the additional radiation modes typically take increasingly large values. An example for the frequency dependence of modal efficiencies for a simulated 2-port antenna system in a USB dongle is shown in Fig. 2.1 [19]. Cyan and blue curves represent efficiencies of the two modes vs. frequency. It can be seen that total antenna system efficiency (2.11) and modal imbalance (2.12) can be strongly dependent on frequency what should be considered in test design.

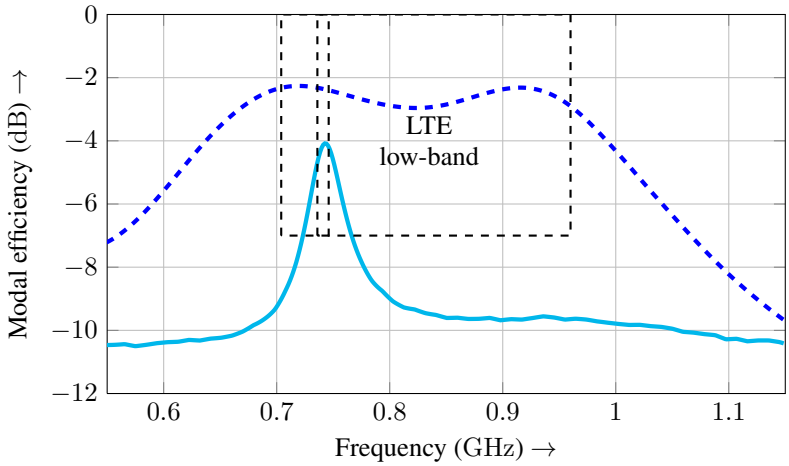

Figure 2.1: Frequency dependence of modal efficiencies for a simulated 2-port MIMO antenna example [19].

2.1.6 Reconfigurable and adaptive antennas

The above mentioned physical limitations in antenna design are reasons for introduction of tunable and reconfigurable or even adaptively matched antenna systems (so as to compensate for antenna detuning in a variable near-field environment, e.g. due to user's head and hand). As a consequence the antenna system can in principle no longer be treated as a linear system block and, in case of adaptive matching, not even as time invariant. It should be noted in particular that with a tunable antenna system the first non-linear system block appears in the receive chain before the band filter. New test cases may therefore be necessary. Moreover, the benefit (or malfunction) of adaptive matching will not be assessed correctly without a properly chosen set of test cases with phantoms, possibly accounting also for time dependence of the adaptation algorithm.

2.2 Receiver system properties

In Downlink (DL) transmission, after signal is received by the antennas, degradation of signal quality can still happen. Several receiver aspects that can cause signal quality degradation are discussed below.

2.2.1 Self-interference and cross-interference

Self-interference is in reality often the most important cause of poor device performance. Conducted measurements are not capable to detect problems caused by coupling of an interfering signal to the antennas [20]. Cross-interference is important for devices which are connected to a host device such as datacards or USB dongles. Interference from the host computer may differ dramatically between e.g. different laptop models. A standard mock-up is necessary to make comparable measurement for this type of devices.

2.2.2 Receiver noise figure

The noise figure of a receiver is defined as the additional noise power level at a receiver's output as compared to an ideal receiver. If the effect of non-linear distortion is approximated as Additive White Gaussian Noise (AWGN) it may be subsumed under the noise figure and the latter be taken as a quality measure for the analog and mixed signal system blocks in the UE's receive chain. In an "end-to-end" measurement it is not possible to separate receiver noise figure from antenna efficiency. It is therefore necessarily included in MIMO OTA measurements.

2.2.3 Baseband algorithms

The quality of the algorithms implemented in the digital baseband of UE is crucial for receiver performance and reporting quality (Channel State Information (CSI)). These aspects, however, can at much lower cost and with superior repeatability be tested in conducted measurements with the full flexibility to apply time-dependent faded channels, different Doppler spectra, birth–death scenarios with the help of today's sophisticated fading emulators. In the sequel it is therefore silently assumed that such conducted tests have been performed separately and the digital baseband is not considered in the context of MIMO OTA measurement.

3 Generic propagation model

In communication theory the radio channel comprises the propagation channel and the antennas at either side of the link. Since antennas are discussed in Section 2.1, this chapter is devoted to the interaction of a multi-path propagation scenario with the UE antenna system.

3.1 Generic multi-path scenario, constellations

Consider a single sub-carrier frequency of an OFDM DL supporting M parallel data streams. The complex amplitudes of the M sinusoids can be described by a vector $\boldsymbol{s} = (s_0, s_1, \ldots, s_{M-1})^\top$ which is normalized to unit power according to $\frac{1}{2}\|\boldsymbol{s}\|^2 = 1$. In addition L interfering signals may be present and are described in the same fashion by a vector $\boldsymbol{w} = (w_0, w_1, \ldots, w_{L-1})^\top$.

Conceptually we define the DUT as the combination of the UE under test and any possible objects in the near-field such as head or hand phantoms. This allows to consider the DUT as being immersed into a superposition of K plane waves, incident from AOA $\Omega_k = (\theta_k, \phi_k)$, $k = 0, \ldots, K-1$. This superposition is described in terms of the distribution

$$\widehat{\boldsymbol{E}}(\Omega) = \begin{pmatrix} \widehat{E}_\vartheta(\Omega) \\ \widehat{E}_\varphi(\Omega) \end{pmatrix} = E_0 \widehat{\mathbf{C}}(\Omega)\boldsymbol{s} + E_0 \widehat{\mathbf{D}}(\Omega)\boldsymbol{w} \tag{3.1}$$

where E_0 is a calibration factor (see below) and $\widehat{\mathbf{C}}$ and $\widehat{\mathbf{D}}$ are respectively $2 \times M$ and $2 \times L$ matrices of distributions, referred to as constellations below, which describe the multi-path channel for the wanted signals and the interferers, respectively. Both have the same form, viz. $\widehat{\mathbf{C}} = \left(\widehat{\boldsymbol{C}}_0, \ldots, \widehat{\boldsymbol{C}}_{M-1}\right)$ with

$$\widehat{\boldsymbol{C}}_m = \sum_{k=0}^{K-1} \begin{pmatrix} c_{\vartheta,k,m} \\ c_{\varphi,k,m} \end{pmatrix} \delta(\Omega, \Omega_k) \tag{3.2}$$

and likewise for $\widehat{\mathbf{D}}$. This is a generic description which covers any real world scenario as well as any test case. In the context of OFDM, it is sufficient to identify the coefficients in (3.2) with complex numbers provided that path delays do not exceed the guard period.

The received signal vector at the antenna ports is then, in absence of interferers, given by

$$\boldsymbol{b}_0 = \frac{\lambda_0 E_0}{\sqrt{4\pi Z_0}} [\mathbf{T}, \widehat{\mathbf{C}}] \boldsymbol{s} \tag{3.3}$$

where

$$[\mathbf{T}, \widehat{\mathbf{C}}] = \iint\limits_{\mathrm{S}_1(0)} \mathbf{T}(\Omega) \widehat{\mathbf{C}}(\Omega) \, \mathrm{d}\Omega. \tag{3.4}$$

The integral over the unit sphere $\mathrm{S}_1(0)$ evaluates to a $N \times M$ matrix for an N-port antenna system. A similar term with $\widehat{\mathbf{D}}$ exchanged for $\widehat{\mathbf{C}}$ is to be added to include external interferers.

3.2 Channel matrix

In order to obtain the channel matrix in real world units, the factor E_0 in (3.1) must be quantified, i.e. the measurement must be calibrated. As usual in anechoic chamber measurements we express E_0 in terms of the power P_{iso}, fictitiously received by an ideal isotropic antenna in the center of the UE position without the UE (and phantom) in place when subject to a single co-polarized plane wave. In this setting (2.1) reduces to unity and

$$P_{\mathrm{iso}} = \frac{1}{2} \left\| \boldsymbol{b}_0 \right\|^2 = \frac{\lambda_0^2}{4\pi} \frac{E_0^2}{Z_0} \frac{1}{2} \left\| \boldsymbol{s} \right\|^2 = \frac{\lambda_0^2}{4\pi} \frac{E_0^2}{Z_0} \tag{3.5}$$

(due to the normalization of the signal vector) from which E_0 can be calculated. The operation $\|\cdot\|$ denotes the Euclidean norm. Since the channel matrix is conventionally referenced to the "inner antenna ports" in the form

$$\boldsymbol{r} = \mathbf{H}\boldsymbol{s} + \text{noise and interference} \tag{3.6}$$

where $\boldsymbol{r} = (r_1, \ldots, r_{N-1})^\top$ is the received signal vector at the input of the detector, it is convenient to scale the received signal vector according to $\boldsymbol{r} := \frac{1}{\sqrt{F}} \boldsymbol{b}$, where F denotes receiver noise figure. The correct SNR is thus maintained when we simply substitute an AWGN signal $\boldsymbol{n}$ with thermal noise

power $P_{\mathrm{N},0} = k_{\mathrm{B}}TB$ per component for the noise contribution on the Right-Hand-Side (RHS) of (3.6). The resulting expression for the channel matrix is

$$\mathbf{H} = \sqrt{\frac{P_{\mathrm{iso}}}{F}}[\mathbf{T}, \widehat{\mathbf{C}}]. \tag{3.7}$$

An analogous expression can be written for the external interferers to yield upon combination

$$\boldsymbol{r} = \sqrt{\frac{P_{\mathrm{iso}}}{F}}[\mathbf{T}, \widehat{\mathbf{C}}]\boldsymbol{s} + \sqrt{\frac{P_{\mathrm{iso}}}{F}}[\mathbf{T}, \widehat{\mathbf{D}}]\boldsymbol{w} + \boldsymbol{r}_{\mathrm{S}} + \boldsymbol{n}. \tag{3.8}$$

The additional term $\boldsymbol{r}_{\mathrm{S}}$ accounts for self-interference.

3.3 Capacity and throughput approximation

Using the channel matrix in (3.7), the system capacity can be derived using information theory, since LTE was designed with an adaptive Modulation and Coding Scheme (MCS) in order to approach Shannon capacity. For the qualitative considerations which are made later, we may therefore simply consider attainable throughput as proportional to Shannon capacity (with a factor k at the order of 0.75, see [21]). Any throughput measurement with perfect capacity to throughput mapping is an equivalent quantification of system capacity. The derivation in this section is for DL scenarios because Uplink (UL) MIMO is not yet realized in cellular wireless standards. Interferers are exempted from the discussion for sake of simplicity.

3.3.1 Channel capacity in TD mode (Alamouti scheme)

Based on the discussion in Section 3.2 an explicit model expression for the Signal-to-Noise Ratio (SNR) is readily obtained. For the low SNR case, the most beneficial MIMO mode is DL TD mode which uses Space-Frequency Block Coding (SFBC) based on Alamouti scheme.

Since first published, the Alamouti scheme [22] is the most implemented or say the fundamental Space-Time Block Code (STBC). In SFBC two blocks of signals s_0 and s_1 are allocated to different sub-carriers and antennas as shown in Table 3.1. These two transmissions are orthogonal.

Table 3.1: Alamouti scheme in SFBC.

	antenna 0	antenna 1
sub-carrier 0	s_0	s_1
sub-carrier 1	$-s_1^*$	s_0^*

By a single antenna receiver, assuming perfect channel estimation, s_0 and s_1 are approximated as

$$\begin{aligned} \tilde{s}_0 &= (\alpha_0^2 + \alpha_1^2)s_0 + h_0^* n_0 + h_1 n_1^* \\ \tilde{s}_1 &= (\alpha_0^2 + \alpha_1^2)s_1 - h_0 n_1^* + h_1^* n_0 \end{aligned} \tag{3.9}$$

where $h_0 = \alpha_0 e^{\mathrm{j}\,\theta_0}$ and $h_1 = \alpha_1 e^{\mathrm{j}\,\theta_1}$ are channel coefficients seen from antenna 0 and 1, respectively, and n_0, n_1 represent AWGN on sub-carriers 0 and 1.

The corresponding expression for an N-antenna receiver with Maximum Ratio Combining (MRC) reads

$$\begin{aligned} \tilde{s}_0 &= \sum_{n=0}^{N-1} (\alpha_{n0}^2 + \alpha_{n1}^2)s_0 + \sum_{n=0}^{N-1} (h_{n0}^* n_{n0} + h_{n1} n_{n1}^*) \\ \tilde{s}_1 &= \sum_{n=0}^{N-1} (\alpha_{n0}^2 + \alpha_{n1}^2)s_1 - \sum_{n=0}^{N-1} (h_{n0} n_{n1}^* - h_{n1}^* n_{n0}) \end{aligned} \tag{3.10}$$

which corresponds to MRC.

Assuming DL TD mode, a power-normalized signal vector $\boldsymbol{s}$ (see Subsection 3.1) and an N-antenna UE with MRC (if $N > 1$), the effective SNR is given by

$$\mathrm{SNR} = \mathrm{SNR}_0 \left\| [\mathbf{T}, \widehat{\mathbf{C}}] \right\|^2 \tag{3.11}$$

with

$$\mathrm{SNR}_0 = \frac{P_{\mathrm{iso}}}{P_{\mathrm{N},0} F}. \tag{3.12}$$

$\|[\mathbf{T}, \widehat{\mathbf{C}}]\|$ denotes the Frobenius norm of the matrix (3.4). It is noted in passing that the mutual information can be expressed in terms of the above introduced

symbols as

$$C_{\mathrm{MRC}} \approx B \log_2 \left(1 + \mathrm{SNR}_0 \left\| [\mathbf{T}, \widehat{\mathbf{C}}] \right\|^2 \right) \tag{3.13}$$

where B denotes bandwidth.

3.3.2 Throughput approximation in the low SNR regime

Consider here DL TD mode with $M = 2$ (two orthogonal DL signals), and a sequence of constellations $\mathcal{C} = \{\widehat{\mathbf{C}}_i\}$ whose elements are, apart from irrelevant phase factors, of the form

$$\widehat{\mathbf{C}}_i = \begin{pmatrix} 1 & 0 \\ 0 & 1 \end{pmatrix} \delta(\Omega, \Omega_i), \tag{3.14}$$

i.e. only a single AOA Ω_i is encountered per measurement [23].

The factor $\left\| [\mathbf{T}, \widehat{\mathbf{C}}] \right\|^2$ on the RHS of (3.11) therefore simplifies to $\left\| \mathbf{T}(\Omega_i) \right\|^2$ in the i-th measurement. The setting resembles a conventional sensitivity measurement with the modification that two DL signals are routed to the two orthogonal polarizations of a dual-polarized test antenna.

With the assumption of low SNR scenario, one may further approximate (3.13) by $\log_2(1 + x) \approx x / \ln(2)$, for $|x| \ll 1$

$$C_{\mathrm{MRC}} \approx B \, \mathrm{SNR}_0 \left\| \mathbf{T}(\Omega_i) \right\|^2 / \ln(2) \tag{3.15}$$

and the isotropic average

$$\begin{aligned} \overline{C_{\mathrm{MRC}}} &\approx \frac{1}{\ln(2)} B \, \mathrm{SNR}_0 \, \mathrm{tr}(\mathbf{R}) \\ &= \frac{1}{\ln(2)} BN \, \mathrm{SNR}_0 \, \overline{\eta_{\mathrm{tot}}}. \end{aligned} \tag{3.16}$$

Thus it can be concluded that the optimum capacity of a MIMO antenna system in TD mode is proportional to the total antenna system efficiency (2.11). The simplest constellation setup e.g. a dual-polarized horn antenna, is sufficient to characterize this property.

3.3.3 Channel capacity in SM mode

Similarly, provided that "good" channel information is available at the receiver, a situation which would be assumed as a prerequisite for CL-SM mode, the mutual information can be approximated by

$$C_{\mathrm{SM}} \approx B \log_2 \left(\det \left(\mathbf{I} + \mathrm{SNR}_0 [\mathbf{T}, \widehat{\mathbf{C}}][\mathbf{T}, \widehat{\mathbf{C}}]^\dagger \right) \right) \tag{3.17}$$

for a given constellation. Assume now that a sequence of constellations of the form $\widehat{\mathbf{C}} = \left(\widehat{\boldsymbol{C}}_0, \ldots, \widehat{\boldsymbol{C}}_{M-1}\right)$ with

$$\widehat{\boldsymbol{C}}_m = \begin{pmatrix} c_{\vartheta,i,m} \\ c_{\varphi,i,m} \end{pmatrix} \delta(\Omega, \Omega_i) + \begin{pmatrix} c_{\vartheta,j,m} \\ c_{\varphi,j,m} \end{pmatrix} \delta(\Omega, \Omega_j), \tag{3.18}$$

which corresponds to a (doubly) isotropic PAS for both polarizations and both DL signals is applied. Such sequence can be obtained by choosing Ω_i and Ω_j from a proper regular grid on the unit sphere. Obviously then, as angular resolution is increased, the average of the term $[\mathbf{T}, \widehat{\mathbf{C}}][\mathbf{T}, \widehat{\mathbf{C}}]^\dagger$ approaches the radiation matrix $\mathbf{R}$. Applying Jensen's inequality, in the limit one would obtain the isotropic average of (3.17) in the form

$$\overline{C_{\mathrm{SM}}} \lesssim B \log_2 \left(\det \left(\mathbf{I} + \mathrm{SNR}_0 \, \mathbf{R} \right) \right) \tag{3.19}$$

providing the upper bound.

3.3.4 Throughput approximation in the high SNR regime

Since the intention is to test in the high SNR regime one may assume that the SNR is high enough to neglect the identity matrix $\mathbf{I}$ in (3.19) similar to the approach in [24]. The upper bound of the isotropic average in (3.19) can then

be approximated by

$$\begin{aligned}\overline{C_{\mathrm{SM}}} &\lesssim B\log_2\left(\mathrm{SNR}_0^N\cdot\det(\mathbf{R})\right)\\ &= BN\log_2(\mathrm{SNR}_0\,\overline{\eta_{\mathrm{tot}}}) + B\sum_{n=1}^{N}\log_2\left(\frac{\eta_n}{\overline{\eta_{\mathrm{tot}}}}\right)\\ &= BN\log_2(\mathrm{SNR}_0\,\overline{\eta_{\mathrm{tot}}}) + B\log_2\left(\prod_{n=1}^{N}\frac{\eta_n}{\overline{\eta_{\mathrm{tot}}}}\right)\\ &= BN\log_2(\mathrm{SNR}_0\,\overline{\eta_{\mathrm{tot}}}) + BN\log_2\left(\frac{\sqrt[N]{\eta_1\eta_2\cdots\eta_n}}{\overline{\eta_{\mathrm{tot}}}}\right).\end{aligned} \tag{3.20}$$

The first term on the RHS of (3.20) corresponds to the isotropic average of capacity in the optimum case of a balanced N-port MIMO antenna system with total antenna system efficiency $\overline{\eta_{\mathrm{tot}}}$. The second term on the RHS of (3.20) describes the capacity degradation due to modal imbalance. It is always non-positive and equal to zero iff the antenna system is perfectly balanced with equal modal efficiencies $\eta_1 = \eta_2 = \cdots = \overline{\eta_{\mathrm{tot}}}$. The approximation of upper bound in (3.20) can be rewritten in the form

$$\overline{C_{\mathrm{SM}}} \lesssim 3.322BN\left(\mathrm{SNR}_0^{(\mathrm{dB})} + \overline{\eta_{\mathrm{tot}}}^{(\mathrm{dB})} - \beta^{(\mathrm{dB})}\right) \tag{3.21}$$

where superscript (dB) indicates a quantity given in decibels and

$$\beta^{(\mathrm{dB})} = 10\,\mathrm{dB}\log_{10}\left(\frac{\overline{\eta_{\mathrm{tot}}}}{\sqrt[N]{\eta_1\eta_2\cdots\eta_n}}\right) \tag{3.22}$$

is the *imbalance figure* of the UE antenna system as introduced in (2.12). Note that both $\overline{\eta_{\mathrm{tot}}}$ and β are invariant properties of the radiation matrix as discussed in Section 2.1.1.

The characterization of a MIMO antenna system can thus be accomplished by evaluation of a limited number of properties. In low SNR scenarios where UE is likely to be operating in the TD mode, an evaluation of total antenna system efficiency over receiver noise figure is sufficient. In high SNR scenarios where UE can achieve higher throughput using SM modes, in addition to efficiency, one also needs to consider including modal imbalance figure in the measurements.

4 Critical review of proposed MIMO OTA measurement methods

4.1 Measurement methods overview

After an initial request by 3GPP RAN4 directed to COST 2100 to collect proposals for MIMO OTA measurement methods [3, 25] in 2008, several MIMO OTA test methods have been proposed by participants of COST 2100, 3GPP RAN4 and CTIA. The proposals differ significantly in terms of measurement setup and equipment because each approach is trying to solve the issue from a different perspective. After some effort of consolidation and development, four forms of proposed methods have been accepted by 3GPP RAN4 for further investigation [4] and also under discussion in CTIA.

Two large-scale Round-Robin Measurement Campaigns [4] were conducted for the purpose of initial comparison but due to limited device availability, a definite conclusion with respect to advantages and drawbacks of each method was not drawn [6, 7, 26, 27, 28, 29, 30, 31, 32, 33, 34]. A critical review of three main forms of proposed methods which are accepted as candidates for further discussion is given in this section. The questions raised in analyzing these methodologies will be discussed and answered in the next section. The fourth candidate proposal is separately presented and discussed in Chapter 5. Because in 3GPP LTE Rel-8 single user MIMO is only supported in DL, the discussion in this chapter is restricted to DL.

4.1.1 Multi-probe anechoic chamber approach

The concept of the multi-probe anechoic chamber approach is depicted in Fig. 4.1 [35]. The approach was first proposed in [36, 37, 38], with several variants introduced later [39, 40, 41, 42, 43, 44, 45, 46, 47, 48, 49, 50, 51, 52].

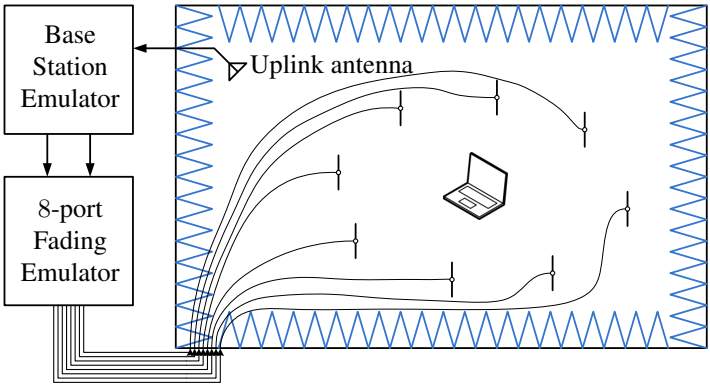

Figure 4.1: Illustration of multi-probe approach inside of an anechoic chamber. The first introduced version (8-probe in azimuthal plane) is presented.

Key elements of this approach are a large anechoic chamber and multi-channel fading emulators. The DUT is placed in the middle of the chamber with many probes (test antennas) surrounding it. The term "probe" used in the description of this method represents a test antenna or a combination of two orthogonally polarized antennas. Each output port of the fading emulators is connected to one of the ports on the probes. This way it is possible to emulate details of a channel model in the measurement (depending on the capability of the fading emulator) e.g. 3GPP Spatial Channel Model Extended (SCME) [53, 54, 55] or Wireless World Initiative New Radio (WINNER) II [56]. The quantity which is measured in these approaches, under conditions of different power levels and different channel models, is throughput.

The proposals of this kind which have been made mainly differ by the number of probes employed in the setup. Each port of the probes requires correspondingly one output port available on the fading emulator. The most advanced fading emulator at the time has 8 ports thus allowing to feed 8 probes with faded signals. The number of fading emulators in the setup hence determines the cost and complexity of the measurement. It requires many fading emulators to implement a complete emulation of a Geometry-Based Stochastic Channel Model (GSCM) model to very detail [57]. In this case, the synchro-

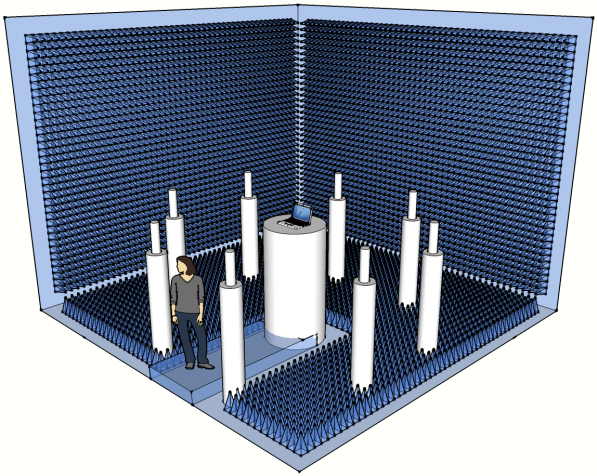

Figure 4.2: A rendering of multi-probe anechoic chamber setup for MIMO OTA measurement. 8 ϑ-polarized probes are illustrated with equal spacing of $45°$. The DUT is placed at the center of chamber with equal distance to all probes.

nization of equipment outside of the chamber is extremely complex.

Probe-ring anechoic chamber approach

A rendering of the initially proposed setup is given in Fig. 4.2 with 8 vertically polarized probes evenly positioned in the azimuthal plane [58]. For a 8-probe setup as in Fig. 4.2, a DL signal vector containing two signal streams $\boldsymbol{s} = (s_0, s_1)^\top$ with independent fading profile is routed to 8 ports of the probes via a fading emulator. This setup correspond to a constellation $\widehat{\mathbf{C}} = \left(\widehat{\boldsymbol{C}}_0, \widehat{\boldsymbol{C}}_1\right)$ of the form

$$\widehat{\boldsymbol{C}}_0 = \sum_{k=0}^{7} c_{\vartheta,k,0}\delta(\Omega, \Omega_k) \quad \text{and} \quad \widehat{\boldsymbol{C}}_1 = \sum_{k=0}^{7} c_{\vartheta,k,1}\delta(\Omega, \Omega_k). \tag{4.1}$$

The applied AOAs Ω_k are in the azimuthal plane with $\Omega_k = (90°, \phi_k), k = 0, 1, \ldots, 7$. The per-stream constellations $\widehat{\boldsymbol{C}}_0$ and $\widehat{\boldsymbol{C}}_1$ depend on the the choice of GSCM and Fixed Reference Channel (FRC).

The received signal vector at the antenna ports of the DUT is $\boldsymbol{r} = (r_0, r_1)^\top$ with

$$\begin{aligned} r_0 &= \sqrt{\frac{P_{\text{iso}}}{F}} \sum_{k=0}^{7} T_{\vartheta,0}(\Omega)\big(c_{\vartheta,k,0}s_0 + c_{\vartheta,k,1}s_1\big)\delta(\Omega,\Omega_k) + r_{\text{S},0} + n_0 \\ &= \sqrt{\frac{P_{\text{iso}}}{F}} \sum_{k=0}^{7} T_{\vartheta,0}(\Omega_k)c_{\vartheta,k,0}s_0 + \sqrt{\frac{P_{\text{iso}}}{F}} \sum_{k=0}^{7} T_{\vartheta,0}(\Omega_k)c_{\vartheta,k,1}s_1 + r_{\text{S},0} + n_0, \\ r_1 &= \sqrt{\frac{P_{\text{iso}}}{F}} \sum_{k=0}^{7} T_{\vartheta,1}(\Omega_k)c_{\vartheta,k,0}s_0 + \sqrt{\frac{P_{\text{iso}}}{F}} \sum_{k=0}^{7} T_{\vartheta,1}(\Omega_k)c_{\vartheta,k,1}s_1 + r_{\text{S},1} + n_1 \end{aligned} \tag{4.2}$$

where $\boldsymbol{r}_{\text{S}} = (r_{\text{S},0}, r_{\text{S},1})^\top$ and $\boldsymbol{n} = (n_0, n_1)^\top$ denote the vectors of self-interference and noise respectively. The channel matrix can in this case be written as

$$\mathbf{H} = \sqrt{\frac{P_{\text{iso}}}{F}} \begin{pmatrix} \sum\limits_{k=0}^{7} T_{\vartheta,0}(\Omega_k)c_{\vartheta,k,0} & \sum\limits_{k=0}^{7} T_{\vartheta,0}(\Omega_k)c_{\vartheta,k,1} \\ \sum\limits_{k=0}^{7} T_{\vartheta,1}(\Omega_k)c_{\vartheta,k,0} & \sum\limits_{k=0}^{7} T_{\vartheta,1}(\Omega_k)c_{\vartheta,k,1} \end{pmatrix} \tag{4.3}$$

with $\boldsymbol{r} = \mathbf{H}\boldsymbol{s} + \boldsymbol{r}_{\text{S}} + \boldsymbol{n}$. Any metric that is measured in this setup depends on channel matrix $\mathbf{H}$ and the DUT's ability to utilize it.

An obvious shortcoming of this approach is that only a single polarization is encountered. Measurements only in one polarization are obviously not sufficient to characterize an antenna system. To include both polarizations in the measurements, it might be tempting to directly route two DL signal streams separately to probe ports representing different polarization, e.g. s_0 to ports representing ϑ-polarization and s_1 to ports representing φ-polarization. It would require all probes to be changed to dual-polarized as well as an additional fading emulator [59]. The constellation is changed accordingly to $\widehat{\mathbf{C}}' = \big(\widehat{\boldsymbol{C}}_0, \widehat{\boldsymbol{C}}'_1\big)$ with

$$\widehat{\boldsymbol{C}}'_1 = \sum_{k=0}^{7} c_{\varphi,k,1}\delta(\Omega,\Omega_k). \tag{4.4}$$

$\widehat{\boldsymbol{C}}_0$ and AOAs Ω_k maintain the same definition as in (4.1). The corresponding

channel matrix $\mathbf{H}'$ is then

$$\mathbf{H}' = \sqrt{\frac{P_{\text{iso}}}{F}} \begin{pmatrix} \sum_{k=0}^{7} T_{\vartheta,0}(\Omega_k) c_{\vartheta,k,0} & \sum_{k=0}^{7} T_{\varphi,0}(\Omega_k) c_{\varphi,k,1} \\ \sum_{k=0}^{7} T_{\vartheta,1}(\Omega_k) c_{\vartheta,k,0} & \sum_{k=0}^{7} T_{\varphi,1}(\Omega_k) c_{\varphi,k,1} \end{pmatrix} \tag{4.5}$$

which gives more information than (4.3). The problem arises in $\mathbf{H}'$ that the setup is highly preferential to dual-polarized DUTs. It is to be expected that DUTs with equally good radiation property for both polarizations (e.g. designs aim to realize MIMO exploiting polarization diversity) would perform well in this setup. On the other hand, DUTs that are radiating mostly with single polarization and exploiting diversity via phase difference or pattern diversity would perform badly in this setup. It is because elements in one of the two columns of $\mathbf{H}'$ would in the latter case be very small in magnitude, thus limiting the condition number of $\mathbf{H}'$. One example of this type of UE is USB dongles when they are tested attaching to laptops with lid open according to normal test requirement [2]. Current excited along the edges of the base part couple predominately to φ-polarized fields whereas ϑ-polarized fields are hardly observed when measurements are restricted to AOAs in azimuthal plane. This observation is confirmed in real measurements with results presented in a later chapter.

The correct approach of polarization configuration in the measurement setup is to measure all possible polarization combinations. The constellations are then necessarily of the form $\widehat{\mathbf{C}}'' = \left(\widehat{\boldsymbol{C}}_0'', \widehat{\boldsymbol{C}}_1''\right)$ with

$$\widehat{\boldsymbol{C}}_0'' = \sum_{k=0}^{7} \begin{pmatrix} c_{\vartheta,k,0} \\ c_{\varphi,k,0} \end{pmatrix} \delta(\Omega, \Omega_k) \quad \text{and} \quad \widehat{\boldsymbol{C}}_1'' = \sum_{k=0}^{7} \begin{pmatrix} c_{\vartheta,k,1} \\ c_{\varphi,k,1} \end{pmatrix} \delta(\Omega, \Omega_k). \tag{4.6}$$

However, the realization of this constellation $\widehat{\mathbf{C}}''$, i.e. emulation of a GSCM snapshot would require 16 independently faded channels. A corresponding setup has not yet been presented.

The setup presented so far limits itself in the azimuthal plane [60]. It is suggested to be acceptable for laptop UE performance evaluation specifically in outdoor scenarios. The argument is that a laptop is like to placed on a horizontal surface and that outdoor scenarios feature predominantly paths with low elevation. However, a full evaluation of UE with handheld or tablet formfactors would require elevation in the measurements [61, 62]. The possible

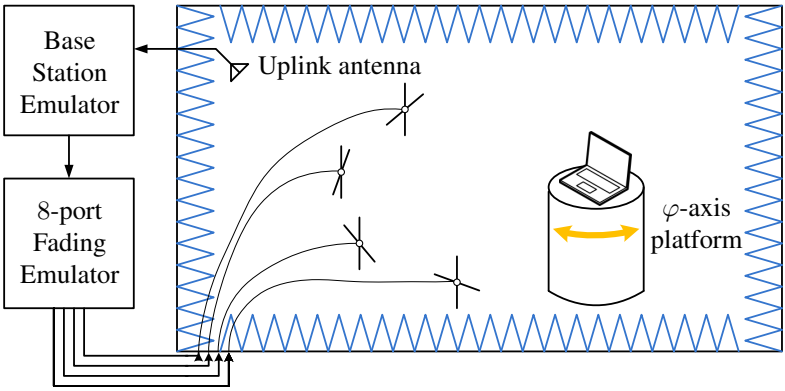

Figure 4.3: Illustration of an alternative setup with lower complexity: single cluster measurement in anechoic chamber with a fading emulator.

solutions would be to add more probes into the chamber or to change the elevation of the DUT or probes during the measurements. The former solution would greatly increase the complexity of the measurement setup because more fading emulators are required for the additional probes. The latter solution requires additional calibration every time when elevation of the DUT or probes has changed.

Single cluster anechoic chamber approach

In order to lower cost and complexity, restriction to emulation of a single cluster has been proposed as an alternative in [63]. The setup is shown in Fig. 4.3. A smaller number of probes is required because the DUT is illuminated from one side only. However, with probes only available at one side, scenarios with multiple clusters cannot be emulated in this approach. The DUT in this setup needs to be placed on a platform which can be rotated around the Z-axis to change the mean AOA of the cluster in the azimuthal plane. The setup is similar to a combined-axis anechoic chamber used for SISO OTA measurement (as in Fig. 1.1) and can be realized using existing chambers with moderate modification.

A rendering of this setup is given in Fig. 4.4. With only 4 probes and $45°$

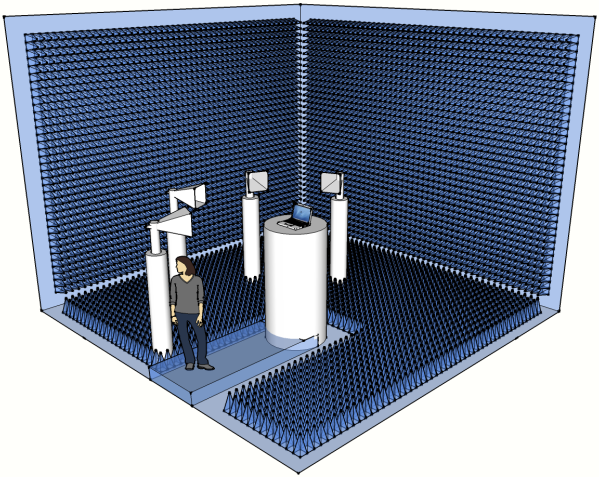

Figure 4.4: A rendering of the anechoic chamber of single cluster MIMO OTA measurement setup with GSCM fading emulation. Four test antennas are placed in the azimuthal plane relative to the DUT from one side of chamber with 45° spacing. Dual-polarized test antennas are used to radiate signal faded by an 8-port channel emulator covering both ϑ and φ polarizations. The DUT is mounted on a platform which is capable of rotating 360° in the azimuthal plane.

spacing between them, a 8-port fading emulator is sufficient to emulate simple GSCM profiles for both polarizations. A "single cluster" of GSCM profile is synthesized at the DUT by multiple radiated copies of a single DL signal stream from one side of the chamber [63].

Calibration for multi-probe approaches

The use of multiple probes in an anechoic chamber results a challenging calibration process as being reported in [64, 65]. In such setup, correlated copies of signals are transmitted from multiple probes. In order to generate predictable superpositions of these signals at the DUT, for each polarization, Path Loss (PL) between probes and the DUT must be calibrated. Even with perfect calibration, simple 'displacement' of the DUT can cause dramatically

different power distribution of the signal superimposed on the DUT [66].

For a setup with 8 ϑ-polarized probes as illustrated in Fig. 4.2, the calibration procedure requires a reference dipole vertically placed at the center of measurement zone. Equal distance is to be calibrated between the reference dipole and all probes in the chamber. For each probe, attenuation between the ports and the reference dipole is measured separately [67]. The reference dipole shall be rotated around the Z-axis in the procedure to observe the stability of PL measurement, in order to verify that the reference dipole is placed at the geometric and rotational center of the chamber [64]. After per-probe calibration, the whole setup shall be calibrated by sending exact copies of signal simultaneously to all probes [67]. A ripple test is required to be performed.

Cable and Basestation Emulator (BSE) calibration follows the standard procedures used in SISO OTA measurements [2] with the exception to consider BSE to be with two output ports instead of one. The fading emulator calibration requires a spectrum analyzer to compare power level of each output port under different displayed output level settings of the fading emulator. Actual output power vs. displayed output level shall be recorded for each port. A reference magnetic loop antenna is used instead of dipole to repeat the same calibration process to φ polarization. There exist also proposals to use dual-polarized horn as reference antenna [65]. However in the setups with multiple probes, signals transmitted from one probe are reflected by other probes. The superposition of these copies can only be correctly received thus calibrated using reference antennas with uniform pattern in the azimuthal plane. Horn antennas which have high directive patterns are not suitable for this purpose.

4.1.2 Reverberation chamber approach

Reverberation chambers are also proposed to be used for MIMO OTA measurements [15, 68, 69, 70, 71, 72]. The in situ superposition of signals on the DUT caused by multiple reflections and mode stirring is already a form of multi-path propagation and it is believed to be suitable for MIMO OTA measurements in the chamber. Multiple test antennas are mounted in the chamber without direct LOS path to the DUT as illustrated in Fig. 4.5. Similar to reverberation chamber setup used in SISO OTA measurements, DUT is mounted in the chamber on a platform which is capable of rotating around the Z-axis.

A rendering of this setup is given in Fig. 4.6. Multiple transmitting test antennas are located at the top of the chamber walls. Two out of multiple test antennas are selected in a 2×2 DL measurement.

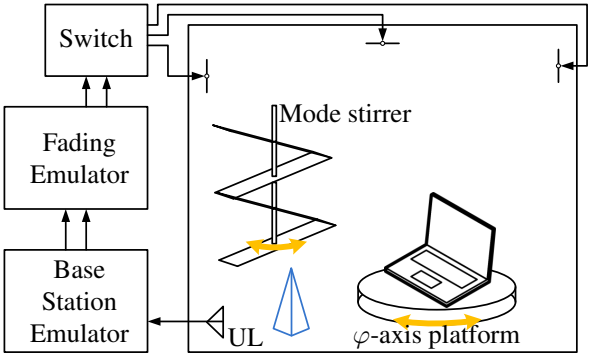

Figure 4.5: Structure of a reverberation chamber proposed for MIMO OTA measurements.

The reverberation chamber provides a statistically isotropic channel environment which is suitable for SISO OTA measurements. Power level applied to the measurement is the only meaningful parameter to adjust. When a chamber is extended for MIMO OTA measurements, it is necessary to have additional control over the channel in the chamber [73]. This is accomplished by placing additional mode stirrers in the chamber [74]. Channel specifications can be modified by changing the placement and mechanical behavior of the mode stirrers in the chamber. This includes the existing three methods of mode stirring methods in the setup [11].

- First method is the platform on which the DUT is mounted. It can rotate 360° around the Z-axis, providing azimuthal sampling and statistical averaging of the measurement results.
- Second method is to rotate the mode stirrers in the chamber, this is also the main method of creating statistically isotropic environment. Absorbers or other lossy materials can also be included in the chamber to achieve wider coherence bandwidth [11].
- The third method is through selection of transmitting test antennas. From multiple test antennas in the chamber, when each one is separately calibrated, selection of a smaller number to be used in the measurements

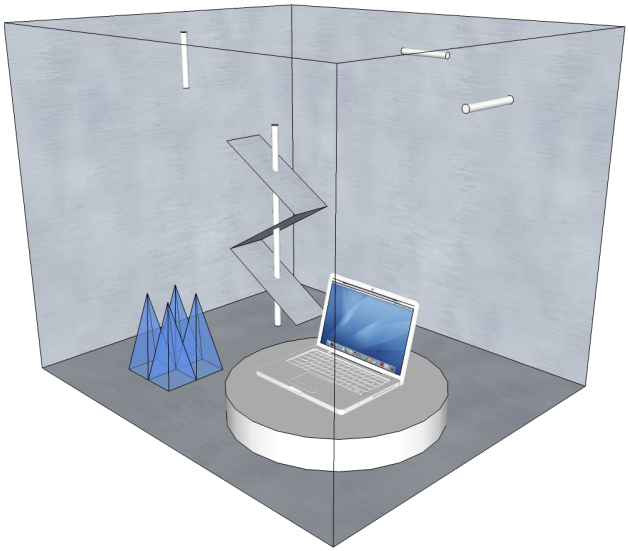

Figure 4.6: A rendering of reverberation chamber used in SISO OTA and proposed to be used in MIMO OTA measurements. The DUT is mounted on a platform which is able to rotate around the Z-axis and same to the mode stirrers. Three orthogonally polarized test antennas are located at the top of the metallic chamber walls. Additional absorbers can be placed in the chamber for further adjustment of the channel properties.

provides control over the channel. For instance, with three transmitting test antennas in the chamber, select two to transmit gives three unique combinations (channel environments). Using differently polarized antennas as transmitting test antennas also provides polarization stirring [75], it is useful in providing additional control over polarization distribution in the chamber.

With each configuration of mode stirring and antenna selection, throughput is recorded and average throughput is reported over all configurations for each power level. External fading emulators can be attached to "pre-fade" the DL signal streams before routed to the transmitting test antennas [76]. Any pre-

fading profiles applied on the emulator has to be implemented considering the existing in situ superposition of waves in the chamber [77, 78]. The necessity of this application will be discussed in the later sections of this chapter.

Calibration of reverberation chamber approach

For reverberation chamber used in EMC testing, a rectangular "test volume" is defined and calibrated by placing 8 probes at all the corners of this cube [79]. The plane waves superimposed at each probe is recorded and compared to theoretical derivation.

In the reverberation chambers used for passive antenna measurements, a simpler approach is used. Instead of calibrating the whole setup, an isotropic reference antenna with known properties e.g. efficiency is placed at the center of rotation on the platform. Measurement result which indicates efficiency of the Antenna Under Test (AUT) is directly compared with the result of the reference antenna in the same measurement. A relative metric is sufficient to characterize the AUT with the knowledge of the absolute properties of the reference antenna if the AUT is small enough to be contained in the "test volume" [11, 79]. When the AUT is electrically large, coupling between the AUT and enclosure / stirrers is inevitable and reference antenna has to be measured with AUT's presence in the reverberation chamber.

For active SISO OTA measurements e.g. TIS / TRP measurements in reverberation chambers, a proper calibration procedure is required [80]. Relative metric is not sufficient to describe the performance of the DUT because reference antenna is not able to be measured with comparable setup as the DUT i.e. lack of exact replica of baseband and RF circuits. The calibration procedure requires an isotropic reference antenna to be placed at the center of rotation on the platform. Planned measurement is performed to the reference antenna and the received power is recorded and its average calculated [81]. Assuming the DUT is again electrically small, the signal power superimposed on the DUT during the measurement is hence the same as what was observed by the reference antenna minus its efficiency. The coherence bandwidth of the chamber may have changed when measuring active DUTs comparing to passive ones, methods are proposed to compensate this effect [73]. The proposed MIMO OTA measurement setup could in principle be similarly calibrated by individually calibrating each test antenna.

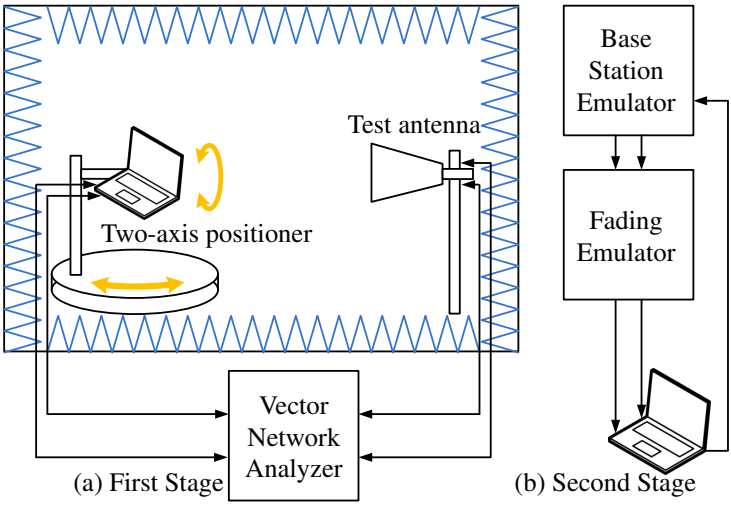

Figure 4.7: Illustration of the proposed two-stage method with (a) antenna pattern measurement and (b) conducted throughput measurements with fading channel emulation.

4.1.3 Two-stage method

The "two-stage" method is an approach that combines antenna pattern measurements with conducted measurements [20, 82, 83]. The first stage is antenna pattern measurements as illustrated in Fig. 4.7a. The second stage is conducted measurements with the antenna radiation pattern emulated by the BSE or the fading emulator as given in Fig. 4.7b. The radiation patterns used in the second stage directly come from the complex pattern measurement result of the first stage. The advantage of this method is that the most time-consuming part of measurements, namely the second stage, is performed as conducted measurements with software aided channel emulation.

As observed in (3.8), the selection of constellation is important to the complexity of the measurement. The two stage method tries to remove the constellations from OTA measurements by separately measuring antenna pattern $\mathbf{T}$ in the first stage. Once $\mathbf{T}$ is known, interaction between antennas and con-

stellations, i.e. operation $[\mathbf{T}, \widehat{\mathbf{C}}]$ can be emulated by software in conducted measurements i.e. the second stage [83].

The first stage can be performed as a passive antenna measurement, the compound radiation pattern of an antenna system in the form of (2.1) is obtained using a 4-port Vector Network Analyzer (VNA) in anechoic chambers. Two ports of the VNA are connected to a dual-polarized test antenna and other two ports are connected to the antenna ports of DUT. Multi-port scattering matrix of the antenna is obtained from the VNA. Measurement shall be repeated over the unit sphere. In this case, radiation patterns of each ports and relative phase between the patterns of antenna ports are obtained. The patterns are used in conducted measurements as substitute of real antennas. Cables are directly connected to the antenna ports and antenna system is replaced by measured patterns in software. The rest of the measurement uses fading emulators to directly feed pre-faded signals to the digital receiver of the DUT. The choice of channel models is flexible but the effort is kept low because the second stage does not require specific chamber or equipment other than BSE and fading emulator.

This approach is able to characterize the DUT by measuring almost all the elements in (3.8), including pattern $\mathbf{T}$, receiver noise figure F, isotropic power level P_{iso} as well as AWGN $\boldsymbol{n}$. However, in conducted measurements, self-interference $\boldsymbol{r}_{\mathrm{S}}$ is unaccounted-for [20]. Recent research suggested to use Reference Signal Received Quality (RSRQ) indication of LTE for self-interference quantification and this suggestion is under investigation [84].

Device self-evaluation support

Passive antenna measurement of an actual DUT however, is not recommended in end-to-end tests. The cables that attached to the antenna ports in the passive measurement can greatly influence the antennas' radiation property. Device assisted pattern measurement procedures can be realized by using information from the channel estimation which is performed by the DUT itself. Magnitude of the radiation patterns of each antenna ports can be obtained performing traditional SISO OTA measurements on individual antenna. With the support from baseband chipset of the DUT, phase information can be extracted from UE estimator by introducing relative phase report [85, 86].

4.2 Relevance of specific aspects in MIMO OTA measurements

The purpose of OTA measurements is to discriminate UE in close correspondence to how they would perform in real-life. All the methods presented in the last section for MIMO OTA evaluation have taken hints from the realistic fading environment and included them into their measurement setup. The relevance of these aspects that are included in the MIMO OTA measurement proposals has to be investigated [6]. Eventually, only a small set of these aspects is allowed in the final MIMO OTA measurement method to keep the complexity low [56, 87, 88, 89, 90, 91].

4.2.1 Approaches of measurement method proposals

MIMO OTA measurement proposals presented so far are different because of their different point of view on solving the problem. One perspective that many proposals have adopted is that MIMO OTA measurements should test the DUT in an environment with multi-path propagation i.e. 'realistic' scenarios which are likely to occur in real use. This is the way to assure the results are highly representative to in-the-field performance. From this point of view, several aspects are relevant in the measurements:

- 3D environment: the AOA of DL signals can be from any direction. Since "realistic" environments are not necessarily isotropic, flexibility to realize many spatial distributions of signal in the chamber is a welcomed feature.

- Spatial diversity: the fundamental reason of introducing MIMO is to exploit spatial diversity of the channel. DL signals from paths with different AOAs enable the usage of MIMO modes to increase data throughput.

- Random polarization distribution is mandatory.

- Realistic phantoms and standard mock-ups: near-field impairments commonly have huge impact to the antenna radiation performance. It is of UE's job to dynamically match and tune for an optimized reception quality [92].

A different perspective is that OTA measurements should concentrate on antenna characteristics. Only properties that are relevant and not able to be tested conducted should be considered in the MIMO OTA measurements.

- Antenna system efficiency: the efficiency of individual antenna is still the foundation of any performance metric. Receiver noise figure and self-interference normally cannot be tested separately.
- Correlation between received signal vectors: the correlation between the received signal vectors decides the channel capacity. This is a combined property of channel correlation and antenna correlation. If the channel matrix is properly estimated and diagonalized, there is no correlation.
- Power imbalance: the SNR imbalance between signal streams (codewords in LTE). Signal streams received with significantly different per-stream SNRs would suggest insufficient channel rank. When one stream is significantly weaker than the other, MIMO modes has to be adjusted accordingly. Although it sounds like a job up to the baseband, this property is dependent on the antenna compound pattern so it should be tested OTA.

Measuring properties other than efficiency needs modifications to the measurement methods and setups. The methods proposed so far each contains a different selection of these listed aspects and properties.

4.2.2 Number of test antennas

Following the discussion in subsection 4.1.1, an important question that has been asked is how many test antennas are required / sufficient in the multi-probe anechoic chamber proposal. Because the purpose of this proposal is to emulate complex channel model (or playback a recorded channel measurement [93]), the accuracy of this emulation depends on the number of test antennas in the chamber. Based on Nyquist sampling theory, the required number of test antennas is

$$K = 2\lceil \frac{\pi D}{\lambda} \rceil + 1 \tag{4.7}$$

where K denotes the number of test antennas, operation $\lceil \cdot \rceil$ representing round up operation, D gives the diameter of test zone and λ as wavelength [35, 94, 95]. This is a relatively large number to fulfill consider the one of the basic

far-field definition conditions is $D \gg 2\lambda$. The minimum number of K would hence be 15 when test antennas are positioned on the boundary of near-field to far-field transition. Numerous proposals have been made suggesting different numbers arguing smaller number of test antennas would still be sufficient, each with their own reasoning [49, 50, 96, 97, 98]. The most common setup in the discussion is to use 8 equaly-spaced test antennas in the azimuthal plane.

The number of test antennas has a large impact on cost, complexity and thereby reproducibility of a MIMO OTA test method. It is therefore important to clarify whether a larger number of test antennas will correspond to a better test method or not.

Without consideration of GSCM emulation, there is an obvious more acceptable lower bound on the number of test antennas. To investigate UE performance in an $M \times N$ MIMO scheme at least $\min(M, N)$ test antennas are required to realize a channel of maximum possible rank. Below we assume $M = N$. The minimum number of test antennas is then $K_{\min} = N = M$.

Use of a larger number of test antennas makes sense only if also additional uncorrelated DL signals are generated. This is possible by applying different time-variant delays or phase shifts and distributing these newly generated signals to different antennas. The resulting $K > K_{\min}$ paths will superimpose in the UE's antenna system to yield again N received signals. We refer to this effect as *in situ fading* which (as opposed to pre-fading, see next subsection) is a physical effect and relates to physical attributes of the UE antenna system.

Formally, in situ fading is a consequence of the linearity and projection property of the sampling operator $[\mathbf{T}, \widehat{\mathbf{C}}]$ showing up in (3.7). In fact, for any constellation $\widehat{\mathbf{C}}^{(K)}$ with $K > K_{\min}$ incoming paths the channel matrix can be represented as a superposition of channel matrices for constellations with only $K_{\min}$ antennas in the form

$$\mathbf{H} = \sqrt{\frac{P_{\text{iso}}}{F}}[\mathbf{T}, \widehat{\mathbf{C}}^{(K)}] = \sqrt{\frac{P_{\text{iso}}}{F}} \sum_i a_i [\mathbf{T}, \widehat{\mathbf{C}}_i^{(K_{\min})}]. \tag{4.8}$$

From the perspective of characterizing physical attributes of the UE, the question is, whether we can obtain significant additional information about the compound pattern $\mathbf{T}$ by applying superpositions of the constellations $\widehat{\mathbf{C}}_i^{(K_{\min})}$ instead of considering them individually. Although the finally recorded metric (e.g. throughput) is not a linear function of the channel matrix, the answer is negative. It has been shown in Section 3.3 that a setup with $K_{\min}$ antennas

is sufficient to characterize the relevant properties of a UE antenna system, in particular total antenna system efficiency and modal imbalance.

4.2.3 Pre-fading

In connection with MIMO OTA test approaches which use more than $K_{\min}$ test antennas, it may be tempting to generate signals for the additional antennas through emulation of a channel model.

A common way to do so is to use a fading emulator to apply a multi-tap Tapped Delay Line (TDL) model to a signal before routing it to a test antenna. This approach is referred as pre-fading. It corresponds to common functionality of fading emulators. Pre-fading is valuable for conducted measurements where it substitutes for the lack of in situ fading in the UE antenna system. It must be emphasized, however, that the introduction of pre-fading in a MIMO OTA test method, where in situ fading is already present, is unphysical and represents an arbitrary deterioration of the channel which does not correspond to reality.

Consider for instance the case of several paths which superimpose in space to create a spatial interference pattern with maxima and minima of available receive power. The diversity performance of a UE antenna system depends on how well it exploits this spatial interference pattern. If the paths are pre-combined before routing them to a test antenna, i.e. generated by means of a TDL filter, the spatial interference pattern is lost and replaced by a purely temporal fading characteristic which is basically sensed in identical form by all UE antennas. Since such proposals nevertheless exist [4] it is worthwhile to take a brief look at the main effect of a pre-faded signal when applied under conditions of a fixed MCS.

To this end it is sufficient to consider a single receiver. Without fading, one shall observe a sudden drop of throughput from nearly 100% to 0% in a small region about the threshold power of the selected MCS as available receive power is reduced below the threshold. This behaviour is approximated by a step function (dashed line) in Fig. 4.8 (the width of the transition region is in the order of $1\,\mathrm{dB}$ to $2\,\mathrm{dB}$ and not relevant for our argument here). The threshold radiated power level at which this transition occurs, assumedly $P_{\mathrm{thr}} = -85\,\mathrm{dBm}$ in Fig. 4.8, uniquely describes the receive quality of the UE in this situation. It reflects antenna efficiency, receiver noise figure and possibly self-interference. In a Rayleigh scenario, the probability that the instantaneous

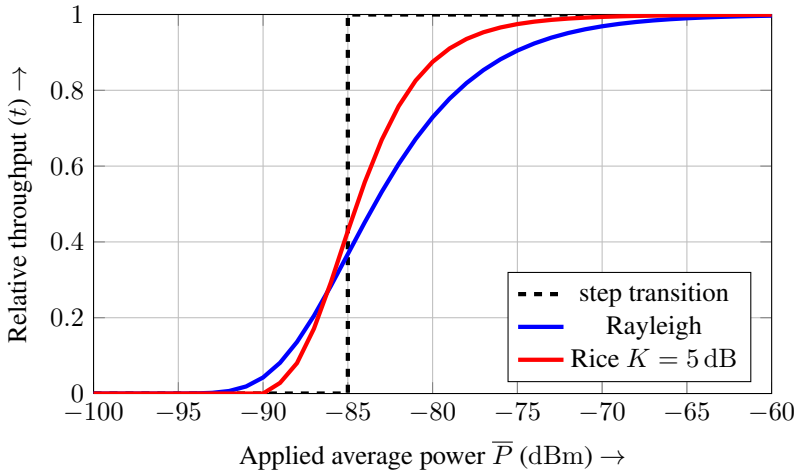

Figure 4.8: Illustration of the effect of Rayleigh fading (blue curve) and Rician fading ($K = 5\,\mathrm{dB}$, red curve) on observed throughput for an MCS threshold power of $-85\,\mathrm{dBm}$. See text for details.

receive power P_r exceeds P for a given average available receive power $\overline{P}$ is

$$\mathrm{Prob}\{P_\mathrm{r} > P\} = \exp(-\frac{P}{\overline{P}}). \tag{4.9}$$

A fading emulator has to emulate exactly this behaviour. The observed average relative throughput $t(\overline{P})$ as a function of average power is then basically given by the convolution of the Probability Density Function (PDF) corresponding to (4.9) with the step function resulting in

$$t(\overline{P}) = \exp(-\frac{P_\mathrm{thr}}{\overline{P}}). \tag{4.10}$$

This dependency is shown in blue in Fig. 4.8. The red curve displays the analogous result for Rician fading with a K-factor of $5\,\mathrm{dB}$. We observe that the desired information about the UE receive quality is just blurred by the statistics of the channel. Differences between results obtained this way are characteristic for the measurement setup (channel) but not for the UEs.

The conclusion of the above discussion is that pre-faded signals should be avoided in MIMO OTA measurements which are done with the purpose of device evaluation. This is easily possible by using just the minimum number of test antennas given by the number of available uncorrelated DL signals.

4.2.4 Emulation of a GSCM

A GSCM is a statistical approximation of channel sounding measurement campaigns. As seen by the receiver, signal transmitted from one transmitter is commonly modeled as a superposition of many copies of the same signal with different AOA. These copies are identified as separate paths but grouped as a cluster. Paths represent refractions and reflections of non-ideal surfaces, they share similar but different transmission distance which means slightly different Path Loss (PL) and with random phase. The modeling of a cluster contains a mean AOA describing the statistical main direction of this group of paths and Angular Spread (AS) denoting the variance of AOA and PL. To successfully emulate such clusters composed by paths, ideally, each path needs to be independently generated and transmitted from its AOA.

Since it is not practical to assign each path to a unique test antenna, many paths have to be synthesized at the DUT by sending correlated copies of the signals through multiple test antennas. Correlated copies of the same signal generate spatial interference pattern and can be seen by an isotropic antenna equivalent to signal received from another AOA. Modifying the power distributed on each test antenna, AOA of the synthesized path can be steered. For an actual DUT, since its pattern is not isotropic, what really is received by the DUT is not the same as an ideally isotropic antenna, even though same signal distribution is superimposed on them. Synthesis of individual path using multiple test antennas is not the same as sending the signal directly from the AOA of the path. Another commonly seen approach is to simply assign each path to the nearest test antenna, in order to avoid synthesis by superposition. However, the end result is not different than applying pre-fading, just with a different fading profile.

4.2.5 MIMO modes and CSI report

So as to design an OTA test method for MIMO UE it is mandatory to have a basic understanding of the underlying communication standard. State-of-the-Art communication standards employ an aggressive switching strategy in

adaptation to the ever-changing multi-path channel. LTE is a perfect example to illustrate this issue. The DL of LTE Rel-8 features already 7 basic transmission modes. Further modes are added in Rel-9 and Rel-10. The most relevant MIMO modes are the DL TD mode and Open Loop and Closed Loop SM modes. Apart from the different transmission modes there are 15 unique combinations of modulation order and coding rate, each referred to in the following context as an MCS (note this is different to the definition of parameter I_{MCS} in LTE). In reality, transmission mode and MCS are adaptively selected by the eNB, taking into account, at its own discretion, CSI feedback from the UE.

In LTE Rel-8, three difference types of reporting are incorporated [99].

- Channel Quality Indication (CQI) is to indicate the suitable MCS to be used in the transmission.
- Precoding Matrix Indicator (PMI) is required in the closed-loop scenarios for selection of precoding matrix feedback.
- Rank Indication (RI) gives the hint of high channel rank and possible exploitation of multi-path environment.

All three indicators are subjects of report both periodically and aperiodically.

Among the different indicators which are returned by the UE and provide CSI feedback to the eNB, the RI is fundamental for the selection of the appropriate MIMO transmission mode. RI is a 1-bit reply from the UE of the capability of channel of supporting SM. In scatter-rich channel environment which is suitable of transmitting multiple signal streams (codewords), the UE should report "$\mathrm{RI} > 1$" to tell the eNB the detected high channel rank. SM is possible only as long as the current rank of the channel is larger than one. Otherwise an "$\mathrm{RI} = 1$" should be reported.

If the channel is in addition not too rapidly varying over time, the eNB can select CL-SM mode and use the PMI information from the UE to select from a predefined set of precoding matrices the one which optimizes the condition number of the channel matrix. In order to maintain a low uplink transmission budget, only phase information of the channel is contained in the PMI reports. For a two-port (layer) antenna system, 2-bit PMI is used. For a four-port (layer) antenna system, 4-bit PMI is used.

If the channel exposes rapid time variation, not allowing for timely update of PMI, the eNB may switch to Open-loop Spatial Multiplexing (OL-SM) mode. In this case random pre-coding is employed in order to assure an at least statistically, on average, good condition number of the channel matrix. In OL-SM

mode Large-delay Cyclic Delay Diversity (LD-CDD) is in addition introduced as a means to enhance diversity of the channel. If the rank of the channel or the SNR do not allow for either of the SM modes, DL TD is available as a robust fallback mode which maximally exploits the diversity of the channel for reliable transmission of single stream (codeword). Note that DL TD mode is nevertheless a MIMO transmission mode. SFBC is used to transmit orthogonal replicas of a single stream from different Basestation (BS) antennas based on the Alamouti scheme [22]. In reality DL TD is the most important mode as it allows for reliable transmission under poor channel conditions.

A further aspect of interest is MCS selection. Based on CQI feedback from the UE the eNB continuously adapts the MCS to current channel conditions. In LTE, CQI reporting is normally 4-bit per each signal stream (codeword). There are 16 CQI levels with index 0 to 15 and 0 explicitly presents "out of range". Each CQI level corresponds to a unique combination of modulation scheme and coding rate. At the eNB side, CQI report is translated to modulation scheme and transmit block size which is the nearest approximation of the coding rate. Modulation scheme and transmit block size has in total 32 levels (with 4 reserved). By means of the CQI the UE indicates allowance for a higher MCS if the current BLER drops below a threshold and requests a lower MCS if the BLER exceeds the threshold.

The final decision of MCS, precoder matrix and rank is made by eNB, but UE's capability of correctly reporting each of the fore-mentioned indicators is relevant to the device performance. When CQI reporting is wrongly reported too high, the corresponding MCS is also high. This causes high BLER in an insufficient SNR. Eventually it may leads to lower throughput during the transmission. On the contrary, lowly reported CQI may guarantee low BLER, but throughput is upper-bound by correspondingly low MCS.

RI reporting is equally important. Although RI has only single bit, it gives indication of whether SM transmission modes are to be used. Wrongly report of $\mathrm{RI} = 1$ in a high rank environment would limit the throughput when a much higher data-rate is possible. On the other hand, $\mathrm{RI} > 1$ should be carefully reported because using SM modes in a single rank channel is likely to cause less throughput than in using transmission modes suitable for such channel e.g. TD.

PMI is only required in closed-loop transmission. Although its effectiveness is no doubt limited since only 2-bit reports are used in a 2×2 transmission. Use of PMI report separates the transmission of signal streams and allows different

CQI report for each signal stream (codeword) for further optimized utilization of the channel.

The above overview is admittedly superficial but considered necessary here to emphasize the role of the interaction between the eNB and the UE in MIMO transmission. Any performance figure like e.g. throughput observed in a real network is a system property which includes not only UE receive performance and UE feedback reporting quality but also the response of the scheduler in the eNB. It is of uttermost importance to be aware of this fact so as not to arrive at a simplistic and erroneous idea of a realistic test case. To be realistic a time-variant, faded multi-path channel is always to be combined with a fully adaptive system comprising not only the UE but also the mode switching and MCS adaptation functionality of the eNB's scheduler. This functionality is, however, neither supported by presently available test equipment, nor is there a standardized scheduler at all. Measurements are presently rather performed under conditions of an FRC which pre-defines transmission mode and MCS. Exposing UE to a random channel under these fixed settings is all but realistic.

The way out of this difficulty is to characterize the physical UE attributes which determine the UE's contribution to overall performance. Part of this task requires for OTA measurements, other properties are more easily and reliably characterized by conducted measurements.

4.2.6 GSCM, adaptivity and averages

The common starting point of any GSCM is the definition of UE velocity. It is directly translated into Doppler shifts. But in addition it is also used to introduce time dependence into the channel, resulting in time-dependent fading where the UE velocity determines the rate of change. Any MIMO OTA measurement performed under these conditions necessarily amounts to the measurement of a time average, e.g. of average throughput. It is tempting to consider such time average to be a particularly "realistic" indicator of UE performance. But there are two major issues with this approach if combined with an FRC:

(a) The condition number of the channel matrix $\mathbf{H}$ is varied over time in a poorly predictable way, i.e. the rank of the channel may change up to the situation that it is in disagreement with a pre-selected MIMO operating mode.

(b) Fading becomes time-dependent and the available receive power is spread out statistically about its average value with the effect that the SNR may be in disagreement with a pre-selected MCS during extended portions of the measurement interval.

Either effect potentially renders the recorded average values meaningless with respect to in-the-field results. In reality, i.e. in a fully adaptive system with a real eNB, the UE would have reported the current rank of the channel and the eNB would have switched to a more appropriate transmission mode (such as TD and OL-SM or CL-SM). During a measurement with time-dependent fading the UE under test may also have desperately reported over parts of the measurement period that it could still attain appreciable throughput if CQI was decremented (i.e. the eNB should switch to a lower order modulation scheme or lower coding rate). But it is not heard. Instead zero throughput is recorded. Similarly the UE may over parts of the measurement period have reported that the channel is good enough for the next higher order modulation scheme or higher coding rate (CQI increment), but the measurement under conditions of an FRC fails to account for the true performance of the UE.

Likewise the rank of the channel may temporarily change when statistically generated and time varying channels are applied but the transmission mode is not adapted. The time response of the UE's channel estimation and correctness of feedback information is a relevant issue for device testing. But there is no need for doing so OTA.

It can be concluded that time averages taken with respect to a time-variant channel do not correspond to any real situation if taken under conditions of an FRC. But as opposed to average values empirical outage probabilities may still convey useful information.

4.2.7 GSCM and near-field impact

A lot of attention has been given to accurate emulation of geometrical detail of the SCME models such as AS in anechoic chambers [100]. In reality however, such "free-space detail" is seldom visible to the UE at all. It is rather masked and strongly modified by the near-field environment of the UE, in case of hand-held devices e.g. by the user's hand or head. Measurements with appropriate phantoms are well established in existing OTA test plans (e.g. [2]). Since the performance of MIMO UE is potentially more susceptible to the near-field environment than that of a single antenna UE, the quest for realistic

test conditions will have to include them.

5 Proposed test plan for MIMO OTA measurements

5.1 A measurement method based on direct device characterization

A way to arrive at a simple but effective OTA method of characterizing MIMO antenna system is to directly evaluate the properties that are relevant to MIMO transmission [101, 102, 103, 104, 105]. The realization of this goal should follow the principles:

(i) OTA measurements are designed to correspond to those physical UE attributes which cannot be characterized by conducted measurements but must be characterized by OTA measurements [106, 107].

(ii) The discretionary introduction of features from channel models for which a UE antenna system is transparent, in particular time dependent fading, are to be avoided. Such features are likely to dominate measurement results and obliterate differences between devices [88, 108].

(iii) In order to assure reproducibility and accurate calibration, each test case should be stripped down in complexity to what is essential for the result.

(iv) The influence of the measurement setup on results must be clearly understood and traceable.

(v) Test setups which allow for reuse of existing OTA chambers are preferred.

Meaningful and realistic test cases can only be defined in agreement with the fundamental features of a MIMO communication standard, the most important of which is adaptation of the MIMO transmission mode to the channel properties.

The investigation of throughput in SM transmission mode is not meaningful unless it is assured that both the rank of the channel is larger than one and the SNR is sufficiently high. Otherwise the result will just show that a poor channel is applied, a situation in which TD transmission mode would be invoked in reality. A MIMO-favourable channel is mandatory to evaluate MIMO performance in SM transmission modes.

Conversely, diversity performance cannot be evaluated if the channel is good enough to achieve constant maximum throughput with a single antenna. Diversity performance is best described by sensitivity under poor channel conditions. The MIMO transmission mode which in reality is used in the low SNR regime is TD and hence should also be used for testing in this context.

Two basic test cases are derived from the above consideration which will be shown to cover the relevant physical attributes of UE:

(1) evaluation of noise limited performance in TD mode using a sensitivity based metric,

(2) evaluation of peak performance in SM mode using a throughput based metric.

They correspond to poor and MIMO-favourable channel conditions, respectively [102, 103, 104].

The definition of the metrics which are to be reported must follow the purpose to provide a criterion for in-the-field performance. UE should perform reasonably well in each of a large variety of propagation scenarios which can only be described statistically. Average quantities are not apt to characterize UE in this respect. An appropriate metric is the *outage probability* of a performance criterion [109, 110, 111]. Statistical metrics allow for a comparison of UE in terms of the probability that a prescribed minimum performance will be achieved or, conversely, in terms of outage probability of a given transmission mode and MCS. The probabilities are directly related to user experience and network efficiency.

As opposed to averages, observed *outage probabilities* relative to some performance criterion gathered over a set of fixed, identically reproducible propagation scenarios, also remain meaningful under conditions of an FRC.

The proposed test plan therefore defines statistical metrics in terms of the Cumulative Distribution Function (CDF) or Complementary Cumulative Distribution Function (CCDF) of sensitivity or throughput, respectively, under identically reproducible conditions as the metrics to be reported.

5.2 Sensitivity measurement in noise-limited scenario

5.2.1 Goal

DL TD mode is meant to provide link reliability and fair throughput under non-optimum channel conditions. The appropriate test case amounts to a characterization of UE sensitivity in a noise-limited scenario, akin to traditional TIS measurements for SISO devices. Differences to traditional TIS measurements arise (i) from the fact that at least $M = 2$ orthogonal DL signals are available in DL TD mode which carry the same information, and (ii) from the presence of multiple receive antennas and the possible support of Receive Diversity (RD) in the UE. Note that TD and RD are completely independent methods for improvement of link quality. TD is in general based on the Alamouti scheme, in LTE for instance in form of SFBC. RD can be realized by MRC which is the optimum approach and is taken as reference case below. Both schemes work together so as to combine the total available power from all M downlink signals and all N UE antennas in order to maximize the SNR. The sensitivity is recorded in terms of the received power which is required for not exceeding a specified BLER threshold.

5.2.2 Procedures

This test case uses a conventional OTA test chamber equipped with a single dual-polarized test antenna, for example a quad-ridged horn antenna. Two output ports of the MIMO BSE, carrying the two orthogonal DL TD signals are routed to the two polarizations of the test antenna simultaneously and with equal power.

The transmission mode is set to transmit diversity. P_{iso} is defined as power available from an isotropic antenna at the UE position. In the TD scheme, two orthogonal signals are routed to the two polarizations of the the test antenna simultaneously and with equal power (half the total power each).

For each constellation, with established connection between BSE and the DUT, search of sensitivity threshold starts from a high P_{iso} level. Decrease of P_{iso} will cause the BLER rise from 0% to 100%. The purpose is to record the BLER vs. P_{iso} curve and find the specific P_{iso} for target BLER. The procedure for the DL sensitivity measurement is described in more detail in a later chapter

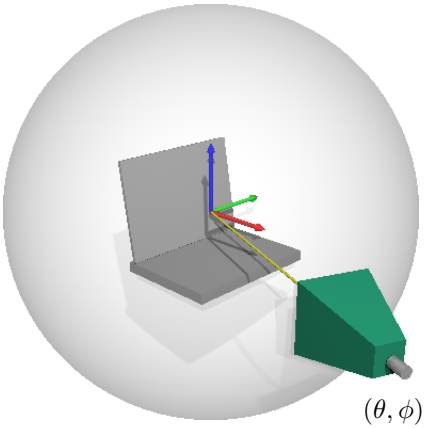

Figure 5.1: Test setup for sensitivity measurement in noise-limited scenario in TD mode using single dual-polarized test antenna.

and in [103]. Repeat the measurement with test antenna moving or the DUT rotating until a defined grid of the unit sphere is visited. In principle all relevant AOAs shall be accessed as in Fig. 5.1 in the same way as in conventional SISO OTA test plans.

5.2.3 Metric

Based on the discussion in Subsection 3.3.2 an explicit model expression for the capacity of a MIMO system in low SNR region is readily obtained. If a sequence of different constellations $\widehat{\mathbf{C}}$ is applied, different values of SNR are observed. The distribution of these SNR values and hence the statistics of sensitivity observed over the sequence of constellations characterizes important features of the compound pattern of the UE's antenna system.

The constellation applied in this measurement is the same as described in Subsection 3.3.2 with $\mathcal{C} = \{\widehat{\mathbf{C}}_i\}$ whose elements are, apart from irrelevant phase factors, of the form

$$\widehat{\mathbf{C}}_i = \begin{pmatrix} 1 & 0 \\ 0 & 1 \end{pmatrix} \delta(\Omega, \Omega_i), \tag{5.1}$$

i.e. only a single AOA Ω_i is encountered per measurement [23].

Let $\mathrm{SNR}_{\mathrm{thr}}$ denote the threshold SNR level on the Left-Hand-Side (LHS) of (3.11) below which the specified BLER threshold is exceeded for the selected FRC. The corresponding value $P_{\mathrm{iso}} = P_{\mathrm{iso,thr}}$ on the RHS of (3.12) gives the sensitivity at AOA Ω_i, the *directional compound sensitivity*

$$\frac{1}{P_{\mathrm{iso,thr}}(\Omega_i)} = \frac{1}{\mathrm{SNR}_{\mathrm{thr}}\, P_{\mathrm{N},0}} \frac{\|\mathbf{T}(\Omega_i)\|^2}{F}. \tag{5.2}$$

Note that the RHS of (5.2) is essentially the compound antenna gain over receiver noise figure at given AOA Ω_i. The average of (5.2) over the unit sphere is the Total Compound Isotropic Sensitivity (TCIS)

$$\frac{1}{\overline{P_{\mathrm{iso,thr}}}} = \frac{1}{\mathrm{SNR}_{\mathrm{thr}}\, P_{\mathrm{N},0}} \frac{\mathrm{tr}(\mathbf{R})}{F} = \frac{1}{\mathrm{SNR}_{\mathrm{thr}}\, P_{\mathrm{N},0}} \frac{N\overline{\eta_{\mathrm{tot}}}}{F}. \tag{5.3}$$

$\mathbf{R}$ is the radiation matrix (2.5), $\overline{\eta_{\mathrm{tot}}}$ denotes the total antenna system efficiency after (2.11) and N is the number of UE antenna ports. Note that (5.3) completely characterizes the most important UE attribute: the ratio of total antenna system efficiency over receiver noise figure.

It is remarkable that the most relevant MIMO OTA performance figure, TCIS, equivalent to total antenna system efficiency over receiver noise figure, can be obtained with actually less effort than suggested in existing SISO OTA test plans which require separate measurements for each polarization. But the test procedure which has been sketched above is suitable also to obtain a more significant statistical metric at no additional cost. As well known from income statistics, average values don't tell the full story. A UE with the same value of TCIS may still exhibit different outage probabilities. Receive diversity performance will be rated the better the less it depends on the accidental directions of the incoming paths, i.e. on the variation of the total power received from both polarizations over all possible AOAs. The FOM to be reported is therefore the empirical CDF of sensitivity which is readily obtained from recorded directional sensitivity values (5.2). The proposed metric is formally introduced as a function of applied power P_{iso} by

$$\mathrm{CDF}_{\mathrm{sensitivity}}(P_{\mathrm{iso}}; \mathcal{C}, \mathrm{FRC}, \mathrm{BLER}) = \mathrm{Prob}\{P_{\mathrm{iso,thr}} < P_{\mathrm{iso}}\} \tag{5.4}$$

and of course depends on choice of FRC, threshold BLER and applied sequence of constellations $\mathcal{C}$. The CDF (5.4) allows for comparison of devices in terms of outage probability of a given FRC at given power level for arbitrary AOA, a quantity which is expected to bear a close relation to the probability of dropped service in an arbitrary propagation scenario.

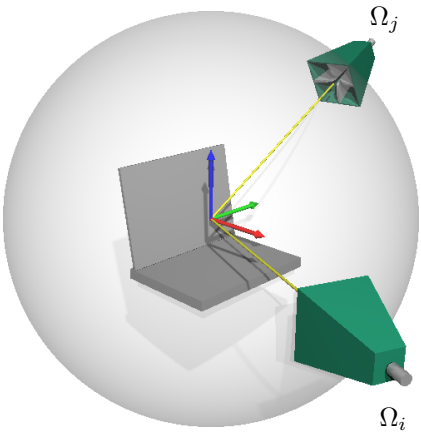

Figure 5.2: Test setup for e.g. a 4×2 or 2×2 MIMO scheme using two dual-polarized test antennas. The AOAs Ω_i and Ω_j are independently selected on the unit sphere.

5.3 Peak throughput in MIMO-favourable scenario

5.3.1 Goal

The capability of a device to benefit from multi-path propagation by providing high throughput can only be tested if the propagation environment is suitable for such transmission. MIMO peak performance is to be measured for SM modes under conditions of a full rank propagation channel and high SNR. A throughput-based metric is appropriate to evaluate whether the UE antenna system meets the performance target. The metric and accompanying test procedure which is proposed below covers the physical UE attributes modal efficiencies and modal imbalance and is therefore complementary to what was obtained by sensitivity measurement in a noise-limited scenario in the previous section.

5.3.2 Procedures

Fig. 5.2 depicts the concept of a test setup with two dual-polarized horns which can independently be set to AOA Ω_i and AOA Ω_j, respectively. For each pair of AOAs all possible combinations of polarizations can be realized. The setup therefore allows for full characterization of the UE with $N = 2$ antennas. In this context it can accommodate for a 2×2 MIMO scheme. It is also expected that the setup after Fig. 5.2 is still sufficient for evaluation of UE with 4 antennas even though it does not provide all degrees of freedom required to span the space of possible receive signal vectors $\boldsymbol{r}$ in a general 4×4 MIMO channel. The reason is that the setup closely mimics what also is to be expected in reality for BS antenna systems built from antenna pairs with $\pm 45^\circ$ inclination of polarization. For evaluation of UE with more than 4 antennas additional test antennas have to be added.

For the presently proposed approach we consider the simple case of a 2×2 MIMO transmission in SM mode. Among all possible constellations which can be realized with the setup after Fig. 5.2 we restrict ourselves to those which are of the simple form

$$\widehat{\mathbf{C}} = \begin{pmatrix} c_{\vartheta,0} & 0 \\ c_{\varphi,0} & 0 \end{pmatrix} \delta(\Omega, \Omega_i) + \begin{pmatrix} 0 & c_{\vartheta,1} \\ 0 & c_{\varphi,1} \end{pmatrix} \delta(\Omega, \Omega_j) \tag{5.5}$$

with exactly one element in either matrix on the RHS of (5.5) equal to one and the other zero. Each of the two orthogonal, equal power downlink signals is then routed to exactly one out of the 4 available ports at a time. The measurement procedure involves a sequence of such constellations with Ω_i and Ω_j taken from a predefined grid on the unit sphere for all possible combinations of polarization, i.e. (ϑ, ϑ), (ϑ, φ), (φ, ϑ) and (φ, φ). Throughput is recorded for each measurement.

Before turning to the proposed statistical metric for the present test case, some considerations with respect to the MIMO transmission modes which may be selected for the measurement, i.e. CL-SM or OL-SM, are necessary. In view of the above discussion CL-SM appears to be well suited for the intended characterization. It comes with the additional advantage to minimize possible bias introduced through the test scenario by virtue of adaptive pre-coding. Investigation of CL-SM performance, however, makes sense only if the eNB emulator supports adaptive pre-coding based on the UE's PMI report and adaptive per-stream CQI-based MCS selection. It must further allow to have the UE's RI report ignored. These features are not yet in general supported by test

equipment. OL-SM comes with an inherent randomization of the channel via LD-CDD and random pre-coding. As a consequence, throughput observed in each particular constellation represents by itself a statistical average of different channel realizations. Furthermore, when using OL-SM mode meaningful statistics can be gathered under conditions of an FRC provided that the power level P_{iso} is selected properly.

5.3.3 Metric

The proposed metric is the empirical CCDF of observed relative throughput t_{obs} written as function of relative throughput t in the form

$$\mathrm{CCDF}_{\mathrm{throughput}}(t; \mathcal{C}, \mathrm{FRC}, P_{\mathrm{iso}}) = 1 - \mathrm{Prob}\{t_{\mathrm{obs}} < t\}, \qquad (5.6)$$

where $\mathcal{C}$ denotes the set of applied constellations and P_{iso} is the applied power level.

For each constellation, a corrective weighting factor is to be applied to the contribution it makes to the CCDF (5.6). This weighting factor depends on the product of relative areas represented by two AOAs of constellations on the unit sphere. (This is in analogy to the $\sin(\vartheta)$ weighting of measurements in conventional TIS or TRP measurement.)

5.3.4 Selection of constellations

The above presented measurement procedure and derivation in Subsection 3.3.4 has been made only for the purpose of a qualitative interpretation of the significance of throughput measurements in the high SNR regime. It is neither necessary nor feasible to choose the AOAs Ω_i, Ω_j from a grid on the unit sphere with resolution fine enough to accurately approximate $\mathbf{R}$ in (3.19). Even for a setup with 2 test antennas only, there are 4 degrees of freedom $(\theta_1, \phi_1, \theta_2, \phi_2)$. Hence, at an angular resolution comparable to traditional TIS / TRP measurement, instead of say $2K$ samples (2 polarizations times K grid points on the unit sphere), $2K^2 - K$ samples would be required. It must be emphasized that this observation holds equally for measurements in an anechoic chamber and in a reverberation chamber. The number of samples, i.e. different constellations required for sampling with a prescribed resolution can also *not* be reduced by employing more antennas. It should be clearly understood that with a larger number of test antennas we can only generate linear combinations of

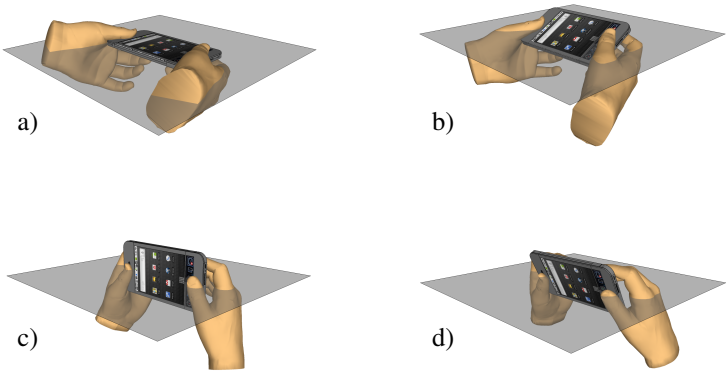

Figure 5.3: Selection of "2D-cut"s: a), b), c), d) are different examples of usage scenarios.

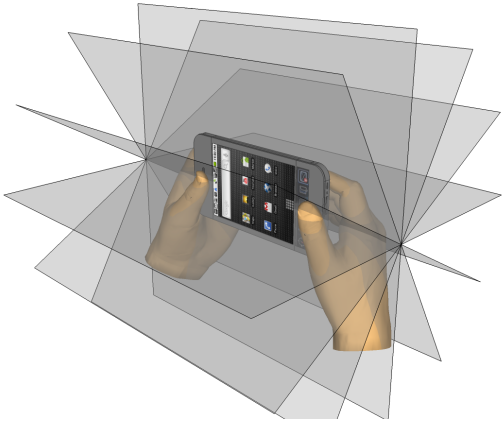

Figure 5.4: Example of 30° step selection of measurement planes.

those constellations which were also realizable with the smaller number of test antennas. Only when taking a larger number of samples, i.e. resorting to a longer sequence of different constellations, further independent samples can be obtained. It is therefore inevitable, but also sufficient (as to be addressed by simulation in a later chapter), to resort to a sequence of constellations which is just large enough to deliver trustworthy statistics of throughput [112]. There are some minimum requirements on the selection of such sequence of constellations which are experimentally confirmed and will be illustrated with examples in Chapter 7:

(a) It is mandatory to consider both polarizations in all cases, i.e. for each pair of AOA Ω_i, Ω_j all 4 possible combinations of polarizations must be accounted for.

(b) It is mandatory to achieve a fair representation of the assumed PAS. An "economization" of MIMO OTA measurement by e.g. restriction to AOAs which are exclusively in the azimuthal plane may yield grossly misleading results.

Economization by limiting constellations in the azimuthal plane is frequently seen in channel models based on realistic channel measurements as well as measurement method proposals using them. It is based on the observations that channel sounding results tend to contain more DL paths with low elevation AOA.

- In outdoor environment, BS is commonly located on top of a nearby building, the elevation of a path AOA is likely to be low.
- In indoor / outdoor scenarios, feasible paths connecting BS and UE are through windows, which suggests low elevation as well.
- Indoor environment with BS and UE inside the same room can have high elevation of path AOAs, but it is not an important scenario in cellular networks.

This economization approach is undoubtedly worth of consideration for DUTs with form-factor laptops or USB dongles which require a laptop as the host. It is because these DUTs are likely to be placed on a horizontal surface when they are used. Hand-held DUTs e.g. phones or tablets on the other hand, should not be assumed to have a standard position like the laptops do. Their orientation can be totally arbitrary.

A suitable reduced set of constellations can, e.g. for a hand-held device derived from considerations illustrated in Fig. 5.3 [102, 113]. The consideration here is to evaluate the possible usage scenarios and constellations with low probability for real life scenarios can be omitted. The most relevant orientations of the device relative to the horizontal plane correspond to standing (a), sitting (b) and lying (c,d) positions of the user. These cases can be covered by first selecting a small set of measurement planes as e.g. the 6 planes shown in Fig. 5.4. A measurement plane is understood in this context to be defined by the origin of the UE coordinate system and the positions of the two test antennas. Within each measurement plane a set of angular offsets between the two measurement antennas in the range from 0° to 180° is considered. Finally the UE is rotated about its vertical axis using a pre-defined step size. At a base resolution of 30° this scheme would for example result in $6 \times 7 \times 12 = 504$ constellations – a number comparable in magnitude to what is used in traditional TIS or TRP measurement.

The extent by which the number of constellations can be reduced for economization of the procedure is subject of further investigation. Fastest way of this investigation is to use a simulation tool to verify the convergence of FOM with respect to a smaller set of constellations.

6 Simulation

6.1 Goals of using simulations

With many MIMO OTA measurement methods proposed, it is of standardization bodies' interest to evaluate each proposal for its ability to distinguish "good" and "bad" devices. As discussed in Section 4.2, many features and aspects that can be introduced to the measurements have to be investigated and their importance in MIMO OTA measurements evaluated. To fulfill these requests, large amount of measurements are required. However, it is neither manageable nor economically justified to have everything accomplished via measurements. Simulation is an acceptable alternative to validate measurement methods.

6.2 Simulation chain overview

Based on existing system link level LTE simulation chain [114] provided by TU Vienna, an OTA simulation chain is developed in order to validate measurement proposals [8, 115]. An overview of the simulation chain is given in Fig. 6.1.

The original MATLAB-based simulation chain follows the classic communication theory structure. It is constructed by three major modules: transmitter, channel and receiver. The purpose of the simulation chain is to evaluate the end-to-end communication at system level and it is further incorporated into network and system planning simulators. The classic communication definition of 'channel' is too general for the purpose of simulating OTA measurements. It needs to be divided into two modules representing propagation and antenna separately. The transmitter and receiver modules can be reused with little to no modification. When simulating DL MIMO, the transmitter is set as eNB and receiver as UE. In real measurements, the transmitting antenna i.e. test antenna or probe is with known property, a separate modeling is not re-

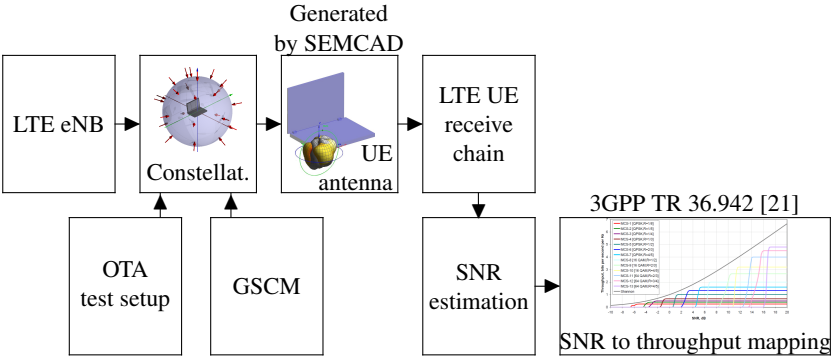

Figure 6.1: Top level view of the simulation chain.

quired. Properties of test antennas are merged with propagation and presented in the simulation chain as constellations introduced in Chapter 3.

The simulation chain has the following modules as illustrated in Fig. 6.1.

- An LTE eNB module served by transmitter module from the original simulation chain. Time domain baseband signal streams are generated to per-port (layer) level. The number of ports can be configured.

- A new constellation module. This module represents the combined function of OTA measurement setup and GSCM emulation. Signal streams from the eNB module are faded and distributed to virtual test antennas. OTA setup (e.g. number and location of test antennas) can be individually changed as well as GSCM emulation parameters.

- The new UE antenna module representing the compound multi-port antenna pattern $\mathbf{T}$ of the DUT. It receives the signals from all possible AOAs (outputs of the constellation module) and superimpose them before sending to the receiver. This module can load different antenna pattern without interfering with other modules.

- An LTE UE receive chain from the original receiver module with little modification.

- A post-processing module for capturing and analyzing results

6.3 Module specifications

All modules and their important functions are explained in the following subsections in detail.

6.3.1 LTE eNB

The LTE eNB module is directly taken from TU Vienna system link layer LTE simulation chain. It generates random payload, along with all possible modulation, interleaving and layer-mapping up to four ports (layers). 5 out 7 LTE MIMO modes are supported including TD and OL-SM. Output of the eNB module is per antenna-port (layer) sequences of baseband signals in time domain. Most of the transmitter parameters are implemented and can be configured with little effort.

In addition to the original output, a modification is done to send a replica of output signals with 'genie' flag for the other modules to access a noise-free version of the sent signals.

6.3.2 Constellations: propagation and GSCM

Constellation module implements the definition of $\widehat{\mathbf{C}}$ from Chapter 3. The constellations take the form $\widehat{\mathbf{C}} = \left(\widehat{\boldsymbol{C}}_0, \ldots, \widehat{\boldsymbol{C}}_{M-1}\right)$ for an M-transmitter DL scenario with $\widehat{\boldsymbol{C}}_m, m = 0, 1, \cdots, M-1$ representing the applied 3D power distribution and fading profile of signal transmitted from the m-th transmitting antenna. The structure of $\widehat{\boldsymbol{C}}_m$ following (3.2) contains power distribution of signals over AOAs and their corresponding Path Loss (PL) and fading profile. The AOAs are defined as the spatial location of K test antennas $\Omega_k = (\theta_k, \phi_k), k = 1, 2, \cdots, K$. The length of vector $\widehat{\boldsymbol{C}}_m$ is the number of test antennas. In simulations, for each AOA, two-element vector $\left(c_{\vartheta,k,m}, c_{\varphi,k,m}\right)^\top$ as in (3.2) is given to represent the separate modeling of ϑ and φ polarization.

To summarize, the OTA measurement setup is modeled by $\widehat{\mathbf{C}}$ which has $M \times 2K$ elements covering the mapping from transmitters to test antennas considering both their AOAs and polarization. The data structure in this module in fact disregards the physical locations of test antennas (which limits how many AOAs are considered in this module) and simply consider K as a finite grid on the unit sphere with its resolution identical to what antenna pattern is obtained with. The location of test antennas is only a subset of a larger matrix

and other points can be filled with zero. It may sound unnecessary but it is useful in the next module because the list of AOAs in this case is aligned with the sampling points of the antenna patterns.

Elements in $\widehat{\mathbf{C}}$ are single complex numbers representing PLs and pre-fading is not implemented. Generation of constellations is performed with following considerations.

- Clusters in GSCM are modeled as groups of paths, all the discussion follows is per-path if not stated otherwise.
- Each path has its large-scale PL with random phase. The PL corresponds to the spatial distribution functions of choice e.g. Laplacian distribution (in SCME [116]) in azimuthal plane or wrapped Gaussian distribution (as in WINNER II [117]),
- Each path is mapped to the test antenna corresponding to its AOA, if the AOA is not directly represented by any of the test antennas, it is assign to the nearest test antenna.

Passing M DL signal streams through the constellations would results $2K \times M$ copies of the original signal streams. Instead of convolving constellations with the signal streams in this module, the $2K \times M$ constellation $\widehat{\mathbf{C}}$ and the DL signal streams $\boldsymbol{s}$ are sent directly to the next module.

6.3.3 UE receive antenna

The UE antenna module implements the compound radiation pattern $\mathbf{T}$ described in Section 2.1.1. It has the exact form as (2.1) with Ω defined as the sampling points when pattern is obtained from antenna measurements or as simulation resolution when pattern is obtained by full-wave simulation software. Applying pattern $\mathbf{T}$, constellation $\widehat{\mathbf{C}}$ and signal streams $\boldsymbol{s}$ into (3.8), one can obtain

$$\boldsymbol{r} = \sqrt{\frac{P_{\mathrm{iso}}}{F}}[\mathbf{T}, \widehat{\mathbf{C}}]\boldsymbol{s} + \boldsymbol{r}_{\mathrm{S}} + \boldsymbol{n} \tag{6.1}$$

with receiver noise figure F, self-interference $\boldsymbol{r}_{\mathrm{S}}$ and thermal noise $\boldsymbol{n}$ all modeled as AWGN.

The size of matrix from operation $[\mathbf{T}, \widehat{\mathbf{C}}]$ as given in (3.4) is $N \times M$ because the constellation $\widehat{\mathbf{C}}$ contains $2K \times M$ elements and the radiation pattern of an N-port antenna has $N \times 2K$ elements. The inner product $[\cdot, \cdot]$ requires integral

over the unit sphere $\mathrm{S}_1(0)$. It can be calculated as a summation of K results from all AOAs with weighting factors correspond to the area each point on the grid represents on the unit sphere. Pattern $\mathbf{T}$ contains simple complex values because radiation properties of patterns for narrow band are modeled as flat.

Another point of discussion is how power normalization and AWGN are handled in the modules. An intuitive approach seen in many simulation chain is to normalize power level or noise ground to one and directly use Signal to Noise and Interference Ratio (SNIR) as power indicator. Although SNIR is the performance indicator that the post-processing module can direct utilize, this approach would require all modules to have a reference power level which does not change in the whole simulation chain. Neither signal power level nor total noise power level is suitable to be defined as reference. It is actually more straightforward that all the power levels in the simulation chain correspond to actual power levels that one can observe in the measurements instead of normalized ones. SNIR evaluation can be obtained later. The advantage of this change is that the power levels of noise and signals are uncorrelated and parameter configuration is correspondingly simpler.

As discussed earlier, receiver noise figure F, self-interference $\boldsymbol{r}_{\mathrm{S}}$ and thermal noise $\boldsymbol{n}$ are all modeled as AWGN but they contribute to the total SNIR in a different way. Instead of summing them up to a total noise figure whose correct power level is difficult to determine, thermal noise is added to $\boldsymbol{s}$ and self-interference and receiver noise figure are added to $\boldsymbol{r}$. In application, part of the noise power is added before convolving $[\mathbf{T}, \widehat{\mathbf{C}}]$ with $\boldsymbol{s}$ and the rest after the convolution.

6.3.4 LTE UE receive chain and channel estimation

The LTE UE module is also taken from TU Vienna system link layer LTE simulation chain. It analyzes the received signal vectors $\boldsymbol{r}$ and gives report whether the payload is correctly received. Channel is estimated using reference symbols of the received signals. Multiple estimation methods are implemented e.g. Minimum Mean-Square Error (MMSE) or Least-square (LS) estimation. Hybrid Automatic Repeat Request (HARQ) function can also be activated to have retransmissions. Modifications are of course necessary to make this module to cooperate with the others.

One example of implemented modifications is the “perfect” channel estimation. In the original module, perfect channel estimation is taken directly from channel parameter generation. In this simulation chain, channel matrix

as in (3.7) is both complicated in structure and with unaccounted noise figure if directly used. Direct use of existing estimation method e.g. MMSE would introduce another layer of uncertainty because the performance of estimator may be different in low SNIR and high SNIR scenarios. A method is introduced for the receiver estimator to make similar estimation for all SNIR level. The method utilizes the 'genie' replica of the M DL signal streams which is introduced in the eNB module. The replica is processed through the simulation chain by the exact procedures as the original transmitted signal streams except noise which is not applied. Received by the UE module, the replica represents a copy of the original signal through identical channel but noise-free. Using the reference symbols from the replica, one can ensure the estimator to make similar level of channel estimation for all possible noise levels.

6.3.5 SNR evaluation

The UE module is already able to provide report for many important signal quality indications including SNR, BER and BLER. However, to reach this stage of report, one would need to pass the received signal through the digital decoder which is time-consuming. A shortcut is to quickly obtain equivalent SNR information before the decoder by evaluating Error Vector Magnitude (EVM) of each received signal stream. It is again realized by comparing noise-free 'genie' replica of the signal streams to the ones with noise. Since all power levels in all modules reflects the actual levels in the measurements, the power of the 'genie' replica gives exactly the received power level of the transmitted signal vectors. The sum of squared magnitude of difference between noisy and noise-free versions of signals gives the noise power.

BLER can also be quickly evaluated in the early stage of decoding by extracting the internal report of HARQ. Once the correctness of payload is decided, later stages of decoder can be skipped. To reach a trustworthy BLER, one needs to have many frames transmitted until the statistics converge.

6.3.6 Result post-processing

Post-processing module delivers FOM from signal quality indications e.g. SNR, BER or BLER. It also takes consideration of transmission mode, MCS etc. to correctly generate result corresponding to what one would observe in real measurements. The algorithm of calculating throughput is based on counting retransmissions according to [118, G.2]. Throughput can calculated from frame

length L_{frame}, number of successfully transmitted frames N_{ACK}, modulation index I_{mod} (with 2 for QPSK, 4 for 16QAM and 6 for 64QAM), coding rate R_c and total time period of transmission by

$$\text{Throughput} = \frac{L_{\text{frame}} \times N_{\text{ACK}} \times I_{mod} \times R_c}{\text{Time}}. \tag{6.2}$$

To reduce simulation time, a much simplified approach can be used. Throughput is estimated based on observed per spatial stream SNR (calculated from EVM) before decoding. A continuous interpolation of the throughput over SNR relationship provided in [21, A.2] is used.

6.4 Simulation setups and results compilation

This section contains a collection of simulation results [8, 101, 109, 111, 115]. The subsections give comparison of simulation results focus on different aspect of the measurements to provide insight on how actual measurement should be constructed.

Four patterns are used in simulations in this section. Two canonical example and two realistic patterns are given in Fig. 6.2.

(a) A canonical collinear dipole arrangement with half wavelength distance. This example has two dipoles with canonical "donut" pattern in ϑ polarization and the half wavelength separation between the dipoles provides orthogonality in phase.

(b) A fictitious terminal with cross-polarized dipoles (ϑ and φ). This pattern is referred as the optimal antenna setup for the receiver because two dipoles in this case are orthogonal in polarization. One can expect it to have good performance because cross-polarized antennas are commonly used in BSs.

(c) A laptop with data-card featuring a realistic two-antenna pattern in cellular low band. The weird appearance is typical for this kind of devices because of the influence from the laptop. The compound pattern is to some extent pattern selective and polarization selective.

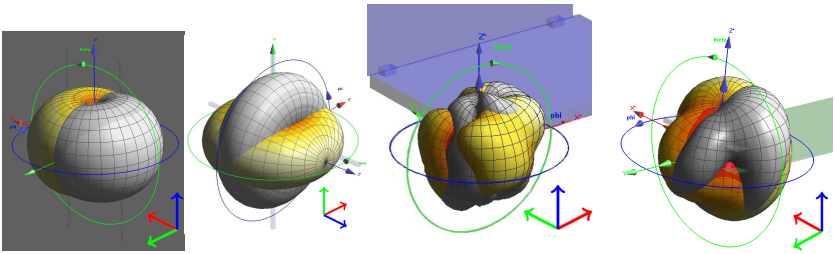

(a) (b) (c) (d)

Figure 6.2: Compound antenna patterns used in the simulations: (a) canonical collinear dipoles, (b) cross-polarized dipoles, (c) a realistic datacard pattern in cellular low band and (d) a good dual-PIFA headset for E-UTRA band class 2. All patterns are simulated by SEMCAD software.

(d) A dual-PIFA headset design for Evolved Universal Terrestrial Radio Access (E-UTRA) band class 2 (PCS band at 1.9 GHz). This is a well performed headset design with symmetric antenna.

The patterns are obtained by full-wave simulation and under the assumption of lossless structures. The coloured and gray scale portions in the figures correspond to the magnitude of two different patterns of the antenna. Red, green and blue axes represent X, Y and Z-axis respectively. Phase and polarization is not presented in the picture but all antennas are properly matched (with low CECC) and with maximum efficiency they can have.

6.4.1 On choice of constellations and MIMO modes

The first comparison focuses on how the choice of constellations and MIMO mode affects the measurement results. The results are obtained during the development phase of the simulation chain [8, 115]. Three simplified test setups are compared.

The two patterns in Fig. 6.2, the cross dipoles (b) and datacard (c), are chosen to investigate the difference in result caused by choice of constellations. TD mode and OL-SM are investigated in a 2×2 MIMO configuration for 5 MHz bandwidth with signal power equally distributed on two spatial streams. Static

channels with AWGN are considered with HARQ switched off. Total noise power corresponds to an SNR of $6.7\,\mathrm{dB}$, which is the boundary between MCS-7 (Quaternary Phase-Shift Keying (QPSK) with coding rate $4/5$) and MCS-8 (16 Quadrature Amplitude Modulation (QAM) with coding rate $1/2$) of LTE. Noise power is applied as receiver noise figure after the signal streams are convolved with channel matrix. In each simulation run a long single sub-frame with QPSK is transmitted which is sufficient to obtain a stable EVM estimate. Throughput is approximated by 0.75 of channel capacity. It is equivalent to a perfect MCS adaptation.

- **Constellation set 1a: Single Dual-Polarized Probe / Full Sphere.** This constellation set is taken from Subsection 5.2.2. It mimics LOS conditions and corresponds to a test setup with a single dual-polarized probe where the DUT is rotated about two axes the same way as in a conventional CTIA SISO OTA TIS measurement. For TD mode this setup is actually a generalization of TIS measurement to MIMO-enabled UE since application of the Alamouti scheme is equivalent at the UE side to MRC [22, 23, 108]. Angular resolution is 5° in θ and ϕ.

- **Constellation set 1b: Single Dual-Polarized Probe / Azimuthal Plane.** With almost identical configuration to Constellation 1a, this set of constellation limits itself in the azimuthal plane. Results for a simulation in the azimuthal plane only are given for comparison to investigate the difference between 2D and 3D measurements.

- **Constellation set 2: Two Test Antennas / Azimuthal Plane.** This constellation set considers two incoming paths with different AOA in the azimuthal plane. All possible (relative) positions of the two test antennas over a circle enclosing the DUT in the azimuthal plane are sampled with a resolution of 5°. All possible combinations of polarizations i.e. (ϑ, φ), (ϑ, ϑ), (φ, φ) and (φ, ϑ) are included in the simulation. This corresponds to a test setup with one fixed and one moveable test antenna in azimuthal plane.

- **Constellation set 3: 8 Probes / Angular Spread.** Following the approach taken in several proposals for OTA testing as described in Subsection 4.1.1, this constellation set applies incoming clusters with Laplacian distribution in azimuthal plane corresponding to an AS of 35°. The angular spread is "synthesized" by distributing power over 8 probes which

are equally spaced with 45° separation along a circle enclosing the DUT in azimuthal plane. The clusters are superimposed at the DUT. In this simulation experiment the two streams are mapped to vertical and horizontal polarization respectively and follows the description of the setup (4.5) in Subsection 4.1.1.

TD Results of cross-polarized dipoles in Fig. 6.2b Fig. 6.3 denotes the CCDF of throughput for the cross-polarized dipoles (pattern Fig. 6.2b) in TD mode assuming a perfect SNR to throughput mapping. Constellation set 1a (1 dual-polarized test antenna in full sphere) gives the antenna system efficiency measurement as discussed in Subsection 3.3.2. To save simulation time, throughput is used instead of sensitivity which is proposed in Section 5.2.2 is because the latter would require many sub-frames transmitted in order to reach target BLER level. Throughput which is proportional to capacity is sufficient to indicate the efficiency difference between DUTs. As for the statistical metrics, CCDF of throughput is used instead of CDF of sensitivity.

To the 2D vs. 3D comparison, constellation set 1b (1 dual-polarized test antenna in the azimuthal plane) does not provide significantly different result comparing to set 1a. This is because one of the cross-polarized dipoles in the simulations is positioned along the Z-axis. In constellation set 1b, ϑ polarization is well covered by this dipole in the azimuthal plane. According to what is described in Subsection 3.3.2, good throughput result is expected in TD mode.

Results from two multi-cluster simulations i.e. constellation set 2 and 3 are also similar. The introduction of AS emulation in the simulations does not introduce much difference to the simulation results for canonical models like cross-polarized dipoles. Comparing between two pairs of simulations (sets 1a and 1b which use single probe and sets 2 and 3 which use multiple probes), one could easily distinguish diversity gain provided by multiple spatial streams.

OL-SM Results of cross-polarized dipoles in Fig. 6.2b The difference between results becomes more significant when one forces to use OL-SM transmission mode in the simulations as presented in Fig 6.4. Fixing on OL-SM mode is not realistic in-the-field because when channel rank is low, eNB should switch to TD to maintain connection quality. This can be confirmed when one compare Fig. 6.3 and Fig. 6.4. Although the latter enables higher throughput in more than 50% of cases in all constellations applied, it also gives sometimes low throughput even no connection at all. Nevertheless, it is worthwhile to see what knowledge we could gain from this simulation.

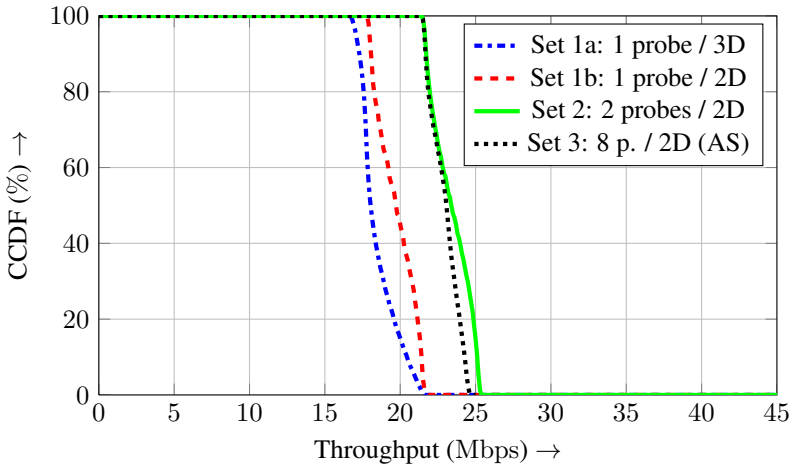

Figure 6.3: The throughput CCDF of the pattern cross-polarized dipoles (pattern Fig. 6.2b) in TD mode for different constellation sets.

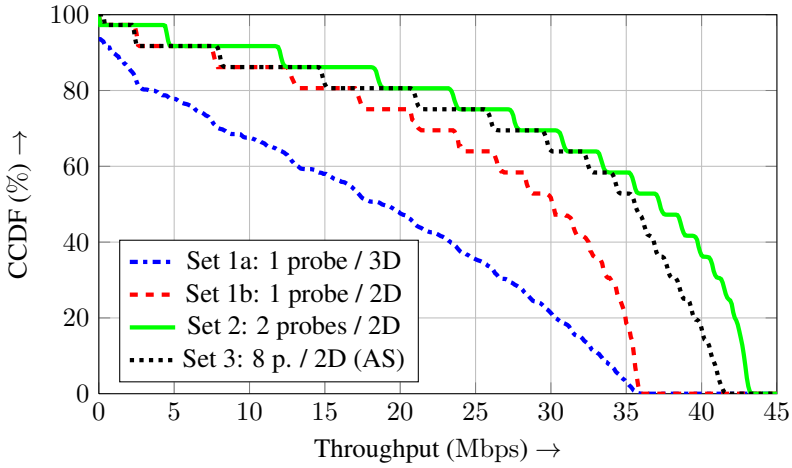

Figure 6.4: The throughput CCDF of the pattern cross-polarized dipoles (pattern Fig. 6.2b) in OL-SM mode for different constellation sets.

The two multi-cluster simulations i.e. constellation set 2 and 3 (green and black repectively) still have similar results in Fig. 6.4 confirming what we have observed in Fig. 6.3 thus AS emulation does not convey additional information. The curves representing constellation sets 1a and 1b as given in blue and red in Fig. 6.4 however, are significantly different to each other unlike Fig. 6.3 in which they are similar. As we are still confident that set 1a gives a complete antenna efficiency evaluation, the cause of this difference has to be the choice of constellations. Similar to what is stated for the TD mode, with constellation set 1b applied on cross-polarized dipoles, ϑ polarization is always well covered by one of the two dipoles. Throughput in OL-SM mode only depends on the φ polarization of the other dipole. Constellation set 1a, which contains constellations in 3D, has more chances of having low throughput because both polarizations can meet the troughs on the patterns. Limiting constellations in azimuthal plane as in set 1b is falsely suitable for cross-polarized dipoles and gives higher throughput results than it should.

The stepped behaviour of the curves in Fig. 6.4 is caused by insufficient angular sampling resolution in simulations using canonical patterns. The symmetry of canonical patterns and precise angular sampling in full-wave simulation software gives limited choice of outcome. This behaviour is expected to disappear when a realistic pattern is used in the simulations or in the measurements when positions of test antenna are not as precise.

TD Results of data-card patterns in Fig. 6.2c For a more realistic pattern like the datacard given in Fig. 6.2c, the same comparison between constellation sets is made for both TD (Fig. 6.5) and OL-SM mode (Fig. 6.6). The observation that CCDFs curves in Fig. 6.5 are not as steep as the curves of cross-polarized dipoles suggests the patterns of data-card are not as rounded as a canonical dipole. In Fig. 6.5, the largest difference is between the simulation results of constellation sets 2 and 3. The AS emulation in constellation set 3 may have "smeared" the the peaks and troughs in the pattern causing a steeper CCDF curve with lower average throughput. It is also worth noticing that the CCDF curve representing results using constellation 1b in Fig. 6.5 has distinct shape which is against theoretical expectation. It comes from the insufficiently chosen constellations in the set.

OL-SM Results of data-card patterns in Fig. 6.2c In OL-SM mode, trends observed in Fig. 6.6 are similar to what is observed in TD mode (in Fig. 6.5). The curves in Fig. 6.6 are mostly smooth comparing to what are presented in

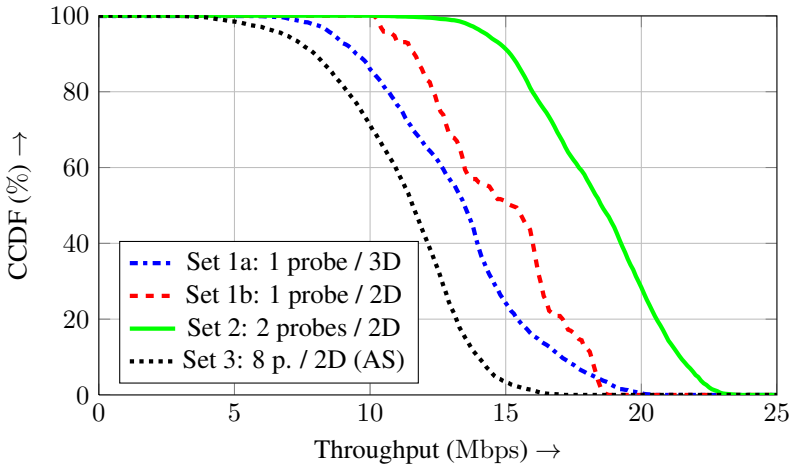

Figure 6.5: The throughput CCDF of a data-card in laptop (pattern Fig. 6.2c) in TD mode for different constellation sets.

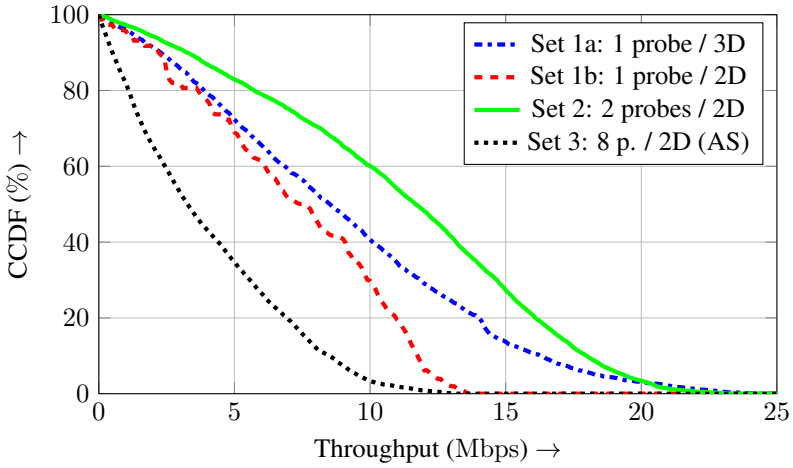

Figure 6.6: The throughput CCDF of a data-card in laptop (pattern in Fig. 6.2c) in OL-SM mode for different constellation sets.

Fig. 6.4 indicating this level of resolution is sufficient for realistic patterns. The AS emulation in constellation set 3 has heavier impact to throughput distribution even than in TD mode and the throughput in OL-SM mode is most probably always lower than in TD mode. If the DUT is placed in-the-field, it would continuously report low rank and keep TD mode in most of the cases. Making measurement with complex channel effect but lacking mode switching does not provide a fair quantification of device performance.

Observations and conclusions from this simulation What are observed or can be concluded from this simulation are following points:

- Choice of constellation gives significantly different results.
- Economization of constellation to 2D (comparing sets 1a and 1b) would ends with grossly misleading results.
- To observe the benefit of introducing MIMO e.g. diversity gain, OTA setup has to include multiple spatial streams from different AOAs (comparing set 1a with set 2 and 3).
- Application of fading channel (comparing sets 2 and 3) is only meaningful with MIMO mode adaptation.

6.4.2 On device discrimination

Another simulation comparison is provided to see how measurement is able to discriminate devices [111]. Two constellation sets are investigated.

First constellation set is the same one labeled as constellation set 1a in the last subsection. It mimics LOS conditions and corresponds to a test setup discussed in Subsection 5.2.2. This constellation represents an OTA setup where a single dual-polarized test antenna and the DUT is rotated about two axes the same way as in a conventional TIS measurement according to CTIA SISO OTA test plan. The transmission mode used is TD.

The second constellation set is configured to simulate two clusters of incoming plane waves with details as below:

- Two clusters are simulated with one vertically polarized, one horizontally polarized.
- 24 dual-polarized probes in the azimuthal plane with uniform spacing of 15°.

- Each cluster is individually mapped to the 24 probes according to a wrapped Gaussian distribution (as in WINNER II model [117]) with variance of 10°.
- All possible combination of cluster center-positions over a 5° spaced set of sampling angles in the azimuthal plane are taken into account.
- Transmission mode is set to OL-SM mode with perfect adaptation to TD.

The simulations are similarly configured as the last subsection. For both TD and OL-SM mode, signal power is equally distributed on two spatial streams. Static channels with AWGN are considered with HARQ switched off. Total noise power corresponds to an SNR of $6.7\,\mathrm{dB}$, which is the boundary between MCS-7 (QPSK with coding rate $4/5$) and MCS-8 (16QAM with coding rate $1/2$) of LTE. For each constellation an AWGN channel with half of the noise power treated as correlated (applied to the DL signal vectors $\boldsymbol{s}$) and the other half as uncorrelated noise (as receiver noise figure) is simulated. In each simulation run a long single sub-frame with QPSK is transmitted which is sufficient to obtain a stable EVM estimate. Throughput is approximated by 0.75 of channel capacity. It is equivalent to a perfect MCS adaptation.

Results for four different pattern examples in two different constellation sets The TD throughput CCDF curves of all 4 patterns with first constellation set are given in Fig. 6.7 provides very obvious insight on antenna system efficiency. With similar reasoning as given in the last subsection, throughput CCDF is used as FOM instead of sensitivity CDF to save simulation time. The FOM is nevertheless proportional to channel capacity because perfect MCS adaptation is used. Three out of four (namely, Fig. 6.2a,b,d) has very similar throughput average although the curves differ depending on the shape of the pattern. The datacard pattern suffers at the efficiency because of its low working frequency and limited physical size, and it is clearly seen in the figure. The collinear dipole arrangement (Fig. 6.2a) which has only a single polarization has its high efficiency correctly appreciated.

The OL-SM throughput CCDF statistics with optimal fallback to TD mode for all four examples using second constellation set are given in Fig. 6.8. The cross-polarized dipole arrangement (Fig. 6.2b) yields the best result in connection with the two orthogonally polarized clusters. The laptop / data-card example (cellular low band) shows the worst performance. The handset antenna (in horizontal orientation) which is designed for the PCS band performs

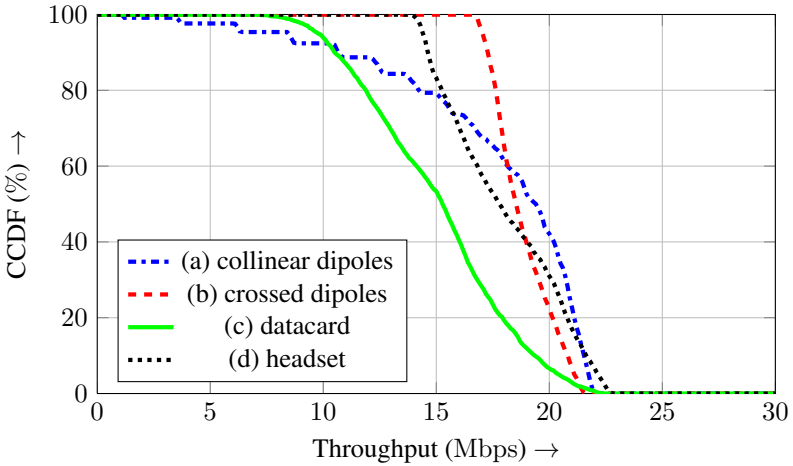

Figure 6.7: The TD throughput CCDF of all 4 patterns in Fig. 6.2 with first constellation set.

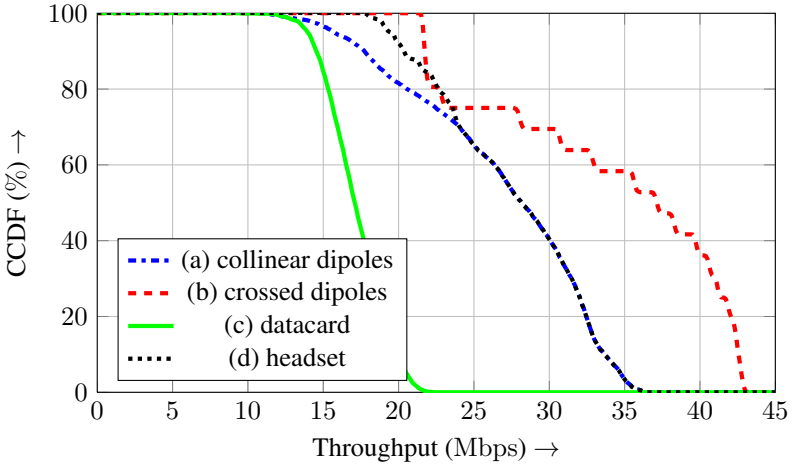

Figure 6.8: The OL-SM throughput CCDF of all 4 patterns in Fig. 6.2 with second constellation set and optimal MIMO modes adaptation (OL-SM and TD).

similarly to collinear dipoles in OL-SM case but its polarization diversity gives better lower-bound of throughput in TD mode hence it achieves overall better results than collinear dipole arrangement. The higher operating frequency and larger real-estate obviously permits the headset to have a better design than the data-card.

Conclusions Measurement in TD mode as proposed in Section 5.2 fulfill its promise of distinguish devices with different antenna efficiency. It does not have preferences in antenna design and is able to discriminate devices purely based on their efficiency. Statistical metrics provide much more insight on antenna properties than averaged metric. Even within devices with comparable efficiency performance, statistical metrics is able to distinguish them in sense of their diversity performance and roundness of their polarimetric patterns.

6.4.3 On choice of SNR with FRC in measurements

The above simulations obviously take for granted that SNR to throughput mapping is perfect. However, as discussed in Subsection 4.2.6, adaptive mode switching does not exist in practice. The adaptation behaviour of eNB is not and will not be standardized. Introducing real-life-like scheduling behaviour in the measurements does not necessarily provide more representative results. Instead, measurements are conducted in FRC with fixed MCS and transmission mode.

Within each FRC, only limited range of SNR can generate meaningful measurement results. When SNR is too high, in the field, the UE would request the eNB to increase the MCS-level (CQI in LTE) for higher throughput. But in FRC, this request is discarded and UE can only maintain the maximum throughput of the current MCS and it's performance is unappreciated. Conversely when SNR is too low for the signal quality to be sustainable, UE may request a decrease of MCS in order to have a lower but stable connection. In FRC, this situation can lead to a disconnection. Through simulations, it is possible to illustrate the importance of choosing correct SNR in FRC [109].

This simulation uses the datacard pattern of Fig. 6.2c. The FRC is a fixed 2×2 OL-SM mode and signal power is equally distributed on two spatial streams. The constellations involves two test antennas as shown in Fig. 5.2 in Subsection 5.3.2 with Ω_i and Ω_j independently taken from a uniform grid on the unit sphere with 15° resolution. The set of constellations $\mathcal{C}$ comprises all unique combinations of polarizations, i.e. (ϑ, φ), (ϑ, ϑ), (φ, φ) and (φ, ϑ). In

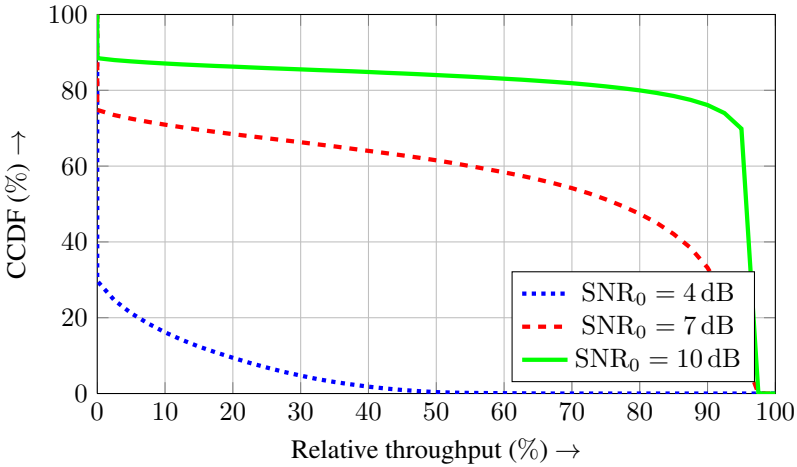

Figure 6.9: Simulated throughput statistics for a 2-antenna LTE datacard in a laptop (Fig. 6.2c) in OL-SM mode with FRC using two dual-polarized test antennas. Results are given for 3 different power levels corresponding to the indicated values of SNR_0.

total, 174724 constellations are present in the set. For each constellation an AWGN channel with half of the noise power treated as correlated (applied to the DL signal vectors $\boldsymbol{s}$) and the other half as uncorrelated noise (as receiver noise figure) is simulated. Three different signal power levels are investigated which correspond to

$$\mathrm{SNR}_0 = \frac{P_{\mathrm{iso}}}{P_{\mathrm{N},0} F} \in \{4\,\mathrm{dB}, 7\,\mathrm{dB}, 10\,\mathrm{dB}\}, \tag{6.3}$$

respectively.

Based on the results in Fig. 6.6, MCS-5 is selected, i.e. QPSK with coding rate of $1/2$. The maximum number of HARQ transmissions is set to 4. The DL channel bandwidth is 5 MHz (25 Resource Blocks (RBs)). To save simulation time in this more qualitative investigation, received signals are captured after the Zero Forcing (ZF) receiver to estimate throughput for the selected MCS based on EVM.

The SNR to throughput mapping is modeled as a step function, when actual

SNR is higher than the threshold of MCS-5, full throughput is recorded. Otherwise, zero throughput is recorded. With higher SNR, the throughput would not increase beyond the maximum throughput of the MCS, mimicking measurement behaviour in FRC. The use of HARQ effectively smooth the results because successful retransmissions would provide intermediate throughput results between 0% and 100%. The CCDF curves of estimated throughput for the three investigated values of SNR_0 are given in Fig. 6.9. The throughput observed for each constellation is weighted with the relative fraction of the surface of the unit sphere it represents, i.e. the data reflect a two-path uniform PAS.

This simulation confirms that for measurements in FRCs, SNR has to be carefully selected. Lets assume that $\mathrm{SNR}_0 = 7\,\mathrm{dB}$ is in fact an appropriate value in this setup. Decrease the SNR_0 by $3\,\mathrm{dB}$, the DUT obviously cannot sustain the transmission with the defined MCS, reporting 70% of time disconnection. An increase of $3\,\mathrm{dB}$ would push the DUT to a very high throughput which is sustainable for at least 70% of the constellations. Any implementation of fading in this scenario would easily introduce a variance to SNR larger than $3\,\mathrm{dB}$. Measurement result in FRC with fading does not depend on the DUT but mostly the fading profile.

6.4.4 On economization of constellations

Another question remains, how many constellations are actually required to sufficiently characterize a device. The question has been addressed by using the simulation results from the last subsection and a convergence test is presented [101]. CCDFs of estimated throughput for $\mathrm{SNR}_0 = 7\,\mathrm{dB}$ for different numbers of randomly selected constellations are given in Fig. 6.10. It is observed that a level of hundreds of constellations is already sufficient for convergence of the CCDF even for a complicated pattern as Fig. 6.2c.

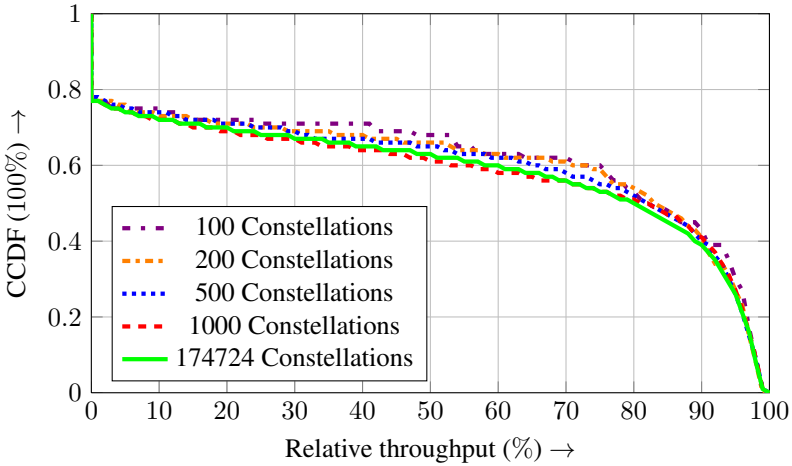

Figure 6.10: Simulated throughput statistics for a 2-antenna LTE datacard in a laptop (Fig. 6.2c) in OL-SM mode with FRC using two dual-polarized test antennas. CCDFs of estimated throughput are presented for $\mathrm{SNR}_0 = 7\,\mathrm{dB}$ for different numbers of randomly selected constellations.

7 Measurements

Detailed description of measurement setups and corresponding results from two rounds of measurements are presented in this chapter. First round of measurements has been conducted in August 2010 in participation of COST2100 round-robin measurement campaign in cooperation with Agilent Technologies and CETECOM GmbH [26, 30]. The measurement setup was based on a combined-axis anechoic chamber in the lab of Hochschule RheinMain. Second round of measurements has been conducted in September 2011 at the site of CETECOM GmbH in Essen [102, 119]. A CTIA certified distributed-axis anechoic chamber was used in the second round.

7.1 COST 2100 round-robin measurement campaign

7.1.1 Measurement setup

The chamber used in the participation of COST2100 Round-Robin measurement campaign 2010 is a standard combined-axis chamber located in the lab of Hochschule RheinMain. A fixed Quad-Ridged Horn antenna is the main test antenna. It is placed at one side of an anechoic chamber close to the wall as presented on the right in Fig. 7.1. A two-axis positioner is placed at the opposite side of the chamber as given on the left in Fig. 7.1. The test antenna and the positioner are in a line which is parallel to the longest axis of the chamber.

A distance of $1955\,\mathrm{mm}$ is measured between the reference plane of the test antenna and the rotation center of the positioner. The positioner has two rotation axes. One axis is a platform which is capable of rotating 360° around the Z-axis. When a DUT is mounted on the arm of the positioner, it provides another 360° vertical rotation. In practice, it is not necessary for both the platform and the arm to rotate a full circle. A half circle of the platform, together with full rotation range of the arm of the positioner, is sufficient to access all possible AOAs.

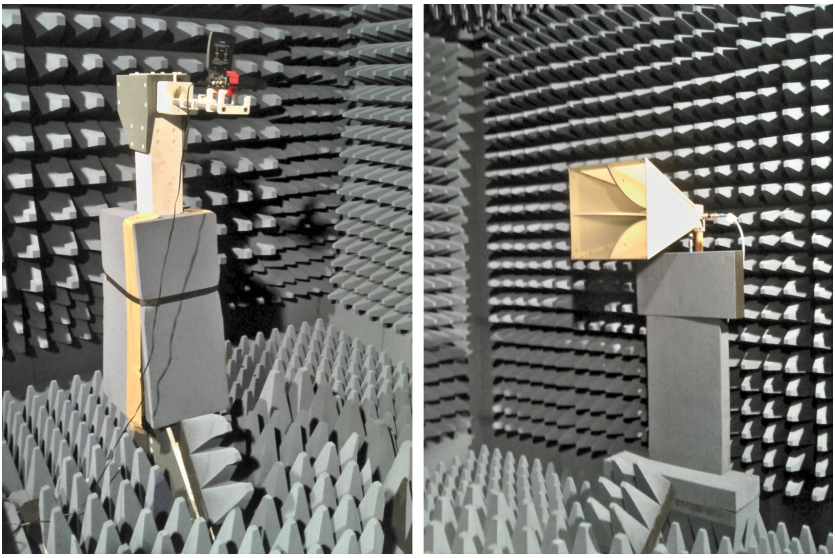

Figure 7.1: The original state of the combined-axis chamber in Hochschule RheinMain with the two-axis positioner on the left and quad-ridged horn antenna as test antenna on the right.

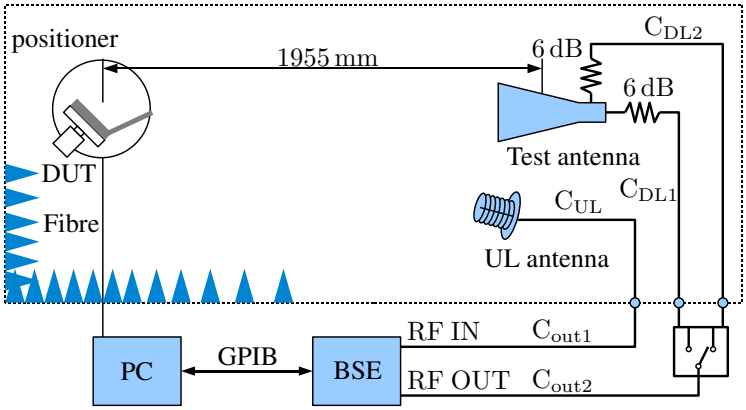

Figure 7.2: Combined-Axis anechoic chamber for SISO OTA measurements schematic, viewed from the Top. Sensitivity measurement for one polarization at a time.

Fig. 7.2 gives a schematic of the anechoic chamber. Two ports of the dual-polarized test antenna representing two polarizations are connected to two ports at the external panel of the chamber. The output signal from BSE is routed to one of the ports. An Agilent 8960 wireless communication tester is used as the BSE. A PC is used to control the positioner and to communicate with the BSE. A circularly polarized helix antenna is placed at the corner of the chamber as the uplink antenna. The uplink antenna is connected to the input port of the BSE. Manually disconnecting and connecting cables to one of two ports at the external panel of the chamber gives access to two polarizations of the test antenna in order to measure two polarizations separately.

Anechoic chamber with single test antenna

In this round of measurements, only High-Speed Packet Access (HSPA) devices with RD support were available. The BSE i.e. Agilent 8960 used in the measurements did not support MIMO modes as well. To measure devices with RD, slight modification was implemented to route one DL stream to two polarizations of the test antenna using a two-port fading emulator. In Fig. 7.3,

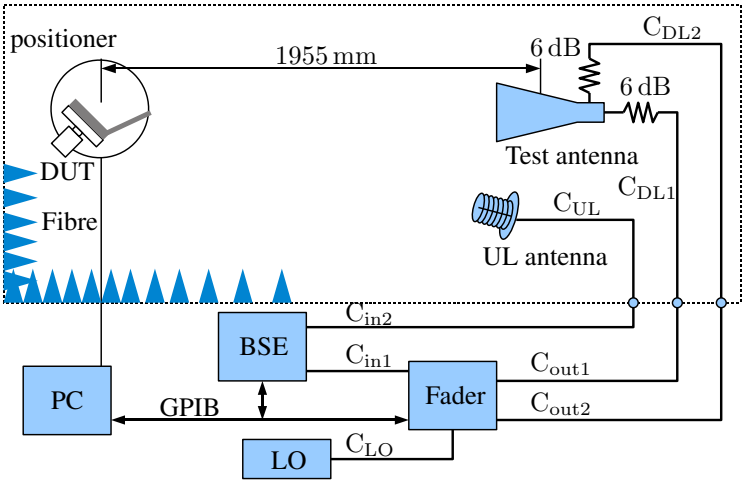

Figure 7.3: Combined-axis anechoic chamber with modification for sensitivity measurements to devices with receive diversity support, schematic viewed from the top. Sensitivity measurement uses both polarizations simultaneously, and is similar to the approach in [23].

an Elektrobit PropSim C2 fading emulator was used to divide the power of a DL signal stream from the output port of BSE to the two ports representing two polarizations of the test antenna. In this case, signals routed to vertical and horizontal polarization must be decorrelated. Ideally, application of a sequence of quasi-random phase shifts would be sufficient. Alternatively, small, opposite Doppler shifts were applied on both polarizations using the fading emulator.

Adding a fading emulator into the setup requires the control over DL power transferred from the BSE to the fading emulator. In this configuration, the BSE has constant output power level. Controlling software was modified to control output power level of the fading emulator via GPIB interface. A signal generator was used to serve as the Local Oscillator (LO) of the fading emulator.

Anechoic chamber with multiple test antennas

To conceptually verify the test setup meant for MIMO peak throughput measurement as described in Subsection 5.3.2, a second test antenna (a single po-

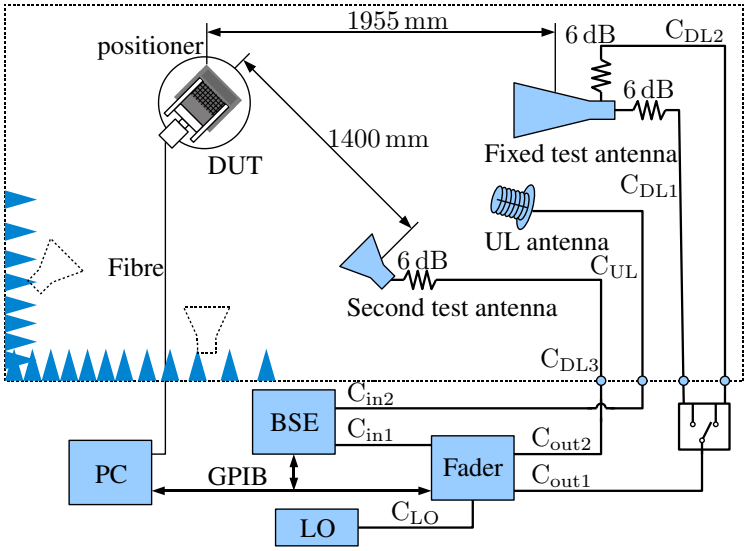

Figure 7.4: Schematic for an azimuthal two-test-antenna setup, view from the top.

larized horn antenna) was added into the chamber. Due to the limited physical size of the chamber, the second test antenna was mounted on one of the three positions, corresponding to $\Delta\phi = 45°$, $\Delta\phi = 90°$ and $\Delta\phi = 135°$ respectively in azimuthal plane as illustrated in Fig. 7.4. Although the second test antenna is not dual-polarized, by manually adjusting its polarization, the setup is capable of realizing all possible combinations of polarizations. The distance between the reference plane of the second test antenna to the rotation center of the positioner is $1400\,\mathrm{mm}$.

For future modification, one could replace the two-axis positioner by a three-axis one. This would allow four degrees of movement freedom which is a possible implementation of two independent AOAs. In this setup, a limited constellation set is chosen to accommodate the existing two-axis positioner.

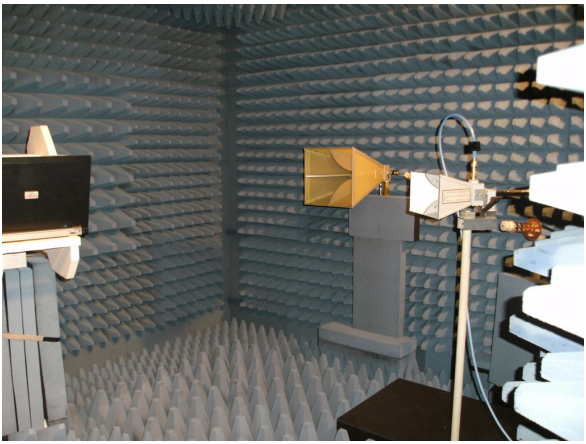

Figure 7.5: The combined-axis chamber with second test antenna placed in the azimuthal plane.

7.1.2 Calibration

Cable calibration

Most of the cables in the setup were measured first using a VNA (Rohde&Schwarz ZVB 20) from 10 MHz to 20 GHz with a resolution of 1 MHz and bandwidth of 10 kHz. The cable losses at the measurement working frequency (DL @ 2.1124 GHz) are shown in Table 7.1.

The other two cables, namely C_{DL1} and C_{DL2} are fixed in the chamber.

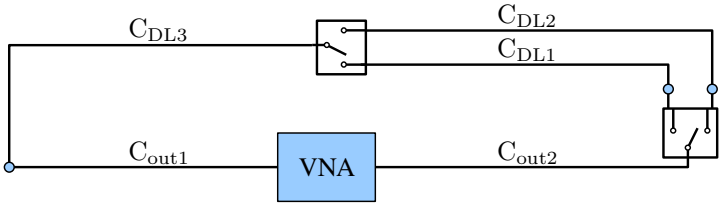

Figure 7.6: Calibration setup for cable C_{DL1} and C_{DL2}.

Cable Name	Cable loss @ 2.1124 GHz (dB)
C_{LO}	0.5
C_{in1}	1.0
C_{in2}	1.6
C_{UL}	2.4
C_{out1}	1.3
C_{out2}	1.0
C_{DL3}	2.2

Table 7.1: Cable calibration: cables directly measured by a VNA.

Cable Name	Cable loss @ 2.1124 GHz (dB)
C_{DL1}	1.8
C_{DL2}	2.0

Table 7.2: Cable calibration: cables measured in conjunction with other cables using a VNA.

They can only be measured in conjunction with other cables in a setup shown in Fig. 7.6. Together with other factors which cause attenuation (ports of the chamber, adapters), two cables were calibrated with results presented in Table 7.2.

Path loss calibration

After cable calibration, the OTA measurement setup has to be calibrated. A single link OTA calibration was performed as shown in Fig. 7.7. It was a complete-link check including Free Space Loss (FSL), cable calibration, reference data of the test antennas etc. The results were in agreement with the expected PL with error within the tolerance of 1 dB.

Similar to what is stated in Subsection 4.1.1, with multiple test antennas in the chamber, it is necessary that all paths to have the same PLs. To verify that the PLs of the two test antennas (as seen by the DUT) is the same, a calibration setup after Fig. 7.8 was used. For the vertical polarization, a dipole was mounted vertically on the positioner. For both test antennas, the platform of the positioner was rotated to assure the dipole is facing the test antenna when measuring each path. When the second test antenna is mounted at different

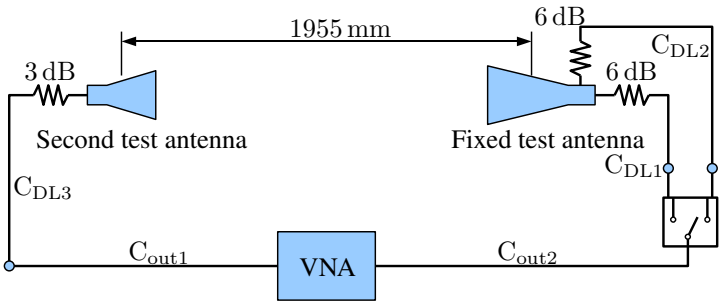

Figure 7.7: Single link calibration setup for the fixed test antenna and PL model using the second test antenna.

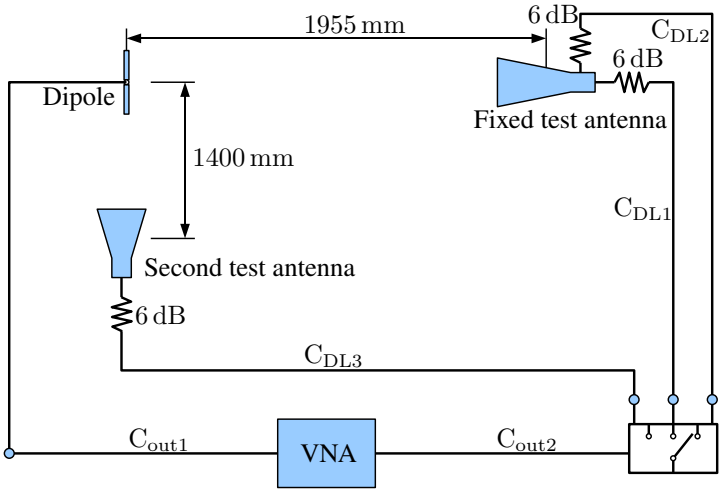

Figure 7.8: Joint verification setup for multiple test antennas using a reference dipole.

Test antenna	FSL	Cables	Gain (dB)	Atten.	Est. PL
Fixed, ϑ	44.8 dB	3.3 dB	12.9 @ 2.12 GHz	6 dB	41.2 dB
Second, ϑ	41.9 dB	3.2 dB	10.4 @ 2.10 GHz	6 dB	40.7 dB
Fixed, φ	44.8 dB	3.1 dB	12.8 @ 2.12 GHz	6 dB	41.1 dB
Second, φ	41.9 dB	3.2 dB	10.4 @ 2.10 GHz	6 dB	40.7 dB

Table 7.3: Estimated total PL, all units in (dB).

Test antenna / Polarization	Corrected PL @ 2.1124 GHz
Fixed test antenna, ϑ	41.3 dB
Second test antenna, ϑ	41.3 dB
Fixed test antenna, φ	40.5 dB
Second test antenna, φ	40.9 dB
On average	41.0 dB

Table 7.4: Measured total PL (corrected).

locations, the platform is also turned to match the angle. The same procedure was also done for the horizontal polarization with dipole mounted horizontally.

A 1 dB to 2 dB difference was observed between the polarizations using the dipole. This was, however, not the case when the horn antenna was used instead of dipole in a follow-up verification. This difference was believed due to the unshielded cables connected to the dipole. Since these cables were not used in the actual measurements, it was concluded that the error in this setup is still within the range of 1 dB.

An estimation of total PL from the BSE (or the fading emulator in the setup with two test antennas) to the DUT is presented in Table 7.3. The measured PL values with corrections are presented in Table 7.4. The average value in Table 7.4 was applied on equipment assuming this approximation was sufficiently accurate in all cases.

Equipment calibration

To calibrate the power readings on the BSE, a spectrum analyzer was connected to the output of the BSE. From a high power level setting to a low power level setting, the values given by both equipment were recorded for every 3 dB. The deviations were in all cases less than 0.35 dB, suggesting a good linear relation

Equipment Name	Function
Agilent 8960 Wireless Communication Test Set	BSE
Electrobit PropSim C2	Signal Fading Emulator
Rohde & Schwarz SMIQ	Signal Generator
Rohde & Schwarz FSP	Spectrum Analyzer

Table 7.5: List of equipment used in the measurements.

between output power level and on-screen power readings of the BSE.

Similar calibration was done for the fading emulator. The BSE in this case was set to a fixed power level. Three different scenarios in the fading emulator were tested: bypass mode (to check the linearity of the output power level with respect to the power settings of equipment), a simple channel model with small Doppler shift and a fading channel model. Two latter cases were used in the measurements. Multiple gain settings in the fading emulator were tested, the results indicates good linearity between the gain setting and measured output power level of the fading emulator. A constant difference of $0.5\,\mathrm{dB}$ was observed and recorded as a correction value for later processes.

7.1.3 Devices under test

Three DUTs with support of HSPA were tested in this round of measurements.

1. DUT1: a Vodafone / Huawei K4505 USB dongle with single internal PIFA antenna. A port was provided for attachment of an external antenna (not available in the time-frame of the measurement).

2. DUT2: a Nokia CS-15 USB dongle with two built-in antennas for the purpose of receive diversity.

3. DUT3: a Dell Latitude E6400 laptop with 2 built-in antennas located at the top of the lid. A HSPA modem in the form of mini-PCIE card was attached on the motherboard of the laptop.

The DUT3 was also used as the host when testing DUT1 and DUT2 with these USB dongles inserted into the same USB port at the LHS of the laptop. The definition of device coordinates is shown in Fig. 7.9.

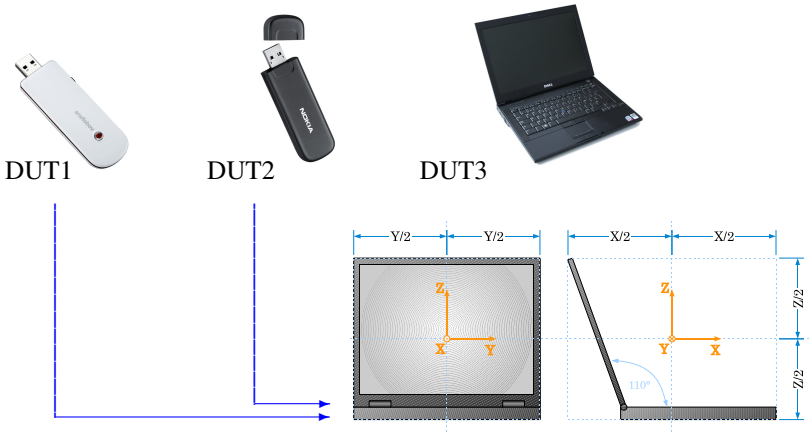

Figure 7.9: DUTs tested in the COST2100 round-robin measurement campaign – DUT1: Vodafone / Huawei K4505; DUT2: Nokia CS-15 and DUT3: Dell Latitude E6400. DUT3 was also used as host when testing DUT1 and DUT2. The dongles were inserted into a USB port at left side of the laptop.

- The X axis is in the azimuthal plane, pointing from the geometric center to the front (towards user).
- The Y axis is in the azimuthal plane, pointing from the geometric center to the RHS of the user.
- The Z axis is orthogonal to the azimuthal plane, pointing upwards.

The center of rotation is the geometric center of the laptop with it's lid opened at $110°$. These definitions are in line with the CTIA definitions [2].

The same definition of coordinate was also applied when testing USB dongles, namely DUT1 and DUT2. The original round-robin test plan suggested to keep the lid closed during the measurements. It was later decided after discussion that to properly test a USB dongle, it is necessary to keep the lid of the host laptop open. It is because when a USB dongle is attached to a laptop, it radiates through current excited on the chassis of the laptop. If the lid is closed, the response to vertical polarization would deteriorate. Keep the lid open when

measuring the laptop but closed when measuring the dongles would also be inappropriate for results comparison.

USB dongles were inserted into the front-most USB port at the LHS of the laptop. The geometric center of USB dongle with laptop was set to the geometric center of the laptop disregarding the physical size of the dongle. It is also in line with the CTIA test plan [2].

The angle of rotation was defined according to orientation of the DUT. If the DUT was mounted differently, the axis and rotation direction were changed accordingly to avoid confusion.

DUT and host laptop settings The laptop (DUT3) was powered by battery, the power management settings were as the following:

- Turn off monitor - never
- Monitor brightness - 100%
- Turn off hard drive - never
- System standby after - never
- Additional power management features by manufacturers - off
- Wireless LAN - off
- Bluetooth radio - off
- Internal HSPA modem - on when measuring laptop, off when measuring dongles

7.1.4 Sensitivity measurements in noise-limited scenario: with receive diversity

Standard TIS measurement described in [2] requires the DUT to be set in loop back mode in sensitivity measurements. Since one of the DUTs did not support loop back mode, the standard procedure of TIS measurement cannot be followed. Instead the following approach was applied:

- Sensitivity measurements were done in an HSPA connection.
- The system was running under H-set 6 (QPSK) with level-set 1.

Parameter	Unit	Value
FRC		H-set 6
DL Channel Frequency		10562
Modulation		QPSK
Nominal Avg. Inf. Bit Rate	Kbps	3219
Inter-TTI Distance	TTI's	1
Number of HARQ Processes	Processes	6
Information Bit Payload	Bits	6438
Number of Code Blocks	Blocks	2
Binary Channel Bits per TTI	Bits	9660
Total Available SML's in UE	SML's	115200
Number of SML's per HARQ Proc.	SML's	19200
Coding Rate		0.67
Number of Physical Channel Codes	Codes	10
Redundancy and constellation version coding sequence		0,2,5,6
Maximum number of HARQ transmission		1

Table 7.6: Simulation Setup in Sensitivity Measurements

Parameter	Unit	Value
P-CPICH_Ec/Ior	dB	-9.9
P-CCPCH and SCH_Ec/Ior	dB	-11.9
PICH_Ec/Ior	dB	-14.9
HS-PDSCH	dB	-5.9
HS-SCCH_1	dB	-7.4
DPCH_Ec/Ior	dB	-5
OCNS_Ec/Ior (Auto.)	dB	-13.3

Table 7.7: Code Power Settings: Level-set 1

Parameter	Unit	Value
Channel Type		12.2k + HSDPA
Paging Services		RB Test Mode
AWGN Power		Off
FRC Type		H-set 6 (QPSK)
UE loopback type		Type 2
PRACH Power Ramp Step	dB	3
Maximum Uplink Transmit Power Level	dBm	33

Table 7.8: Configuration of Agilent 8960

- Frequency of measurement was channel 10562 (2.1124 GHz).
- HARQ was turned off.
- BLER values of multiple power levels were recorded.
- Sensitivity was defined as the power level needed not to exceed 50% BLER.

General settings applied in the measurement system are given in Table 7.6. Code Power Settings (Level-Set 1) were set according to [4] and are given in Table 7.7. Additional configuration that applied to Agilent 8960 Wireless Test Set is detailed in Table 7.8.

Procedures

Three test cases were applied to each DUT:

1. Transmission from horizontal polarization of the test antenna only, in setup as described in Fig. 7.2.
2. Transmission from vertical polarization of the test antenna only, in setup as described in Fig. 7.2.
3. Transmission from both polarizations of the test antenna with half power per polarization and de-correlation, in setup as described in Fig. 7.3.

Case 1 and 2 represent traditional approach to sensitivity measurement that separately measure each polarization. Case 3 is designed to let DUTs with receive diversity to benefit from polarization diversity [23].

Ideally, one should place phase shifters configured with random phase at the two output ports of fading emulator to de-correlate the signals. In this setup, a small Doppler shift with opposite direction was separately applied on two polarizations, resulting two stationary but independently phase-shifted streams. The $3\,\mathrm{km/h}$ pedestrian speed Doppler shift was used to realize at least 10π phase difference during every second of transmission, and it was sufficient to have statistically trustworthy results.

The control by PC was through GPIB interface. A Tcl/Tk program was written to control the platform and the arm of the positioner (through an executable file compiled in C), to communicate with the BSE (via GPIB) and the fading emulator (via GPIB over LAN). The program is able to run semi-automatic to the end of measurement or to continue measurement after interrupt (DUT run out of battery for instance).

The measurement starts with a high transmitting power in DL to setup a connection between the DUT and the BSE.

1. The power level decreases with a large step of $5\,\mathrm{dB}$.
2. At each power level, 1000 frames are transmitted and BLER is recorded.
3. When BLER increases beyond 0%, the power level is switched one step back and a $2\,\mathrm{dB}$ power step is used to continue the measurement.
4. Repeat procedures 2 and 3 and change the power decreasing step to $0.5\,\mathrm{dB}$.
5. Repeat procedures 2 and 3 and change the power decreasing step to $0.2\,\mathrm{dB}$.
6. Starting from current power level, at each power level, 1000 frames are transmitted and all BSE reports including BLER, throughput are recorded.
7. When BLER exceeds 90%, the measurement of this sampling point is finished.

The adaptive power scheme above is based on current and previous BLER values. When the algorithm senses that the power step is too coarse, the power

level is switched back one step higher and measurement continues with a finer resolution. To avoid any possible drop of connection during the procedure, every time when the power level is switched back, a connection check is invoked to verify the transmission status. If connection is lost, transmission re-establishment is handled by calling an external function. When the measurement for one point is done, the positioner is turned for the measurement of the next point.

In some measurements, a regular (rectangular) set of sampling grid was used. For θ from 0° to 180°, ϕ from 0° to 360°, every 15° of θ and ϕ were sampled except for $\theta = 0^\circ$ and $\theta = 180^\circ$ (which represent the top and the bottom respectively, at which one sample is sufficient). A total sum of 266 samples over the sphere were taken in this case.

To save the measurement time, an irregular sampling grid was also applied on some of the measurements. For θ from 0° at the top, to 180° at the bottom with 15° steps, 1, 8, 15, 18, 24, 24, 24, 24, 24, 18, 15, 8, 1 samples were taken uniformly on ϕ. For every possible θ, $\phi = 0^\circ$ was always sampled. A total sum of 204 points were sampled in this case, saving roughly 25% of measurement time.

Post-processing

For each point of measurement, a set of data containing multiple power levels and corresponding BLER values was recorded. Interpolation was necessary to present results in a meaningful way. Curve-fitting was used to present the data-set by a smaller number of metrics. Q function was used as the curve to fit the measured data with an MMSE cost function. Two metrics representing the curve were generated, one describing the slope, the other the 50% BLER middle point. The 50% BLER metric was defined as the sensitivity.

In 2D representation, spline interpolation was used to fill the coarse data into a finer set. For irregular sampling points, ϕ was interpolated first. For 3D plot, Legendre Polynomial interpolation was used.

Measurement results

The sensitivity map of DUTs are rendered in both 3D and 2D, given in Fig. 7.10 and Fig. 7.13 for DUT1, Fig. 7.11 and Fig. 7.14 for DUT2 and Fig. 7.12 and Fig. 7.15 for DUT3 respectively.

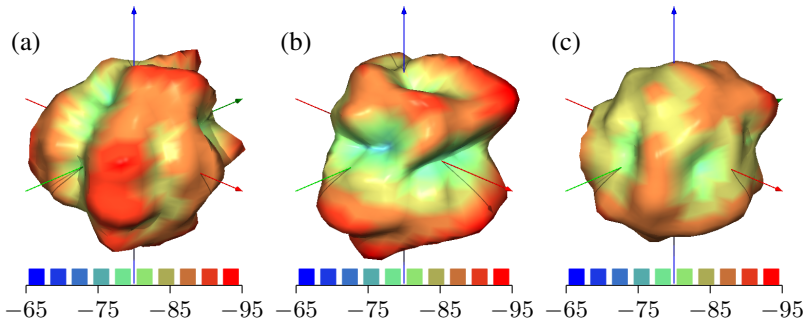

Figure 7.10: 3D sensitivity pattern of DUT1: (a) φ polarised DL signal only, (b) ϑ polarized DL signal only, (c) decorrelated copies of the DL signal with half power each on either polarization.

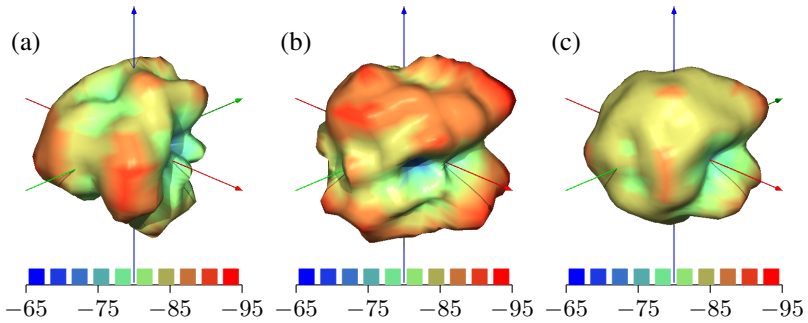

Figure 7.11: 3D sensitivity pattern of DUT2: (a) φ polarised DL signal only, (b) ϑ polarized DL signal only, (c) decorrelated copies of the DL signal with half power each on either polarization.

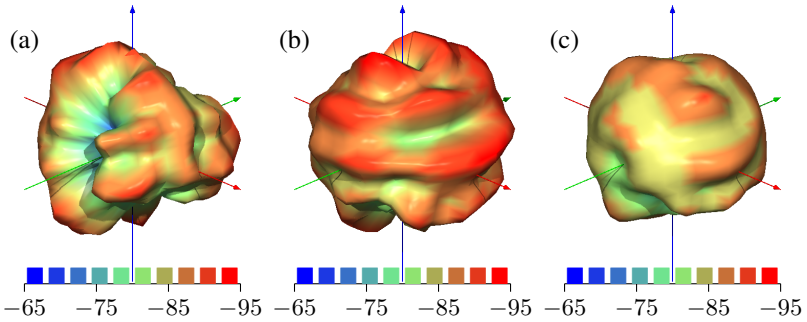

Figure 7.12: 3D sensitivity pattern of DUT3: (a) φ polarised DL signal only, (b) ϑ polarized DL signal only, (c) decorrelated copies of the DL signal with half power each on either polarization.

In all these figures, it is observed that measurement (c), i.e. decorrelated copies of signal with half power on both polarizations gives smoother pattern that the peaks and troughs in sensitivity measurements with single polarization is less visible. The sensitivity maps of DUT1 and DUT2 are similar to each other, it is because the radiation pattern of a USB dongle is highly dependent on the laptop it attached to. Since both DUTs have used DUT3 as host and were attached to the same USB port, their measured patterns are similar. The laptop (DUT3) has obviously superior performance than the other two DUTs.

To illustrate the measurement described in Section 5.2, the CDF of sensitivity is presented in Fig. 7.16, Fig. 7.17 and Fig. 7.18 for DUT1, DUT2 and DUT3 respectively. The total sensitivity, calculated similarly as TIS defined in [2], are given for three DUTs in Table 7.9, Table 7.10 and Table 7.11 for DUT1, DUT2 and DUT3 respectively. The standard deviation σ of sensitivity are also calculated for all measurements performed on three DUTs. It is the square root of variance and sensitivity of each measured point is weighted by the surface of unit sphere this point represents in the measurements.

Fig. 7.19 gives the comparison between CDF curves of measurement (c) for all three DUTs. The ranking of DUTs is obviously in the order of DUT3, DUT1 and DUT2.

Analysis The CDF curves for the measurements with decorrelated copies of the DL signals on both polarizations simultaneously is understandably steeper

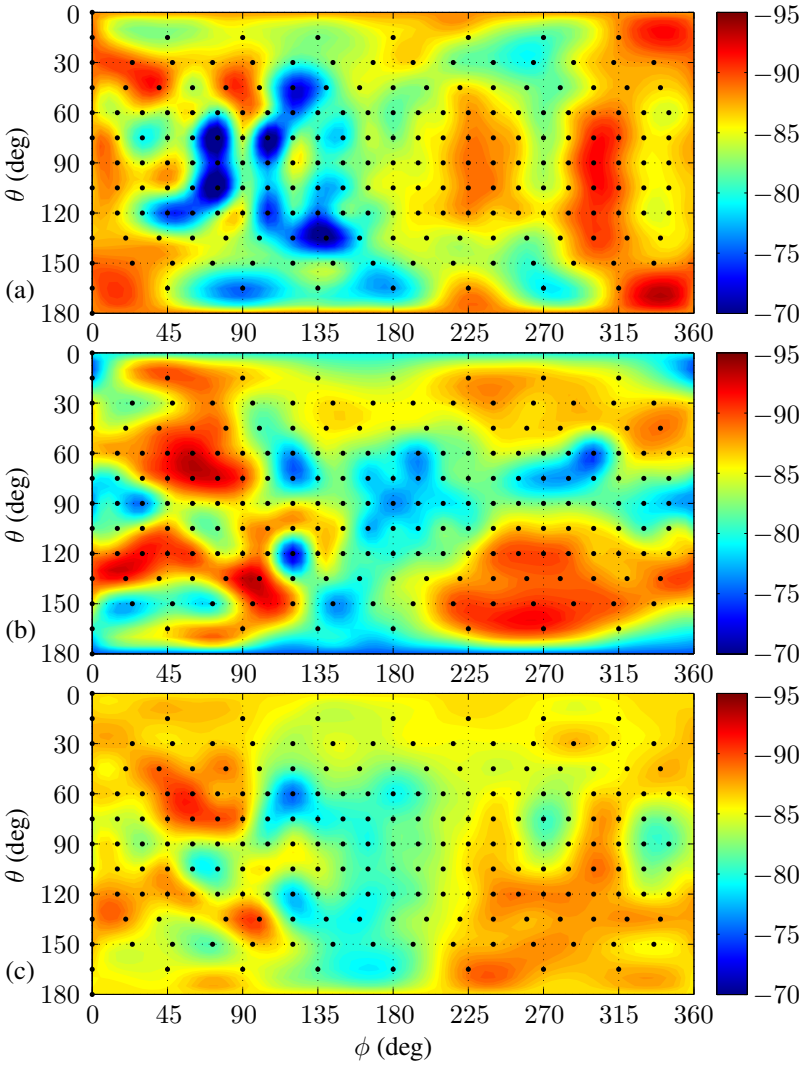

Figure 7.13: 2D sensitivity map of DUT1, with dots representing sampling grid of the measurement. a) φ polarization only, b) ϑ polarization only, c) two polarization transmitting decorrelated copies simultaneously.

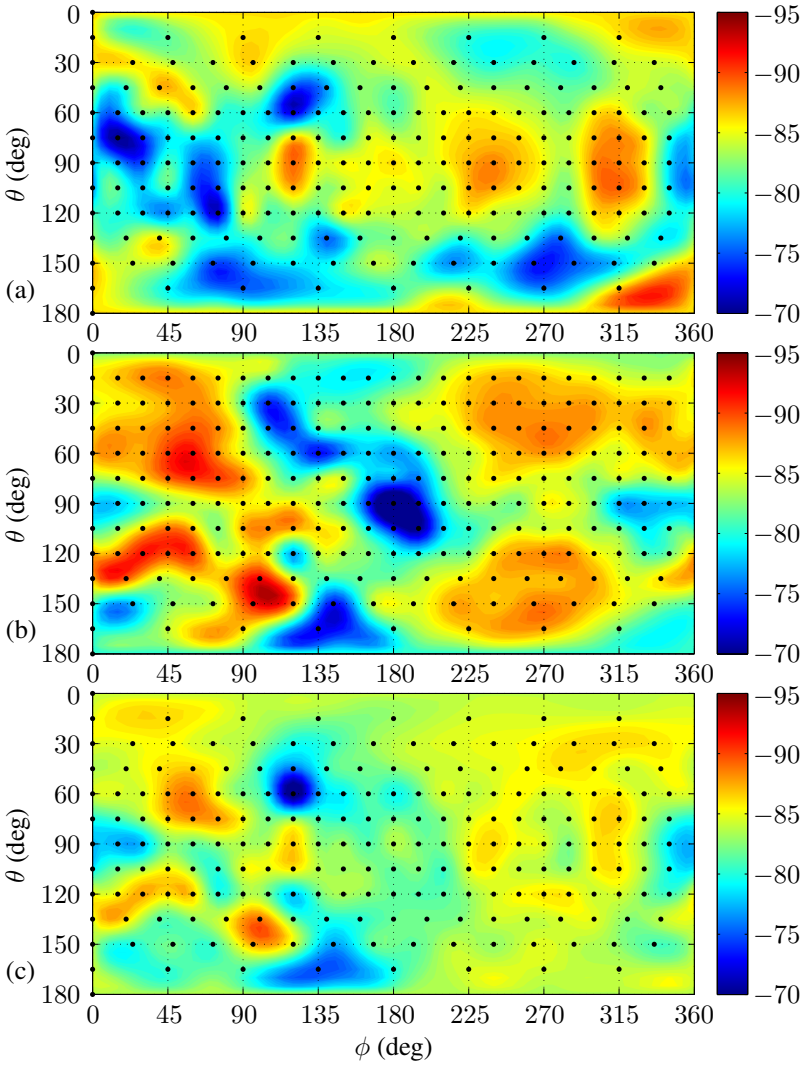

Figure 7.14: 2D sensitivity map of DUT2, with dots representing sampling grid of the measurement. a) φ polarization only, b) ϑ polarization only, c) two polarization transmitting decorrelated copies simultaneously.

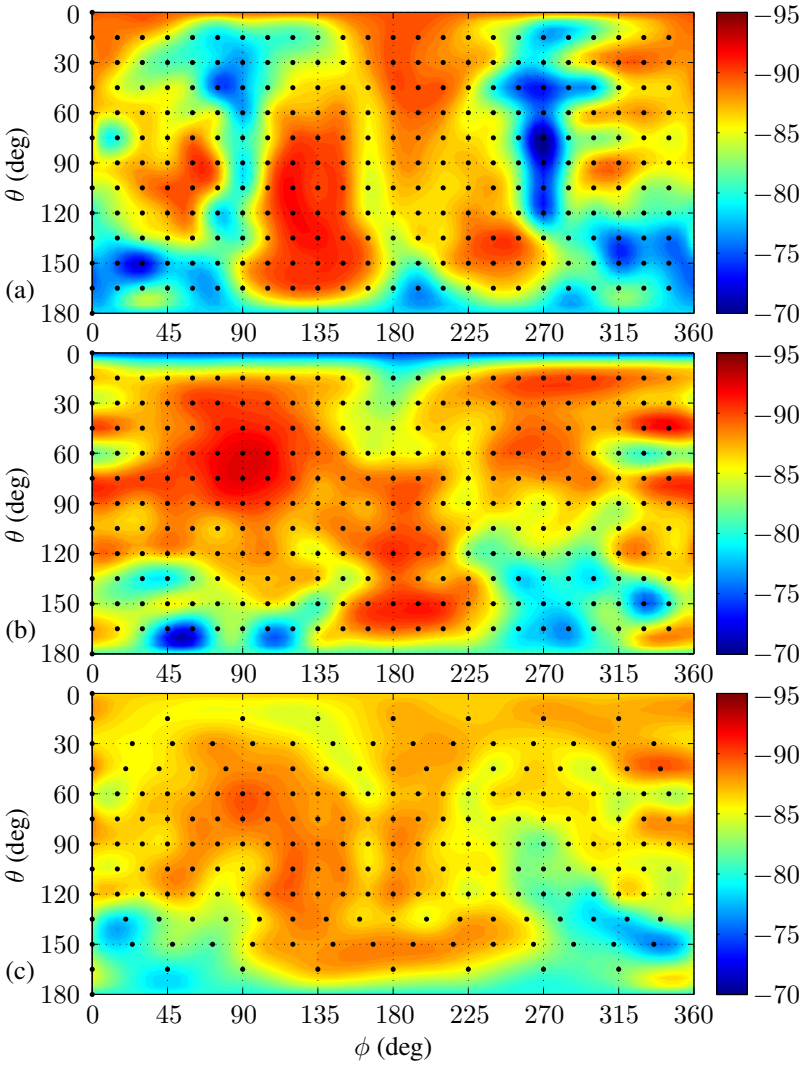

Figure 7.15: 2D sensitivity map of DUT3, with dots representing sampling grid of the measurement. a) φ polarization only, b) ϑ polarization only, c) two polarization transmitting decorrelated copies simultaneously.

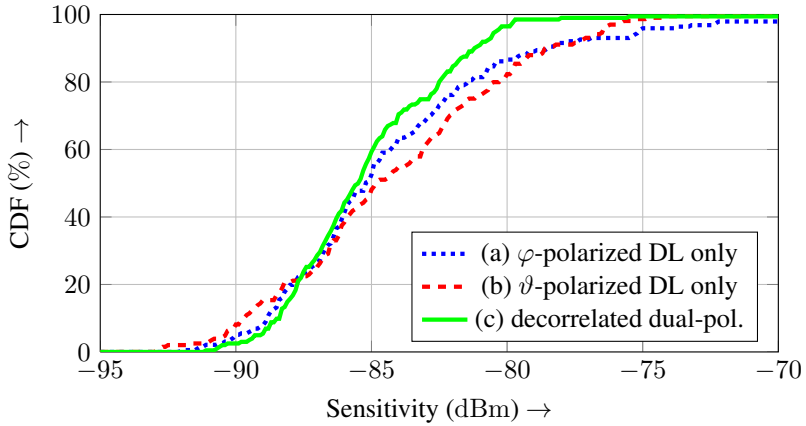

Figure 7.16: CDF of sensitivity measurement results of DUT1: (a) φ polarised DL signal only, (b) ϑ polarized DL signal only, (c) decorrelated copies of the DL signal with half power each on either polarization.

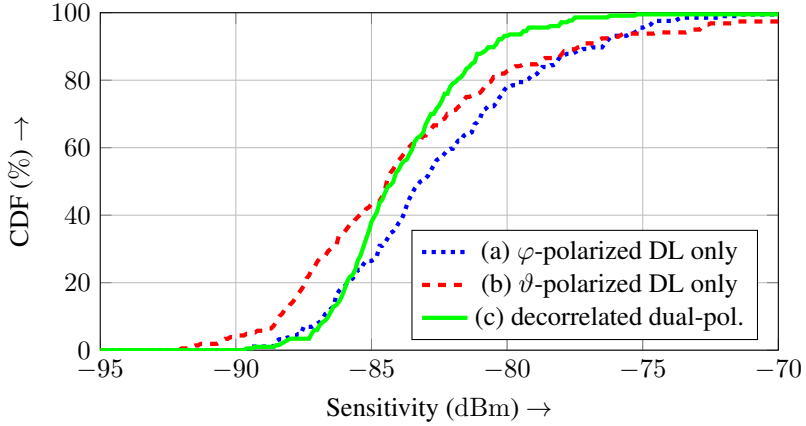

Figure 7.17: CDF of sensitivity measurement results of DUT2: (a) φ polarised DL signal only, (b) ϑ polarized DL signal only, (c) decorrelated copies of the DL signal with half power each on either polarization.

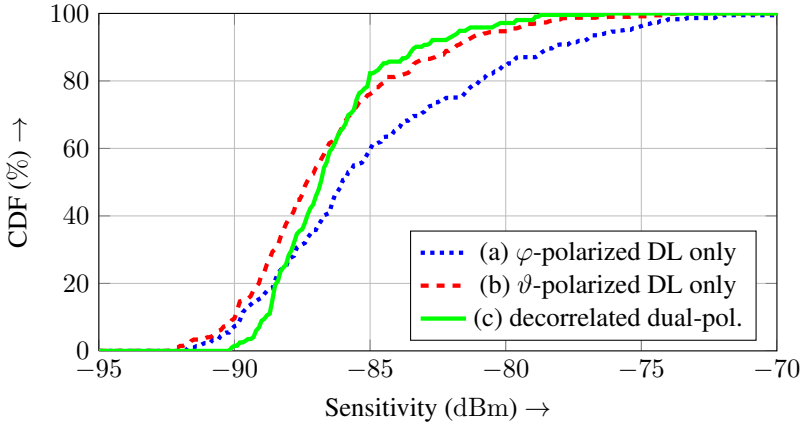

Figure 7.18: CDF of sensitivity measurement results of DUT3: (a) φ polarised DL signal only, (b) ϑ polarized DL signal only, (c) decorrelated copies of the DL signal with half power each on either polarization.

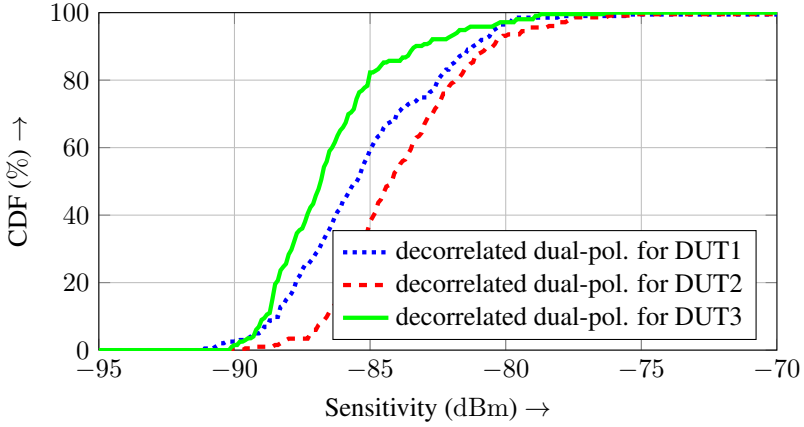

Figure 7.19: Comparison between CDF curves of sensitivity measurement results in case (c): decorrelated copies of the DL signal with half power each on either polarization.

	Total Sensitivity (dBm)	σ (dB)
(a) φ-only	-86.2	4.25
(a) ϑ-only	-85.9	4.56
Two-pol. (CTIA)	-86.1	/
(c) Two-pol.	-85.6	3.30

Table 7.9: Statistics of sensitivity measurement results of DUT1.

	Total Sensitivity (dBm)	σ (dB)
(a) φ-only	-83.8	3.80
(a) ϑ-only	-85.6	5.33
Two-pol. (CTIA)	-84.8	/
(c) Two-pol.	-84.0	2.66

Table 7.10: Statistics of sensitivity measurement results of DUT2.

than the measurements with single polarization only. It is also easy to observe that because DUT1 has only single antenna while the other two have second antenna in the purpose of receive diversity, the steepness of the CDF curves of measurement (c) for the three DUTs is different. The difference is intuitively given in Fig. 7.19. If one ranks the three DUTs in the sense of utilization of diversity, DUT3 is obvious the best with DUT2 falls only slightly behind. Nevertheless, DUT1 with a single antenna can still have better efficiency than DUT2 (which has a multi-port antenna system with receive diversity) because it is better designed. The above conclusion can also be drawn based on data given in Table 7.9, Table 7.10 and Table 7.11, the statistical metric comparison in Fig. 7.19 is more intuitive and easier to understand.

The similarity between patterns of DUT1 and DUT2 confirms that standard mock-up is necessary in testing UEs in the form-factor of USB dongles. Their patterns show significantly bad performance in ϑ polarization in the azimuthal plane. It again confirms that economization of OTA measurements by limiting constellations in the azimuthal plane is not a proper solution.

	Total Sensitivity (dBm)	σ (dB)
(a) φ-only	-86.5	4.48
(a) ϑ-only	-87.8	3.27
Two-pol. (CTIA)	-87.2	/
(c) Two-pol.	-86.5	2.40

Table 7.11: Statistics of sensitivity measurement results of DUT3.

7.1.5 Throughput measurements in a two test antenna setup with receive diversity

The azimuthal throughput measurements with two antennas is a conceptual check of peak performance measurement proposed in Subsection 5.3.2. It differs from the proposal based on the facts that,

- this measurement was applied to HSPA devices,
- no MIMO modes, neither TD nor SM modes are supported.

From the previous measurements and existing documents, it was known that not all DUTs have a second antenna for RD. The measurement should nevertheless indicate the availability of multiple antennas in the results.

- Throughput measurements were done in an HSPA connection.
- The modulation scheme was set to 16QAM to have a larger range of throughput.
- The system was running under H-set 6 (16QAM) with level-set 1.
- HARQ was set to have a maximum of 4 transmissions.
- BLER values and throughput of multiple power levels were recorded.

General settings applied in the measurement system are given in Table 7.12. Code Power Settings (Level-Set 1) are set according to [4] and are given in Table 7.13. Additional configuration that applied to Agilent 8960 Wireless Test Set is detailed in Table 7.14. The FOM in this measurement was throughput statistics.

Two channel models were applied:

Parameter	Unit	Value
FRC		H-set 6
DL Channel Frequency		10562
Modulation		16QAM
Nominal Avg. Inf. Bit Rate	Kbps	4689
Inter-TTI Distance	TTI's	1
Number of HARQ Processes	Processes	6
Information Bit Payload	Bits	9377
Number of Code Blocks	Blocks	2
Binary Channel Bits per TTI	Bits	15360
Total Available SML's in UE	SML's	115200
Number of SML's per HARQ Proc.	SML's	19200
Coding Rate		0.61
Number of Physical Channel Codes	Codes	8
Redundancy and constellation version coding sequence		6,2,1,5
Maximum number of HARQ transmission		4

Table 7.12: Simulation Setup in Throughput Measurements

Parameter	Unit	Value
P-CPICH_Ec/Ior	dB	-9.9
P-CCPCH and SCH_Ec/Ior	dB	-11.9
PICH_Ec/Ior	dB	-14.9
HS-PDSCH	dB	-5.9
HS-SCCH_1	dB	-7.4
DPCH_Ec/Ior	dB	-5
OCNS_Ec/Ior (Auto.)	dB	-13.3

Table 7.13: Code Power Settings: Level-Set 1

Parameter	Unit	Value
Channel Type		12.2k + HSDPA
Paging Services		RB Test Mode
AWGN Power		Off
FRC Type		H-set 6 (16QAM)
UE loopback type		Type 2
PRACH Power Ramp Step	dB	3
Maximum Uplink Transmit Power Level	dBm	33

Table 7.14: Configuration of Agilent 8960

- a simplified SCME model to investigate the influence of pre-fading in the measurement.
- a non-fading scenario with small Doppler shift applied on the two spatial streams with opposite direction for the purpose of de-correlation.

The Doppler shift was the same as the one described in the sensitivity measurements.

Procedures

The measurement starts with a high transmit power level ($-65\,\mathrm{dBm}$) in downlink to setup a connection between DUT and the BSE.

1. The power level decreases with a large step of $6\,\mathrm{dB}$.
2. At each power level, 5000 frames (with SCME model) or 1000 frames (with Doppler shift) are transmitted and BLER is recorded.
3. When the BLER exceeds 20%, the power setting is switched one step back to the last one and the power decreasing step is changed to $4\,\mathrm{dB}$.
4. Repeat procedures 2 and 3 and change the power decreasing step to $2\,\mathrm{dB}$.
5. Starting from this power level, all BSE report including BLER / throughput are recorded over 5000 frames (SCME model) / 1000 frames (with Doppler shift).

6. When BLER exceeds 80%, the measurement of this point is finished.

The adaptive power scheme above is based on current and previous BLER values. When the algorithm senses that the power step is too coarse, the power level is switched back one step higher and measurement continues with a finer resolution. To avoid any possible drop of connection during the procedure, every time when the power level is switched back, a connection check is invoked to verify the transmission status. If connection is lost, transmission re-establishment is handled by calling an external function. When the measurement for one point is done, the platform of the positioner is turned for the measurement of the next point.

In these measurements, θ was fixed to 90°. The two ϕ values assigned to two test antennas were represented by one ϕ value for the fixed test antenna, and $\Delta\phi$ for the relative angle between the two test antennas. The former ϕ value was realized by rotating the platform. The $\Delta\phi$ was given by the 3 mounting locations of the second test antenna. For each $\Delta\phi$, four polarization combinations were realized by routing signals to different polarization of the fixed test antenna and manually changing the polarization of the second test antenna. The $\Delta\phi = 0^\circ$ of relative angle case was realized using both polarizations of the fixed test antenna, but only one polarization combination was available. A resolution of 15° was used in rotating the platform. In total, 24 sampling points were taken in each of the 13 arrangements, summing up to 312 constellations for each DUT per measurement.

Simplified SCME Model The simplified SCME model was based on the standard SCME defined in [116]. The definition of sub-paths in the standard is a list of angles relative to the main direction of path. However in this setup, only two test antennas did exist. The sub-paths were directly mapped to one of the test antennas creating TDL models. The TDL fading models were configured in the fading emulator. The power of each sub-path was calculated from the angle the sub-path relative to the main direction and the given angular distribution.

In SCME model, Laplacian distribution is used to define the relation between angle offset and assigned power of the subpath, as given by:

$$P(\Delta\phi, \sigma) = N_0 \exp(\frac{-\sqrt{2}|\Delta\phi|}{\sigma}) \tag{7.1}$$

where P is the power of the sub-path, $\Delta\phi$ is the angle offset of the sub-path to

Subpath #	angle offset (degrees) for 35° AS	Power (dB)	Delay (ns)
1, 2	±1.5649	−9.88	117.5
3, 4	±4.9447	−10.47	125.8
5, 6	±8.7224	−11.14	135.8
7, 8	±13.0045	−11.89	148.1
9, 10	±17.9492	−12.76	163.6
11, 12	±23.7899	−13.78	184.1
13, 14	±30.9538	−15.04	212.8
15, 16	±40.1824	−16.66	256.4
17, 18	±53.1816	−18.94	333.4
19, 20	±75.4274	−22.84	522.6

Table 7.15: Simplified SCME model: derived Power Delay Profile based on angular offset of sub-paths in SCME.

the main path and σ is the angular spread. N_0 in the equation is the normalization factor which is defined by the integration of the power over all sub-paths, given by

$$N_0^{-1} = \int_{-\pi}^{\pi} \exp(\frac{-\sqrt{2}|\Delta\phi|}{\sigma})\,\mathrm{d}\Delta\phi. \tag{7.2}$$

Similarly, using the FSL model, one can obtain the distance, which can be used as the delay property of the sub-path,

$$\mathrm{PL} = 20\,\mathrm{dB}\log_{10}(d) + c, \tag{7.3}$$

where PL represents the Path Loss (PL) in dB and d is the distance in meters. The simplified SCME model implemented in the measurement is shown in Table 7.15. The velocity which defines the small-scale fading was set to $3\,\mathrm{km/h}$ (pedestrian).

Measurement results

For each constellation, throughput vs. power curves were recorded. The averages over all 312 constellations of the throughput vs. power relation are presented in Fig. 7.20 for simplified SCME channel model and in Fig. 7.21 for the non-fading scenario where copies of signal are de-correlated by small Doppler

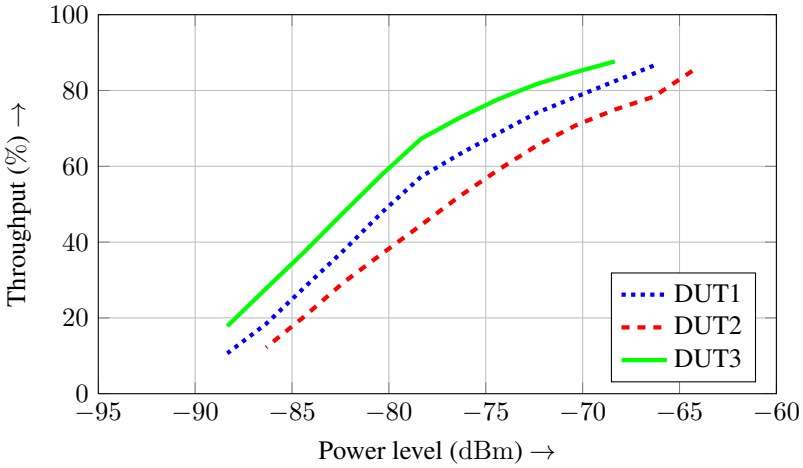

Figure 7.20: Throughput vs. power figure with simplified SCME model.

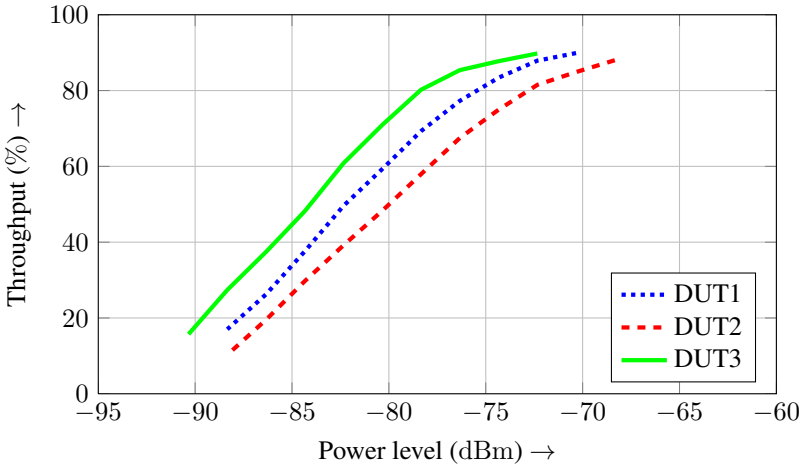

Figure 7.21: Throughput vs. power figure with copies of signal decorrelated by small Doppler shift.

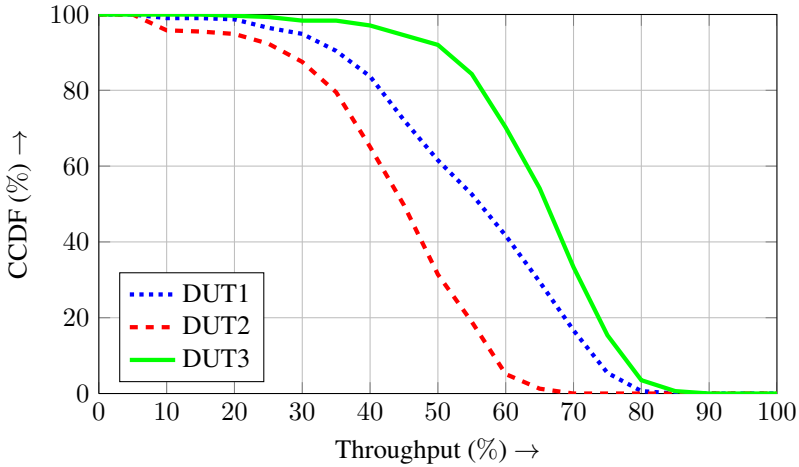

Figure 7.22: The CCDF of throughput for three DUTs at the power level of $-80\,\mathrm{dBm}$ in a simplifed SCME fading channel. 312 constellations in the azimuthal plane were considered.

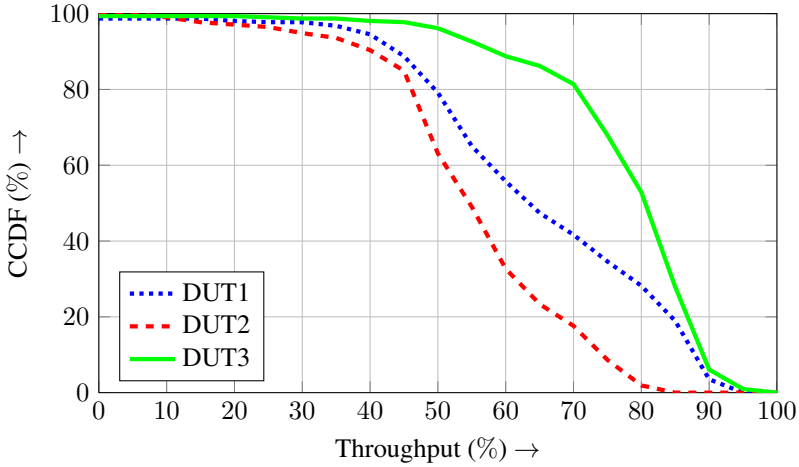

Figure 7.23: The CCDF of throughput for three DUTs at the power level of $-80\,\mathrm{dBm}$ with decorrelation on two copies of signal by small Doppler shift. 312 constellations in the azimuthal plane were considered.

	Simplified SCME	decor. w/ Doppler
DUT1	Mean: 49.5%, σ: 15.9%	Mean: 61.0%, σ: 17.3%
DUT2	Mean: 38.3%, σ: 12.7%	Mean: 49.9%, σ: 14.1%
DUT3	Mean: 59.5%, σ: 10.9%	Mean: 72.7%, σ: 12.1%

Table 7.16: Throughput statistics at $-80\,\mathrm{dBm}$ power level for three DUTs. 312 constellations in the azimuthal plane were considered.

shift. Every curve is the averaged result of 312 curves measured for each DUT in one channel model. The same ranking of the DUTs is observed in both scenarios (simplified SCME model and non-fading).

A more informative presentation of the result is given in Fig. 7.22 and Fig. 7.23 for simplified SCME and non-fading scenario respectively. It shows the outage probability of achieving certain throughput at a given signal power level of $-80\,\mathrm{dBm}$. Since the measured power level is not exactly at $-80\,\mathrm{dBm}$, linear interpolation is used to acquire results in this presentation. Statistics including the mean and standard deviation σ of throughput PDF at this power level is given in Table 7.16.

Analysis It is worth noting that the transmission mode in the measurements is receive diversity. In SM mode, the shape of the CCDF curves would almost definitely be different to what is measured in these measurements. For instance, in SM measurements with FRC, 0% relative throughput points are inevitable because fallback to diversity is disabled. In diversity modes e.g. RD used in this measurement, such 0% points are rarely seen.

Strong similarities are observed between the curves in Fig. 7.20 and Fig. 7.21. Introducing fading in the measurement for this setup is equivalent to a shift in power level. Information is obviously lost in this averaged result presentation.

Statistical metric in Fig. 7.22 and Fig. 7.23 on the other hand suggests a similar UE performance ranking to what is observed in sensitivity measurements and obvious indication of DUT1's lack of second antenna (by observing the steepness of the CCDF curves). Constellations applied in this measurement were limited in the azimuthal plane which were also discriminative against DUT1 and DUT2. One could observe in the patterns generated by the sensitivity measurements that the ϑ polarization of the patterns of both DUT1 and DUT2 are inefficient in the azimuthal AOAs. If 3D constellations were used,

better throughput statistics for these two DUTs are to be expected.

7.2 Measurements of LTE devices

After several LTE terminals became available, another round of measurements was conducted at CETECOM GmbH in Essen in September 2011 for one week. The purpose of this round of measurements was to investigate the applicability of the test plan proposal to actual LTE terminals as well as to verify several theoretical observations.

A CTIA certified distributed-axis anechoic chamber was used in the measurements. The BSE used in the measurements was a Rohde & Schwarz CMW500 which was capable of LTE MIMO measurements (in beta phase). The chamber was a fully automated Rohde & Schwarz system using AMS32 software and OSP control platform.

7.2.1 The CTIA certified chamber

The chamber used was a CTIA certified SISO OTA test chamber with a quad-ridged horn antenna as test antenna. It is a distributed-axis chamber [120] with test antenna mounted on a boom for adjustable elevation θ. A platform capable of 360° rotation around the Z-axis is located at the center of the chamber to serve as DUT mount and to adjust azimuthal position ϕ as shown in Fig. 7.24. Similar to Fig. 1.2, for SISO OTA measurements, the output port of a BSE (in this case the Rohde & Schwarz CMW500) is routed to one of the two ports of the test antenna.

To measure the sensitivity of the DUT in a noise-limited scenario with TD mode as described in Section 5.2, the polarization switch in OSP was bypassed. Two output ports of the Rohde & Schwarz CMW500 were connected directly to the antenna ports corresponding to the two polarizations of the test antenna.

The transmission mode was set to TD. P_{iso} was defined as power received by an isotropic reference antenna at the UE position following Subsection 5.2.2. Two orthogonal signal streams were routed to the two polarizations of the the test antenna simultaneously and with equal power (half the total power each). To be able to compare measurement results directly to TIS results of individual antenna, P_{iso} in this case was defined as the full-band power instead of RS EPRE which is the per sub-carrier power in LTE. TIS results were obtained from official device certification process in the same chamber following

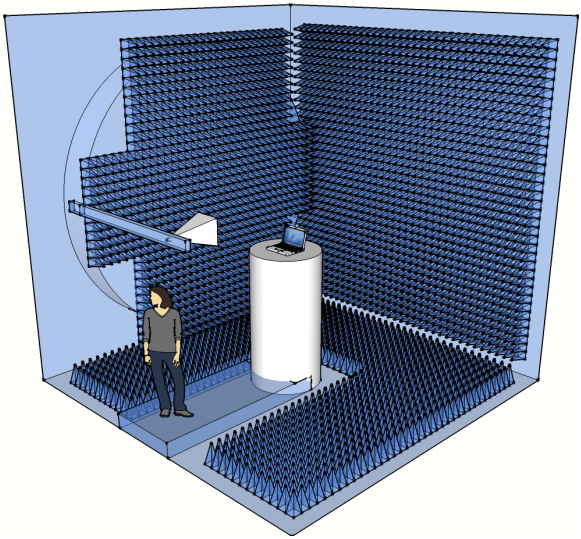

Figure 7.24: Illustration of a distributed-axis chamber.

the standard SISO OTA measurement procedures. The rest of configurations followed what is described in Subsection 5.2.2 and in [103] with equipment configuration given in Table 7.17.

The recorded data was sensitivity defined as the DL power at which 10% BLER is reached. 10% BLER is the designed optimal working condition for each CQI level in LTE. Lower BLER means the transmission condition is better than the one required by this CQI level. A different MCS which is capable of higher throughput is suggested to apply. Conversely, higher BLER normally indicates a request of a lower CQI level for the purpose of stable transmission.

7.2.2 Extended chamber for measurements with two test antennas

To introduce spatial diversity into the chamber, a second test antenna is required. Ideally, an additional dual-polarized test antenna is to be put into the chamber with possibility for a position independent from the first test antenna as illustrated in Fig. 5.2. Two output ports of the BSE are to be routed to two

DL MIMO mode	Transmit Diversity (TD)		
Schedule type	RMC		
Downlink settings		Uplink settings	
Cell bandwidth	10 MHz	Cell bandwidth	10 MHz
Number of RB	50	Number of RB	50
Start RB	0	Start RB	0
Modulation	QPSK	Modulation	QPSK
TBS Idx/value	0	TBS Idx/value	0
Max. throughput	3953 kbps	UL Power Control	Max. power
HARQ retransmission	off		
PDSCH power offset to RS EPRE	$\rho_A = -3\,\mathrm{dB}$ $\rho_B = -3\,\mathrm{dB}$		
AWGN	OFF		
P_{iso} DL power	Full BW		
Number of subframes	2000		
BLER threshold	10%		

Table 7.17: TD communication parameters

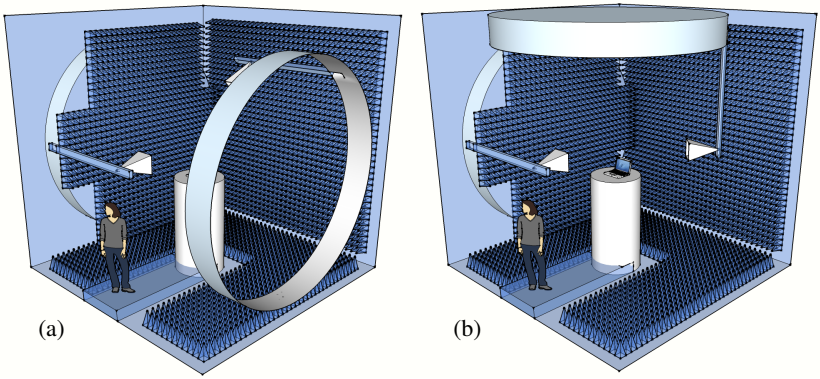

Figure 7.25: Examples for realization of 2-test-antenna setups in a distributed-axis chamber.

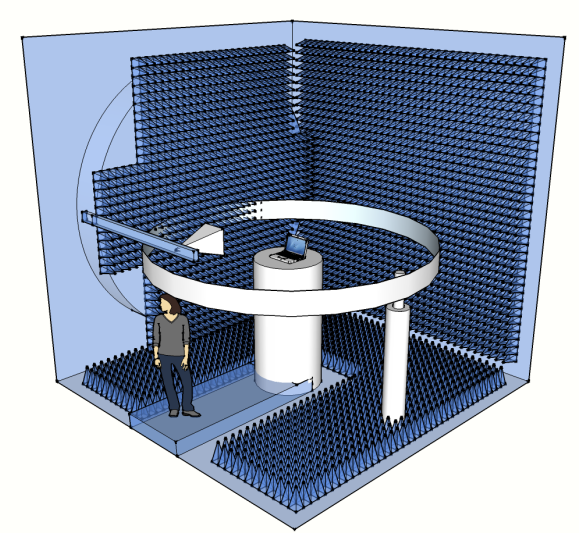

Figure 7.26: Illustration of an equivalent method using a dipole / loop antenna in the azimuthal plane.

of the four ports of the two test antennas, one polarization per test antenna at one time as described in Section 5.3.

In a distributed-axis chamber, there are several ways to place a second test antenna. The implementation by Rohde & Schwarz [31, 103] is to have another boom constructed on the opposite wall of the chamber against the existing one as illustrated in Fig. 7.25a. It was decided in this round of measurements to implement an equivalent setup to the one illustrated in Fig. 7.25b because of the limitation in time and effort, that is to construct a boom to the ceiling of the chamber in order to make the second test antenna movable in the azimuthal plane. Due to the relative small size of the chamber and lack of flexible antenna placing construction, a dipole / loop combination was chosen to be placed in the azimuthal plane instead as given in Fig. 7.26. Polarization switching of the additional test antenna was realized by switching between dipole and loop antenna manually.

OL-SM was the transmission mode because the CL-SM was not yet supported by equipment. P_{iso} was defined as per sub-carrier power received by an

DL MIMO mode	Spatial Multiplexing (SM)		
Schedule type	User defined channel		
Downlink settings		Uplink settings	
Cell bandwidth	10 MHz	Cell bandwidth	10 MHz
Number of RB	50	Number of RB	50
Start RB	0	Start RB	0
Modulation	16QAM	Modulation	QPSK
TBS Idx/value	15	TBS Idx/value	6
Max. throughput 1	15264 kbps	UL Power Control	Max. power
Max. throughput 2	15264 kbps		
Max. throughput total	30528 kbps		
HARQ retransmission	off		
PDSCH power offset to RS EPRE	$\rho_A = -3\,\mathrm{dB}$ $\rho_B = -3\,\mathrm{dB}$		
AWGN	OFF		
P_{iso} DL power	RS EPRE		
Number of subframes	1000		

Table 7.18: OL-SM communication parameters

isotropic reference antenna at the UE position. In the OL-SM scheme, signal streams from each port arrive with equal power at the UE. Unlike the sensitivity measurement, RS EPRE was used as the P_{iso}.

General equipment configuration is given in Table 7.18. The HARQ retransmission is one of the important parameter that can affect measurement results. It should be chosen according to the network setting for the specific FRC. In this measurement, HARQ retransmission was not supported by the BSE.

Throughput was recorded over a predefined set of constellations of the two test antennas, i.e. a set angular positions of test antenna 1 and test antenna 2 as given in each case by $(\theta_1, \phi_1, \theta_2, \phi_2)$ and the 4 possible combinations of polarization of the two dual-polarized test antennas.

Type of PL	FSL	Cable loss	Antenna gain	Attenuator
1st Test Antenna φ	39.1 dB			6.2 dB
1st Test Antenna ϑ	38.9 dB			6.2 dB
2nd Test Antenna φ	40.0 dB	8.7 dB	3.0 dB	/
2nd Test Antenna ϑ	40.0 dB	8.7 dB	3.0 dB	/

Table 7.19: Summary of calibration data for the chamber with second test antenna at the frequency of 2655 MHz.

7.2.3 Calibration

The CTIA certified chamber complies the calibration process defined by CTIA. In principle, since the sensitivity measurement in the method proposed required no modification to the chamber and equipment (including cable), no additional calibration process is required. In reality, the switch (Rohde & Schwarz OSP) was excluded from the sensitivity measurement in this setup comparing to the calibrated SISO OTA setup. Two output ports of CMW500 were directly connected to the chamber input ports via all the cables existed in the chain, except the OSP. The attenuation introduced by OSP (1 dB) was subtracted from the existing calibration data.

For the second test antenna which was later added into the chamber, a quick component calibration was performed to assure equal PLs for both test antennas. Because of the small size of the chamber, only a distance of 90 cm from the center of the chamber was possible for the second antenna to be placed. It corresponds to a 40.0 dB FSL at the frequency of 2655 MHz (Band 7 center frequency). A summary of cable losses and antenna gain is given in Table 7.19. The PL values were set in the BSE and were compensated at the output ports of the BSE.

7.2.4 Devices under test

Three DUTs with different form-factor and working frequency were examined in the measurements.

DUT1: handset with individually switchable antennas The first DUT was an E-UTRA Band 13 LTE handset with two receive antennas. These two antennas can be separately disabled in software thus allowing single antenna mea-

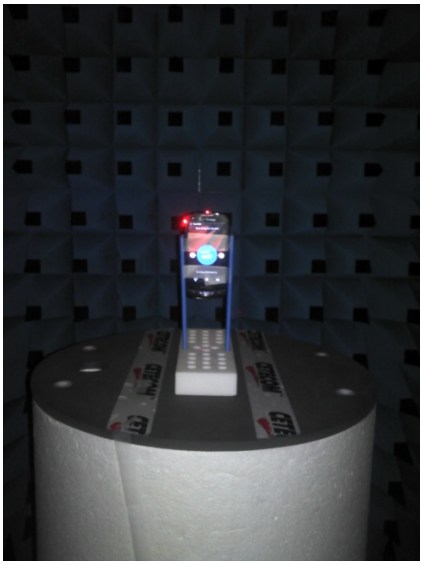

Figure 7.27: E-UTRA Band 13 handset (DUT1) with two receive antennas which can be individually switched off. The center of rotation is the earpiece which is marked by two laser points.

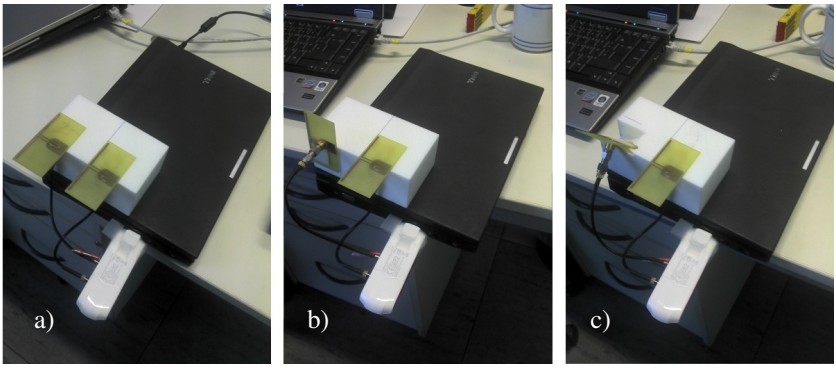

Figure 7.28: E-UTRA Band 7 dongle (DUT3) with external antenna samples, a) collinear dipole arrangement, b) cross-polarized dipoles and c) 45° polarization inclination.

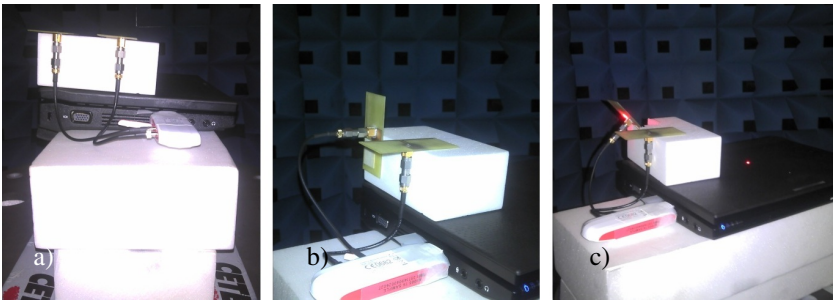

Figure 7.29: E-UTRA Band 7 dongle (DUT3) with external antenna samples when mounted, a) collinear dipole arrangement, b) cross-polarized dipoles and c) 45° polarization inclination. The laser points denote the center of rotation which is geometric center of laptop (horizontal) and height of the external antenna ports (elevation).

surements. The device was mounted inside the chamber according to CTIA test plan for single antenna devices with earpiece as the center of rotation as shown in Fig. 7.27.

DUT2: wireless modem The second DUT was an E-UTRA Band 13 modem with internal battery. It connects to the cellular network and share the data service via wireless LAN. The modem was placed flat on horizontal surface with it's geometric center as the center of rotation.

DUT3: USB dongle with external antennas The third UE under investigation was an E-UTRA Band 7 USB dongle with external antennas. Two band 7 dipoles were connected to the two antenna ports of the USB dongle in three arrangements.

(a) collinear arrangement with half-wavelength separation ("canonical dual dipole arrangement") as shown in Fig. 7.28a,

(b) orthogonal arrangement with half-wavelength separation ("crossed dipoles") as shown in Fig. 7.28b,

(c) similar to (a) and (b) but with 45° inclination between the axes of the two dipoles.

The theoretical patterns of these antenna arrangements are of course disturbed by the presence of the laptop and connecting cables. The external antennas were mounted on a piece of Rohacell above the rear-left corner of a closed-lid laptop as in Fig. 7.28. Because the purpose of this setup was to measure the external antennas instead of the USB dongle, laptop was kept closed to minimize its influence to the patterns of the external antennas. Antenna spacing was half-wavelength across all setups. DUT3 is in fact a set of DUTs with everything identical except the antennas. The center of rotation was azimuthal center of the laptop (see laser point on the laptop lid in Fig. 7.29c) at the height of the external antennas (see another laser point on the 45° mounted dipole).

7.2.5 Sensitivity measurements in noise-limited scenario

The Band 13 DL center frequency was set to $751\,\mathrm{MHz}$; uplink center frequency was set to $782\,\mathrm{MHz}$. The Band 7 DL center frequency was set to $2655\,\mathrm{MHz}$; uplink center frequency was set to $2535\,\mathrm{MHz}$. The bandwidth was $10\,\mathrm{MHz}$ in both bands and both transmission directions.

The sensitivity measurement in TD mode as described in Section 5.2 was performed. Because DUT1 is able to switch on / off individual antenna, two additional measurements were included for the purpose of comparison.

- For each receive antenna, sensitivity measurements for horizontal and vertical polarizations following the conventional TIS measurement procedure described in [2].

- For each receive antenna, sensitivity measurement in TD mode as described in Section 5.2,

The measurement resolution was 30°, both in θ and ϕ. The sensitivity CDF is generated with each sampling point weighted by a factor appreciating the surface it represents on the sphere.

The measurement was fully automatic. Starting with a high power level, AMS32 decided the steps for decreasing power level. The 10% BLER was reached by finding two points on the BLER vs. power level curve between

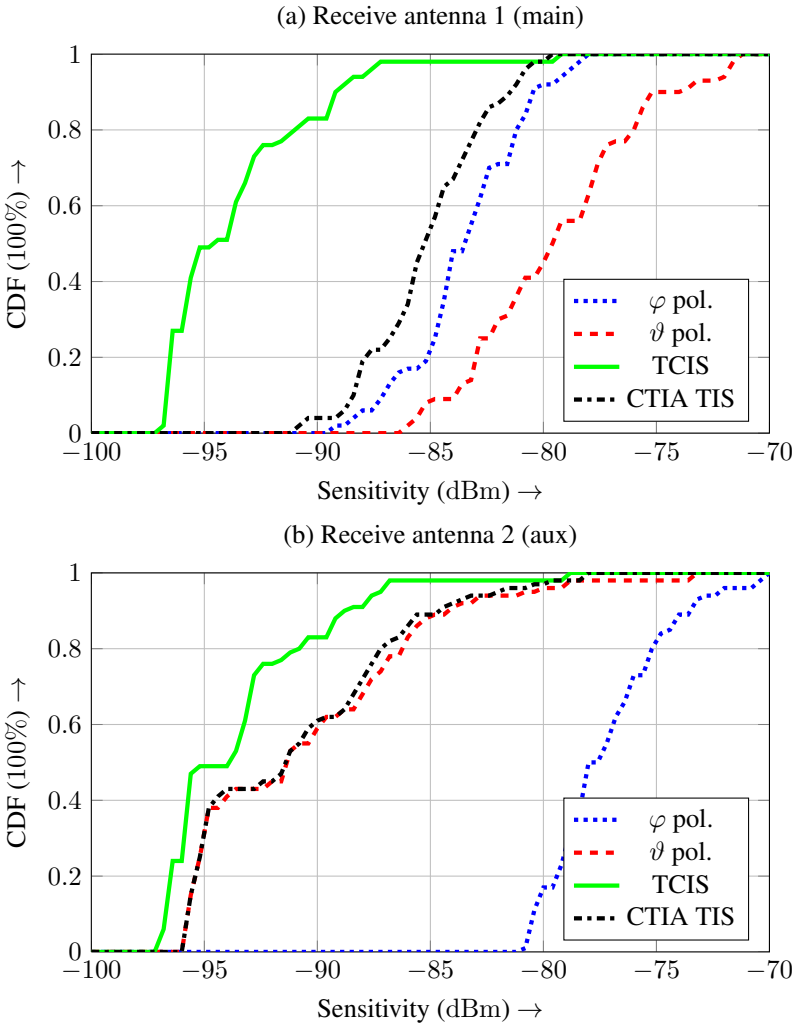

Figure 7.30: E-UTRA Band 13 handset sensitivity measurement for (a) receive antenna 1 and (b) receive antenna 2 of DUT1: Sensitivity CDF for horizontal polarization, vertical polarization, TCIS in TD mode with −3 dB power on both polarizations and combined report according to CTIA TIS definition.

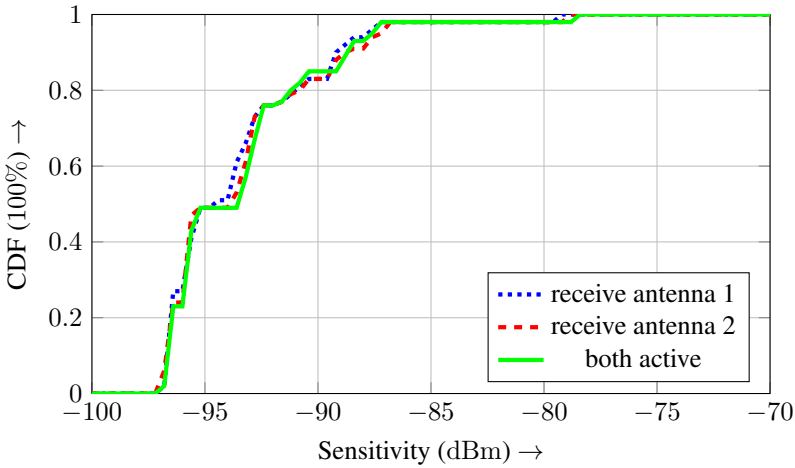

Figure 7.31: E-UTRA Band 13 handset (DUT1) sensitivity measurement in TD mode: for antenna 1 (blue), antenna 2 (red) and both antennas activated (green).

which a power difference of $0.5\,\mathrm{dB}$ and BLER at one point greater and the other less than 10%. The 10% BLER was later interpolated in the post-processing.

The result comparison between traditional TIS measurements and the sensitivity measurements in TD mode is given in Fig. 7.30a for receive antenna 1 (main) of DUT1 and Fig. 7.30b correspondingly for receive antenna 2 (aux) of DUT1. Blue and red curves are the CDF of horizontal and vertical polarization sensitivity. The combined (calculated) sensitivity according to CTIA TIS definition is presented in black. The statistics of TCIS as described in Section 5.2 (sensitivity statistics in TD) mode is plotted as green curve with $-3\,\mathrm{dB}$ correction value to match the power definition used in TIS. The comparison between cases where only one of the two antennas is switched on (single antenna) and both antennas are switched on (multiple antennas) in TD mode is presented in Fig. 7.31.

The measured CDF curves of TCIS for all DUTs are presented in Fig. 7.32. DUT1 and DUT2 were measured in Band 13 with all antennas active and DUT3 with three external antenna arrangements were measured in Band 7. The shaded region denotes a potential rejection criteria of “Better sensitivity than

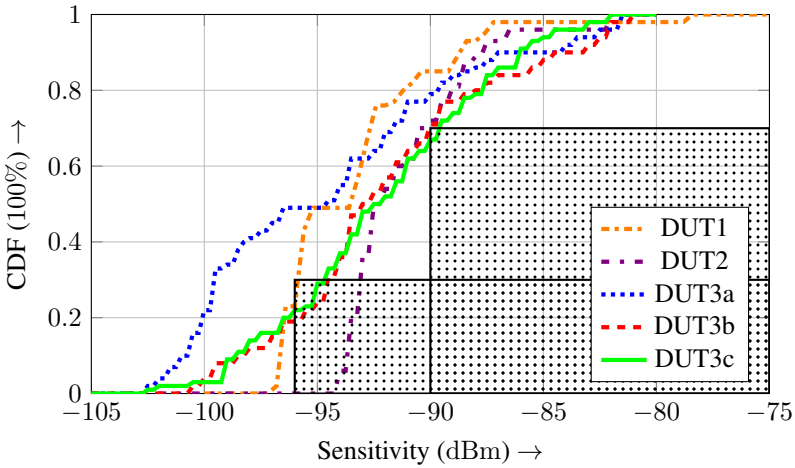

Figure 7.32: Measured CDFs of TCIS for all DUTs with different form-factor, working frequency and external antenna arrangements. The shaded region denotes the potential rejection criteria: "Better sensitivity than $-96\,\mathrm{dBm}$ with the probability of 30% and better sensitivity than $-90\,\mathrm{dBm}$ with probability of 70%".

$-96\,\mathrm{dBm}$ with the probability of 30% and better sensitivity than $-90\,\mathrm{dBm}$ with probability of 70%". Note that the numerical values here are just for illustration and arbitrarily selected. Actual values are likely to be obtained only by comparison of (5.4) against in-the-field results.

Analysis From Fig. 7.30, it is observed that the two receive antennas in DUT1 are different. The receive antenna 2 of this handset is vertically polarized. The conventional sensitivity calculation method relies heavily on the sensitivity results of the dominant polarization of the antenna. It is confirmed by the almost identical black and red CDF curves in Fig. 7.30b. The sensitivity measurement in TD mode (TCIS) can benefit from the weaker polarization through MRC. This effect is more obvious for receive antenna 1 as in Fig. 7.30a.

In Fig. 7.31 which presents the TCIS CDF curves of DUT1 with different antenna switched on, the three curves (receive antenna 1 as blue, receive antenna

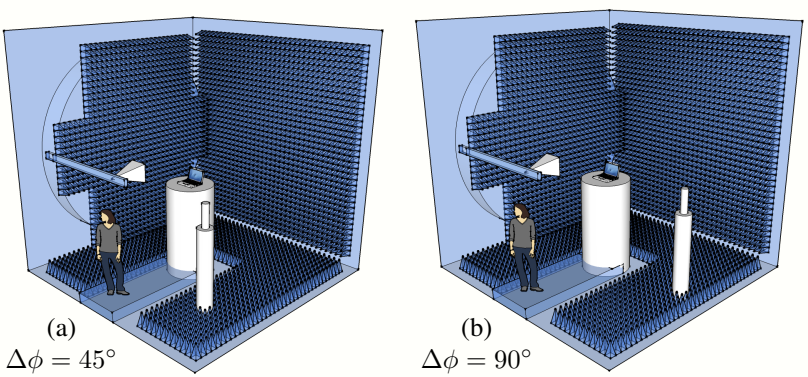

Figure 7.33: Distributed axis chamber with second test antenna positioned at (a) $\Delta\phi = 45°$ and (b) $\Delta\phi = 90°$.

2 as red, two antennas as green) are very similar. This suggests this device does not benefit from having two antennas.

Fig. 7.32 gives an intuitive comparison of the DUTs. The DUT3 with collinear external antenna arrangement (DUT3a in blue) obvious has the best results. Comparing to the other two antenna arrangements of DUT3, the sensitivity measurement in TD mode does not discriminate against arrangements without polarization diversity. This is a confirmation of what being observed in simulations in Subsection 6.4.2 that sensitivity measurement in TD mode is effective in quantifying antenna system efficiency.

7.2.6 Peak throughput measurements in MIMO-favourable scenario

In the peak performance measurement in form of throughput measurement in MIMO-favourable scenario, only DUT3 with external antennas was used. This is because DUT1 and DUT2 support only diversity mode at the time. The procedure generally follows what is described in Subsection 5.3.2 with specifications already given in Subsection 7.2.2. The DL frequency in this case was $2655\,\mathrm{MHz}$ and UL was $2535\,\mathrm{MHz}$ with bandwidth of $10\,\mathrm{MHz}$.

As stated before, the constellations planned for this measurement was equivalent to Fig. 7.25b using a reference dipole / loop set. The polarization was

(a) Sampling grid with $\Delta\phi = 45°$ and $30°$ resolution.

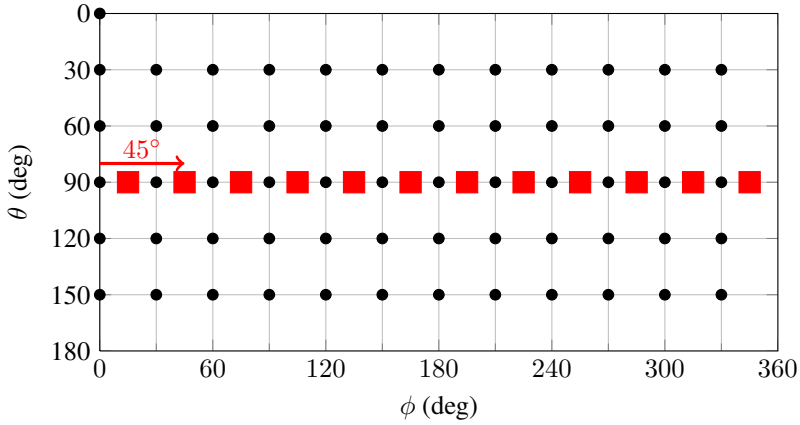

(b) Sampling grid with $\Delta\phi = 90°$ and $30°$ resolution.

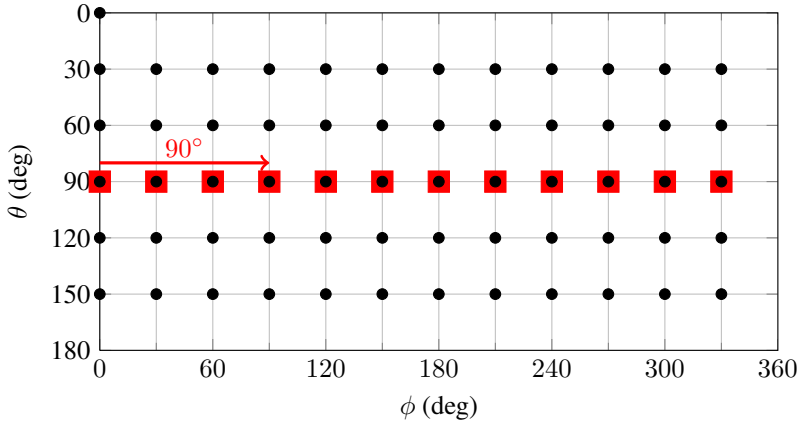

Figure 7.34: Constellations that are measured with setup (a) $\Delta\phi = 45°$ and (b) $\Delta\phi = 90°$ in $30°$ resolution of (θ_1, ϕ_1). Black bullets • represent AOAs of first test antenna (θ_1, ϕ_1), red squares ■ represent AOAs of second test antenna (θ_2, ϕ_2).

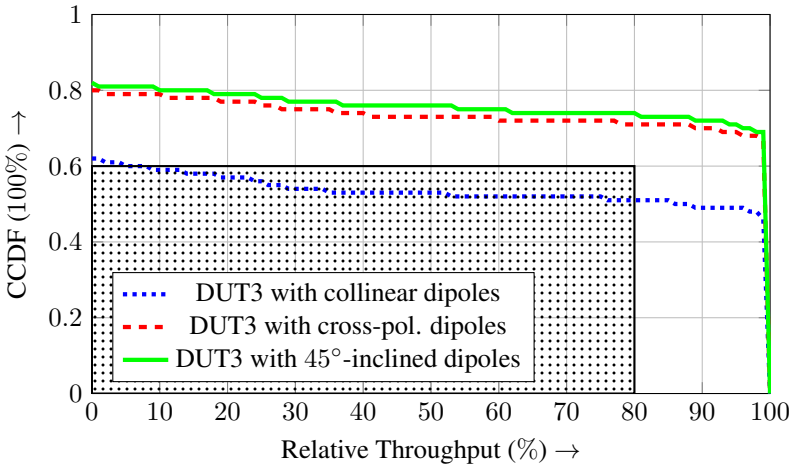

Figure 7.35: E-UTRA band 7 dongle with external antenna in OL-SM mode: throughput statistics for collinear dipoles setup (blue), cross-polarized dipoles setup (red) and 45° polarization inclination (green) at RS EPRE $= -100\,\mathrm{dBm}/15\,\mathrm{kHz}$. Shaded region indicates a possible rejection criterion: "UE should provide at least 80% throughput in 60% of all test cases".

changed by manually replacing the antennas. Instead of $(\theta_1, \phi_1, \theta_2, \phi_2)$, each constellation was presented by $(\theta_1, \phi_1, \Delta\phi)$ where $\Delta\phi = \phi_2 - \phi_1$. The second test antenna was always in the azimuthal plane, hence $\theta_2 = 90°$. To generate constellations, one had to first decide the $\Delta\phi$ and polarization of the second test antenna, the rest, i.e. (θ_1, ϕ_1) movement was realized using existing automation software which in this case was AMS32.

A complete set of constellations would consists all possible $\Delta\phi$ values. Unfortunately due to limited chamber availability, only two cases, that are $\Delta\phi = 45°$ and $\Delta\phi = 90°$ were measured as Fig. 7.33a and b. The resolution of (θ_1, ϕ_1) sampling was 30° and the number of total constellations was 488. Sampling grid for $\Delta\phi = 45°$ case is presented in Fig. 7.34a, $\Delta\phi = 90°$ case in Fig. 7.34b respectively.

The measurement starts with established connection between the BSE and the DUT and a high signal power of RS EPRE $= -90\,\mathrm{dBm}/15\,\mathrm{kHz}$.

1. The power decreases with a large step of $2\,\mathrm{dB}$.
2. At each power level, 1000 frames are transmitted and all BSE report including BLER and throughput are recorded.
3. When the BLER exceeds 0%, the power setting is switched one step back to the last one and the power decreasing step is changed to $1\,\mathrm{dB}$.
4. Repeat 2 until BLER exceeds 80%, the measurement of this point is finished.

Because of the immaturity of software and several compatibility issues, if connection between the BSE and the DUT breaks down, manual reconnection was necessary.

The throughput measurement results in OL-SM mode are given in Fig. 7.35 for all three antenna arrangements with RS EPRE $= -100\,\mathrm{dBm}/15\,\mathrm{kHz}$. The throughput observed for each constellation is weighted in the CCDF with the relative fraction of the surface of the unit sphere it represents, i.e. the data reflect a two-path isotropic PAS. Because the measurement points are not exactly at RS EPRE $= -100\,\mathrm{dBm}/15\,\mathrm{kHz}$ for the DL power level, linear interpolation is used to acquire results.

Similar to the sensitivity measurement results, one may make use of the throughput measurement results in Fig. 7.35 to deliver rejection criteria. The shaded box in Fig. 7.35 illustrates this for the criterion "UE should provide at least 80% throughput in 60% of all test cases". The MNO can specifically tailor this requirement to network conditions and user expectation.

Analysis Despite the fact that the sequence of applied constellations appears insufficient for a full characterization, the results in Fig. 7.35 confirm that we can observe clear differences between the three arrangements. The collinear-polarized arrangement performs worst and one may assume that this observation carries over to in-the-field performance when the other two arrangements benefit from the cross-polarized antennas employed at the BS.

The flatness of the curves is due to the lack of adaptivity support in the measurements. As discussed in Section 4.2, adaptivity of LTE in form of MCS selection, HARQ retransmission and most importantly, mode switching / fallback is the key to utilization of the channel. When measuring in FRC, CL-SM or HARQ retransmission should be available in the measurements. The result of using OL-SM without retransmissions is a rapid transition from 100% to

0% once one of the spatial channels is deteriorated. The results hence contain mostly either 0% or 100% without intermediate ones. In 3GPP Rel-9 and Rel-10, TD is included in all MIMO transmission modes as the fallback mode. It is expected in measurements with CL-SM and fallback to TD, more informative throughput statistics will be obtained.

In addition, separate result plots for the two different $\Delta\phi$ values are presented in Fig. 7.36 with (a) $\Delta\phi = 45^\circ$ and (b) $\Delta\phi = 90^\circ$. It can be seen that the statistics obtained with only two different values of $\Delta\phi$ are not sufficient to characterize all three antenna systems. Differences between the two cases are significant and a larger number of constellations is clearly needed to achieve convergence.

Fig. 7.37 is included to highlight that it is mandatory to include all 4 possible combinations of polarizations of the test antennas. Results obtained with only co-polarized or only cross-polarized test antennas show significant differences.

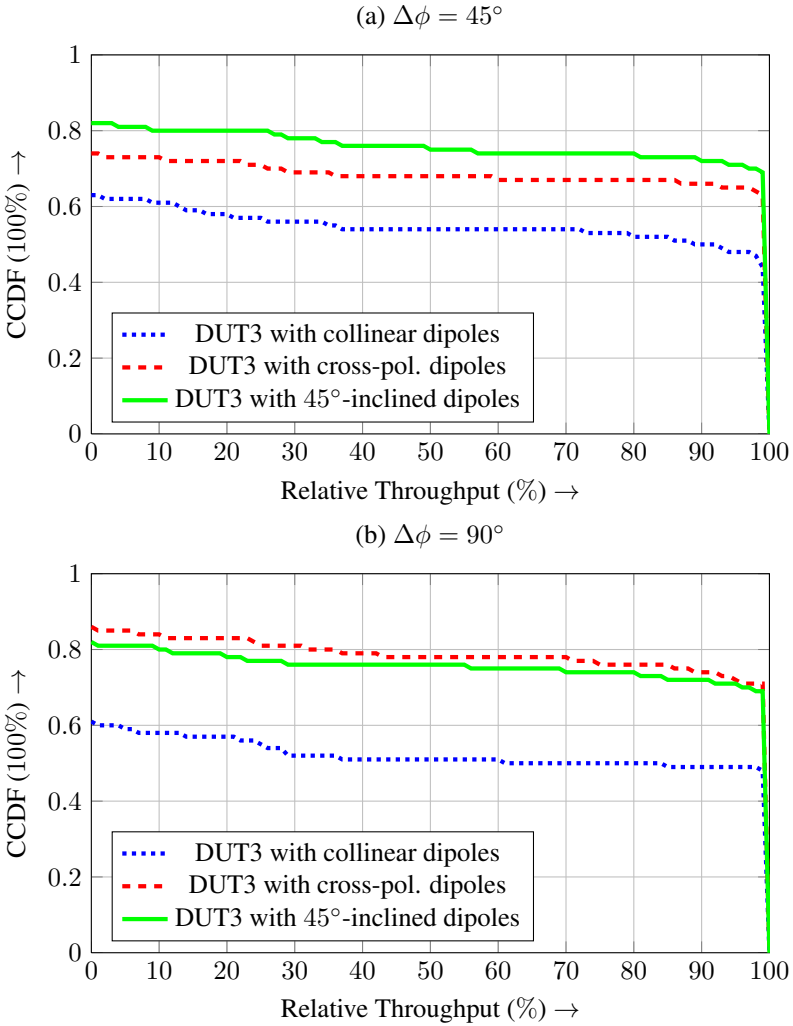

Figure 7.36: E-UTRA band 7 dongle with external antenna in OL-SM mode with constellations (a) $\Delta\phi = 45°$ and (b) $\Delta\phi = 90°$: throughput statistics for collinear dipoles setup (blue), cross-polarized dipoles setup (red) and $45°$ polarization inclination (green) at RS EPRE $= -100\,\mathrm{dBm}\,/15\,\mathrm{kHz}$.

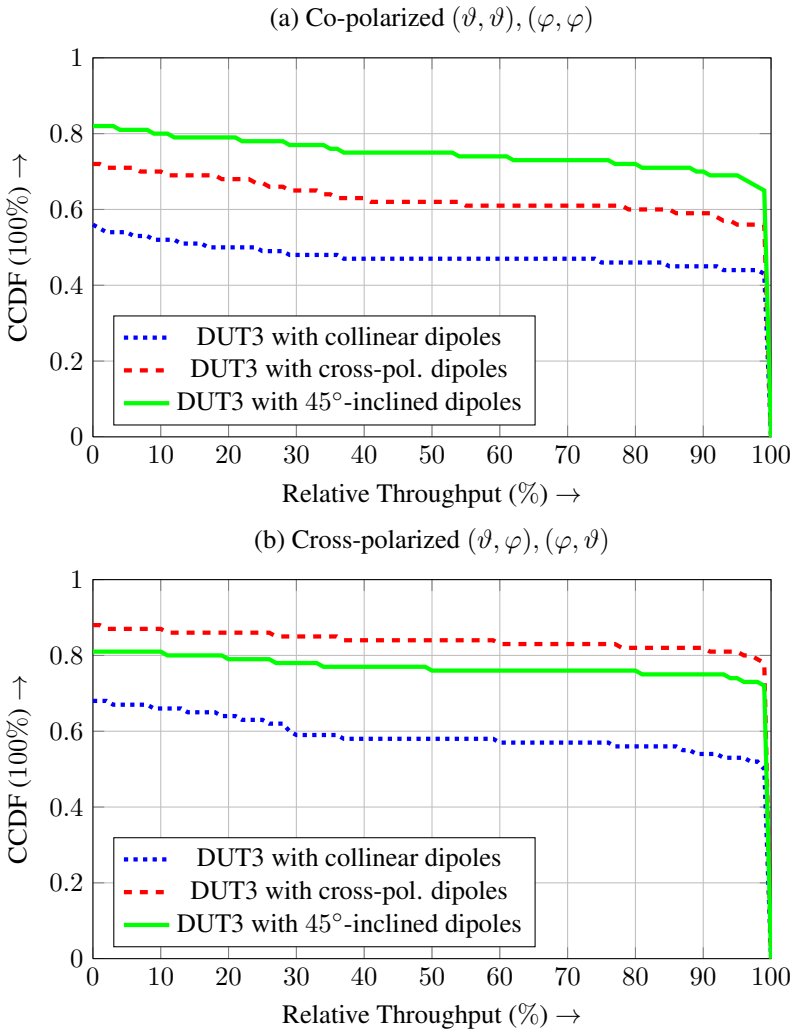

Figure 7.37: E-UTRA band 7 dongle with external antenna in OL-SM mode with (a) with co-polarized constellations $(\vartheta, \vartheta), (\varphi, \varphi)$ and (b) cross-polarized constellations $(\vartheta, \varphi), (\varphi, \vartheta)$: throughput statistics for collinear dipoles setup (blue), cross-polarized dipoles setup (red) and 45° polarization inclination (green) at RS EPRE $= -100\,\mathrm{dBm}\,/15\,\mathrm{kHz}$.

8 Conclusions

This dissertation has investigated the methodologies for MIMO OTA measurements. It starts from a description of existing SISO OTA measurements and the motivation of introducing MIMO OTA measurement methods. A generic antenna model based on compound antenna polarimetric patterns is introduced as well as a propagation model which can be used to describe realistic channels or measurement setups in which a MIMO-enabled terminal is tested. A discussion of the relevance of UE antenna system attributes and channel properties is given.

Every MIMO measurement proposal introduced so far is described using these models and analyzed for its advantages and drawbacks. The motivation of each method is thoroughly presented and discussed. Difference in measurement setups are summarized and their relevance are investigated. Observations and questions raised in this process are addressed and corresponding solutions proposed.

A straightforward test approach which focuses on direct characterization of the physical attributes of UE is presented. Statistical metrics are adopted to adequately represent the variety of possible propagation scenarios. The approach is of low complexity and allows for reuse of existing test sites and equipment. The relevant device properties are covered by two complementary test cases:

The first test case covers total antenna system efficiency, receiver noise figure and self-interference. It bears similarity to traditional TIS measurement in SISO OTA tests. Existing anechoic chambers designed for SISO OTA measurements can be directly used. The statistical metric which is reported directly maps to in-the-field outage probability. Similar to TIS, this FOM gives clear indication of the total antenna system efficiency. In addition, since this test case can be indiscriminately applied to devices with any number of antennas, existence of diversity schemes can be easily observed in the statistics representation.

The second test case covers modal imbalance, pattern and polarization selectivity. The measurement setup in this case realizes a maximum rank channel.

Instead of introducing many test antennas and expensive equipment, this test case requires minimum modification to existing anechoic chambers. Only rotate mechanisms that are already been used in SISO OTA measurements are required in the process of realizing 3D measurements with two AOAs via independently movable test antennas. The statistical metric which is reported describes the probability of attaining theoretical peak throughput in SM mode. The FOM can be tailored specifically according to network conditions and reflects user experience in-the-field.

Simulations are presented for both canonical examples and realistic antenna designs. Part of the results focuses on verification of the test approach and the rest aims at investigating the specific aspects mentioned in earlier chapter to address their relevance and practical limitations. The test plan fulfills its promise in the simulations, showing it is capable to discriminate between "good" and "bad" devices. At the same time, the test plan does not have preferences in a specific type of device design. This is important in the commercial certification process. The simulations also confirm that economization of measurements method can only be achieved by limiting the number of constellations to be measured after the convergence of statistical FOMs. Other approaches including limiting measurements to the azimuthal plane or restricting to measurements with fixed polarization will lead to grossly misleading results.

Results of two rounds of measurement are also presented. One of the two is applied to HSPA devices in participation of the COST 2100 Round-Robin measurement campaign. The effort invested in this international activity was to conceptually check the test approach on "legacy" devices with no TD or SM mode support. In another round of measurements LTE devices with different form-factors were tested. The extensive examples support the conclusion that the test plan is suitable for evaluation of device performance. Some of the features from other proposals are also included in the measurements for the purpose of comparison. Introducing pre-fading, as discussed in an earlier chapter, does not convey useful information but introduced further averaging into the measurement result. Measurements had been done with many different constellation sets and the results support the conclusion that to correctly quantify device performance, constellation sets have to be carefully selected.

The approach which is suggested in this dissertation, as well as all other proposed MIMO OTA measurement methods still requires for a final validation by thorough comparison between lab results and in-the-field observation to verify its capability to predict device performance.

Abbreviations

3GPP	3rd Generation Partnership Project
AOA	Angle of Arrival
AOD	Angle of Departure
AS	Angular Spread
AUT	Antenna Under Test
AWGN	Additive White Gaussian Noise
BER	Bit Error Rate
BLER	Block Error Rate
BS	Basestation
BSE	Basestation Emulator
CCDF	Complementary Cumulative Distribution Function
CDF	Cumulative Distribution Function
CECC	Complex Envelope Correlation Coefficient
CL-SM	Closed-loop Spatial Multiplexing
CQI	Channel Quality Indication
CSI	Channel State Information
DL	Downlink
DUT	Device Under Test
EIS	Equivalent Isotropic Sensitivity
EMC	Electromagnetic Compatibility
eNB	evolved Node-B
E-UTRA	Evolved Universal Terrestrial Radio Access
EVM	Error Vector Magnitude
FOM	Figure of Merit
FRC	Fixed Reference Channel
FSL	Free Space Loss
GSCM	Geometry-Based Stochastic Channel Model
GSM	Global System for Mobile Communications
HARQ	Hybrid Automatic Repeat Request

HSPA	High-Speed Packet Access
LD-CDD	Large-delay Cyclic Delay Diversity
LHS	Left-Hand-Side
LO	Local Oscillator
LOS	Line of Sight
LS	Least-square
LTE	Long Term Evolution
MCS	Modulation and Coding Scheme
MIMO	Multiple Input – Multiple Output
MISO	Multiple Input – Single Output
MMSE	Minimum Mean-Square Error
MNO	Mobile Network Operator
MRC	Maximum Ratio Combining
OFDM	Orthogonal Frequency Division Multiplex
OL-SM	Open-loop Spatial Multiplexing
OTA	Over-The-Air
PAS	Power Angular Spectrum
PDF	Probability Density Function
PIFA	Planar Inverted-F Antenna
PL	Path Loss
PMI	Precoding Matrix Indicator
QAM	Quadrature Amplitude Modulation
QPSK	Quaternary Phase-Shift Keying
RB	Resource Block
RD	Receive Diversity
RF	Radio Frequency
RHS	Right-Hand-Side
RI	Rank Indication
RSRQ	Reference Signal Received Quality
SCME	3GPP Spatial Channel Model Extended
SFBC	Space-Frequency Block Coding
SIMO	Single Input – Multiple Output
SISO	Single Input – Single Output
SM	Spatial Multiplexing

SNIR	Signal to Noise and Interference Ratio
SNR	Signal-to-Noise Ratio
STBC	Space-Time Block Code
TCIS	Total Compound Isotropic Sensitivity
TDL	Tapped Delay Line
TD	Transmit Diversity
TIS	Total Isotropic Sensitivity
TRP	Total Radiated Power
UE	User Equipment
UL	Uplink
UMTS	Universal Mobile Telecommunications System
VNA	Vector Network Analyzer
WINNER	Wireless World Initiative New Radio
ZF	Zero Forcing

List of Symbols

σ	Standard deviation	98
$\mathrm{S}_1(0)$	Unit sphere	18
$(\cdot)^\top$	Transpose	10
φ	Horizontal polarization	9
ϑ	Vertical polarization	9
$\boldsymbol{a}$	Incoming wave quantity (TX $\rightarrow$ antenna)	9
$\boldsymbol{b}$	Outgoing wave quantity (antenna $\rightarrow$ RX)	9
$\boldsymbol{b}_0$	Received wave quantity	10
$\boldsymbol{E}$	Electric field	10
$\boldsymbol{n}$	Thermal noise vector	19
$\boldsymbol{r}$	Received signal vector	18
$\boldsymbol{r}_\mathrm{S}$	Self-interference	19
$\boldsymbol{s}$	Transmitted signal vector	17
$\boldsymbol{T}_n$	Per-port compound polarimetric pattern (of port n)	9
$\boldsymbol{w}$	Interfering signal vector	17
$\widehat{\mathbf{C}}$	Constellation of transmitted signals	17
$\widehat{\mathbf{D}}$	Constellation of interfering signals	17
$\widehat{\boldsymbol{C}}_m$	Constellation of m-th transmitted signal stream	17
B	Bandwidth	19
C	Channel capacity	21
F	Receiver noise figure	18
h	Channel coefficient	20
k_0	Wavenumber in free space	10
k_B	Boltzmann constant	19
P_avail	Available power	10
P_thr	Threshold radiated power	42
r	Radius from the source	10
T	Absolute temperature (in Kelvin)	19
t	Throughput	56
Z_0	Free space impedance	10

References

[1] *User Equipment (UE) / Mobile Station (MS) over the air (OTA) antenna performance; Conformance testing (Release 8)*, 3GPP TS 34.114, Rev. 8.0.0, Dec. 2008.

[2] *Test Plan for Mobile Station Over the Air Performance Rev 3.1*, CTIA – The Wireless Association Std., Jan. 2011.

[3] RP-080766. (2008, Sep.) LS on status of radiated testing methods for MIMO/multiple receive antenna terminals. [Online]. Available: www.3gpp.org/LiaisonsDocs/Outgoing_LSs/Rp-41-meeting.htm

[4] *Measurement of radiated performance for MIMO and multi-antenna reception for HSPA and LTE terminals (Release 10)*, 3GPP TR 37.976, Rev. 1.5.0, May 2011.

[5] D. Kurita, Y. Okano, S. Nakamatsu, and T. Okada, "Experimental comparison of MIMO OTA testing methodologies," in *Proceedings of the 4th European Conference on Antennas and Propagation (EuCAP '10)*, Barcelona, Spain, Apr. 2010, pp. 1–5.

[6] W. L. Schroeder and Y. Feng, "A critical review of MIMO OTA test concepts – lessons learned from actual measurements," in *XXXth URSI General Assembly and Scientific Symposium (11' URSI-GASS)*, Istanbul, Turkey, Aug. 2011, pp. 1–4.

[7] S. Prather, "Comparison of OTA test results from anechoic and reverberation chambers," in *COST 2100, 11th MCM*, Aalborg, Denmark, Jun. 2010, TD(10)11100. [Online]. Available: www.cost2100.org

[8] Y. Feng, A. Krewski, and W. L. Schroeder, "Simulation based comparison of metrics and measurement methodologies for OTA test of MIMO terminals," in *Proceedings of the 4th European Conference on Antennas and Propagation (EuCAP '10)*, Barcelona, Spain, Apr. 2010, pp. 1–5.

[9] Vodafone Group. (2012, Feb.) RP-120272: Verification of radiated multi-antenna reception performance of UEs in LTE/UMTS. [Online]. Available: http://www.3gpp.org

[10] I. Szini, "Reference antennas proposal for MIMO OTA," in *COST IC1004 2nd MCM*, Lisbon, Portugal, Oct. 2011, TD(11)02009. [Online]. Available: www.ic1004.org

[11] P.-S. Kildal, X. Chen, C. Orlenius, M. Franzén, and C. L. Patané, "Characterization of reverberation chambers for OTA measurements of wireless devices: Physical formulations of channel matrix and new uncertainty formula," *IEEE Trans. Antennas Propagat.*, vol. PP, 2012, to be published, Early Access Article.

[12] K. Rosengren, P.-S. Kildal, J. Carlsson, and O. Lundén, "A new method to measure radiation efficiency of terminal antennas," in *IEEE-APS Conference on Antennas and Propagation for Wireless Communications, 2000*, Waltham, MA, Nov. 2000, pp. 5–8.

[13] P.-S. Kildal, "Definition of effective diversity gain and how to measure it in a reverberation chamber," *Microwave and Optical Technology Letters*, vol. 34, no. 10, pp. 56–59, 2001.

[14] K. Rosengren, P.-S. Kildal, C. Carlsson, and J. Carlsson, "Characterization of antennas for mobile and wireless terminals by using reverberation chambers: improved accuracy by platform stirring," in *IEEE Antennas and Propagation Society International Symposium, 2001*, vol. 3, Boston, MA, Jul. 2001, pp. 350–353.

[15] P.-S. Kildal and C. Orlenius, "TRP and TIS/AFS measurements of mobile stations in reverberation chambers (RC)," Mar. 2009, CTIA Certification Program Working Group Contribution RCSG099401.

[16] M. Rumney, "Efficacy criteria of MIMO OTA test," in *COST 2100, 9th MCM*, Vienna, Austria, Sep. 2009, TD(09)925. [Online]. Available: www.cost2100.org

[17] J. W. Wallace and M. A. Jensen, "Termination-dependent diversity performance of coupled antennas: Network theory analysis," *IEEE Transactions on Antennas and Propagation*, vol. 52, no. 1, pp. 98–105, Jan. 2004.

[18] W. L. Schroeder and A. Krewski, "Total multi-port return loss as a figure of merit for MIMO antenna systems," in *European Microwave Conference (EuMC)*, Paris, Sep. 2010, pp. 1742–1745.

[19] A. Krewski, "private communication."

[20] M. Rumney, "Selecting figures of merit and developing performance requirements for MIMO OTA," in *COST 2100, 10th MCM*, Athens, Greece, Feb. 2010, TD(10)10028. [Online]. Available: www.cost2100.org

[21] *Evolved Universal Terrestrial Radio Access (E-UTRA); Radio Frequency (RF) system scenarios; (Release 9)*, 3GPP TR 36.942, Rev. 9.2.0, Dec. 2009.

[22] S. M. Alamouti, "A simple transmit diversity technique for wireless communications," *IEEE J. of Selected Areas in Communications*, vol. 16, no. 8, pp. 1451–1458, Oct. 1998.

[23] Y. Feng and W. L. Schroeder, "Extending the definition of total isotropic sensitivity (TIS) and total radiated power (TRP) for application to MIMO over-the-air (OTA) testing," in *COST 2100, 8th MCM*, Valencia, Spain, May 2009, TD(09)866. [Online]. Available: www.cost2100.org

[24] R. Tian, B. K. Lau, and Z. Ying, "Multiplexing efficiency of MIMO antennas," in *Antennas and Wireless Propagation Letters, IEEE*, vol. 10, 2011, pp. 183–186.

[25] R5-070371. (2007, Feb.) New work item proposal: Conformance test aspects - multiple input multiple output antennas (MIMO) for FDD. 3GPP TSG-RAN5 Meeting #34. [Online]. Available: http:/www.3gpp.org

[26] R4-103763. (2010, Oct.) COST2100 MIMO OTA Round Robin Measurement Campaign, summer 2010 - first results & conclusions from measurements performed at RheinMain University of Applied Sciences -. [Online]. Available: http://www.3gpp.org

[27] Z. Wen, Y. Jing, and H. Kong, "MIMO OTA round robin test report: throughput measurement results for multiple probe antenna based method and two-stage method," in *COST 2100, 12th MCM*, Bologna, Italy, Nov. 2010, TD(10)12055. [Online]. Available: www.cost2100.org

[28] Y. Jing, Z. Wen, and H. Kong, "MIMO OTA round robin test report: capacity, correlation and power imbalance measurement results for multiple probe antenna based method and two-stage method," in *COST 2100, 12th MCM*, Bologna, Italy, Nov. 2010, TD(10)12056. [Online]. Available: www.cost2100.org

[29] C. L. Patené, A. Skårbratt, M. Franzén, J. Åsberg, C. Orlenius, and L. Carlén, "OTA round robin measurement campaign: Experiences from measurements in reverberation chambers," in *COST 2100, 12th MCM*, Bologna, Italy, Nov. 2010, TD(10)12082. [Online]. Available: www.cost2100.org

[30] Y. Feng, J. Jonas, W. Schroeder, R. Acharkaoui, and M. Rumney, "Results from the COST2100 SWG 2.2 MIMO OTA Round Robin Measurement Campaign," in *COST 2100, 12th MCM*, Bologna, Italy, Nov. 2010, TD(10)12086. [Online]. Available: www.cost2100.org

[31] C. von Gagern and A. Tankielun, "Report on test results from the RAN4 round robin test on LTE MIMO devices," in *COST IC1004 1st MCM*, Lund, Sweden, Jun. 2011, TD(11)01046. [Online]. Available: www.ic1004.org

[32] A. Scannavini, "LTE MIMO OTA round robin testing results," in *COST IC1004 1st MCM*, Lund, Sweden, Jun. 2011, TD(11)01052. [Online]. Available: www.ic1004.org

[33] D. Reed and M. Foegelle, "3GPP round robin OTA measurement results, pool 3," in *COST IC1004 1st MCM*, Lund, Sweden, Jun. 2011, TD(11)01056. [Online]. Available: www.ic1004.org

[34] H. Kong, Y. Jing, X. Zhao, M. Rumney, and S. Duffy, "Preliminary LTE MIMO OTA test results using two-stage method," in *COST IC1004 1st MCM*, Lund, Sweden, Jun. 2011, TD(11)01062. [Online]. Available: www.ic1004.org

[35] P. Kyösti, T. Jäsmä, and J.-P. Nuutinen, "Channel modelling for multiprobe over-the-air MIMO testing," *International Journal of Antennas and Propagation*, vol. 2012, no. 615954, 2012. [Online]. Available: http://www.hindawi.com/journals/ijap/2012/615954/

[36] P. Kyösti, J. Kolu, J.-P. Nuutinen, and M. Falck, "OTA testing for multiantenna terminals," in *COST 2100 6th MCM*, Lille, Oct. 2008, TD(08)670. [Online]. Available: www.cost2100.org

[37] A. Scannavini, L. Foged, K. Rutkowski, P. Iversen, and S. Issartel, "Radiated performance testing of diversity and MIMO enabled terminals," in *COST 2100 6th MCM*, Lille, Oct. 2008, TD(08)618. [Online]. Available: www.cost2100.org

[38] J. Krogerus, P. Mäkikyrö, and P. Vainikainen, "Towards an applicable OTA test method for multi-antenna terminals," in *COST2100 6th MCM*, Lille, Oct. 2008, TD(08)671. [Online]. Available: www.cost2100.org

[39] J. Welinder, P. Hallbjörner, T. Bolin, and Z. Ying, "Multipath simulator - over-the-air test equipment," in *COST2100 7th MCM*, Braunschweig, Feb. 2009, TD(09)704. [Online]. Available: www.cost2100.org

[40] J. Takada, "Handset MIMO antenna testing using a RF-controlled spatial fading emulator," in *COST2100 7th MCM*, Braunschweig, Feb. 2009, TD(09)742. [Online]. Available: www.cost2100.org

[41] J.-P. Nuutinen, P. Kyösti, M. Falck, P. Heino, H. Lehtinen, and T. Jääskö, "Experimental investigations of OTA system," in *COST2100 7th MCM*, Braunschweig, Feb. 2009, TD(09)753. [Online]. Available: www.cost2100.org

[42] P. Kyösti, J.-P. Nuutinen, and T. Jämsä, "MIMO OTA test concept with experimental and simulated verification," in *Proceedings of the 4th European Conference on Antennas and Propagation (EuCAP '10)*, Barcelona, Spain, Apr. 2010, pp. 1–5.

[43] P. Kyösti, J.-P. Nuutinen, and M. Falck, "Proposal for standardized test procedure for OTA testing of multi-antenna terminals," in *COST2100 7th MCM*, Braunschweig, Feb. 2009, TD(09)766. [Online]. Available: www.cost2100.org

[44] J. Krogerus, M. Nurkkala, and P. Mäkikyrö, "Discussion on some topical issues related to the spatial fading emulation based OTA test method for multi-antenna terminals," in *COST2100 7th MCM*, Braunschweig, Feb. 2009, TD(09)780. [Online]. Available: www.cost2100.org

[45] J. Welinder, L. Fast, T. Bolin, and L. Manholm, "Towards a low cost over the air performance test method," in *COST2100 8th MCM*, no. 07, Valencia,Spain, May 2009. [Online]. Available: www.cost2100.org

[46] A. Scannavini, J.-P. Nuutinen, P. Heino, L. Durand, M. A. E. Anouar, and F. T. Talom, "Practical considerations on MIMO OTA testing," in *COST 2100, 8th MCM*, Valencia, Spain, May 2009, TD(09)854. [Online]. Available: www.cost2100.org

[47] A. Scannavini, L. J. Foged, M. A. E. Anouar, N. Gross, and J. Estrada, "OTA throughput measurements by using spatial fading emulation technique," in *Proceedings of the 4th European Conference on Antennas and Propagation (EuCAP '10)*, Barcelona, Spain, Apr. 2010, pp. 1–5.

[48] A. Scannavini, L. J. Foged, and N. Gross, "OTA throughput testing of multi-antenna terminals by using StarMIMO test range," in *Proceedings of the 5th European Conference on Antennas and Propagation (EuCAP '11)*, Rome, Italy, Apr. 2011, pp. 1554–1557.

[49] A. Yamamoto, "MIMO performance evaluation in a street microcell using a spatial fading emulator in comparison with a radio propagation test," in *COST 2100, 9th MCM*, Vienna, Austria, Sep. 2009, TD(09)912. [Online]. Available: www.cost2100.org

[50] T. Sakata, "Throughput measurement of MIMO array on WLAN IEEE 802.11n system using a RF-controlled spatial fading emulator," in *COST 2100, 9th MCM*, Vienna, Austria, Sep. 2009, TD(09)920. [Online]. Available: www.cost2100.org

[51] J. Kallankari, S. Laukkanen, J. Nuutinen, P. Kyösti, and A. Scannavini, "Test plan for OTA throughput comparison measurements in a fading channel environment," in *COST2100, 9th MCM*. Vienna, Austria: Nokia, Elektrobit and Satimo, Sep. 2009, TD(09)964. [Online]. Available: www.cost2100.org

[52] J.-P. Nuutinen, P. Kyösti, J. Malm, and M. Foegelle, "Experimental investigations of MIMO performance of IEEE802.11n device in MIMO OTA test system," in *COST2100, 9th MCM*. Vienna, Austria: Elektrobit and ETS-Lindgren, Sep. 2009, TD(09)972. [Online]. Available: www.cost2100.org

[53] P. Kyösti, J.-P. Nuutinen, and A. Byman, "Verification of MIMO OTA set-up via simulations and measurements," in *COST2100, 9th MCM*. Vienna, Austria: Elektrobit, Sep. 2009, TD(09)990. [Online]. Available: www.cost2100.org

[54] A. Yamamoto, "Procedure of designing the structural parameters of a spatial fading emulator with a laplacian angular power spectrum of incoming wave," in *COST 2100, 10th MCM*, Athens, Greece, Feb. 2010, TD(10)10016. [Online]. Available: www.cost2100.org

[55] T. Hayashi, "Effect of delay waves on MIMO OTA throughput evaluation of a handset MIMO array using a spatial fading emulator," in *COST 2100, 10th MCM*, Athens, Greece, Feb. 2010, TD(10)10018. [Online]. Available: www.cost2100.org

[56] X. Gao, X. Wang, B. K. Lau, and T. Bolin, "On simplifying WINNER II channel model for MIMO OTA performance evaluation," in *Proceedings of the 5th European Conference on Antennas and Propagation (EuCAP '11)*, Rome, Italy, Apr. 2011, pp. 2942–2946.

[57] T. Laitinen, P. Kyösti, T. Jämsä, and P. Vainikainen, "Generation of a power angular spectrum of a single cluster in a MIMO-OTA test system based on multiple OTA antennas," in *COST 2100, 11th MCM*, Aalborg, Denmark, Jun. 2010, TD(10)11054. [Online]. Available: www.cost2100.org

[58] P. Kyösti and L. Hentilä, "Criteria for physical dimensions of MIMO OTA multi-probe test set-up," in *2012 6th European Conference on Antennas and Propagation (EuCAP)*, Prague, Czech, Mar. 2012, pp. 2055–2059.

[59] A. Byman, L. Rudant, J.-P. Nuutinen, T. Jämsä, and J. Meinilä, "MIMO OTA system performance measurement of a compact MIMO antenna," in *COST 2100, 11th MCM*, Aalborg, Denmark, Jun. 2010, TD(10)11055. [Online]. Available: www.cost2100.org

[60] P.-S. Kildal, "Comparison of small antenna performance in horizontal 2-D and isotropic 3-D multipath environments," in *COST 2100, 10th MCM*, Athens, Greece, Feb. 2010, TD(10)10037. [Online]. Available: www.cost2100.org

[61] S. Obayashi, T. Ohishi, and Y. Karasawa, "Effect of vertical angle spread of propagation channel on MIMO OTA measurement method," in *Asia-Pacific Microwave Conference Proceedings (APMC)*, Yokohama, Dec. 2010, pp. 1934–1937.

[62] W. A. T. Kotterman, A. Heuberger, and R. S. Thomä, "On the accuracy of synthesised wavefields in MIMO-OTA set-ups," in *Proceedings of the 5th European Conference on Antennas and Propagation (EuCAP '11)*, Rome, Italy, Apr. 2011, pp. 2560–2564.

[63] D. Reed, "Measuring device antennas with spatial and uniform channels," in *COST 2100, 10th MCM*, Athens, Greece, Feb. 2010, TD(10)10092. [Online]. Available: www.cost2100.org

[64] P. Hallbjörner, J. Welinder, and T. Bolin, "Mutual coupling in multipath simulator antenna array and its impact on measurement accuracy," in *COST 2100, 11th MCM*, Aalborg, Denmark, Jun. 2010, TD(10)11003. [Online]. Available: www.cost2100.org

[65] D. Parveg, T. Laitinen, A. Khatun, and V.-M. Kolmonen, "MIMO-OTA EM calibration procedure," in *COST IC1004 2nd MCM*, Lisbon, Portugal, Oct. 2011, TD(11)02060. [Online]. Available: www.ic1004.org

[66] W. Fan, J. O. Nielsen, X. Carreño, O. Franek, M. B. Knudsen, and G. F. Pedersen, "Impact of probe placement error on MIMO OTA test zone performance," in *COST IC1004 3rd MCM*, Barcelona, Spain, Feb. 2012, TD(12)03044. [Online]. Available: www.ic1004.org

[67] M. Foegelle, "Calibration and validation of an anechoic chamber based MIMO OTA system," in *COST 2100, 11th MCM*, Aalborg, Denmark, Jun. 2010, TD(10)11102. [Online]. Available: www.cost2100.org

[68] L. Garcia-Garcia, B. Lindmark, N. Jaldén, and C. Orlenius, "MIMO capacity of antenna arrays evaluated using radio channel measurements, reverberation chamber and radiation patterns," *Microwaves, Antennas and Propagation, IET*, vol. 1, no. 6, pp. 1160–1169, Dec 2007.

[69] T. A. Laitinen, J. Krogerust, M. Mustonen, P. Suvikunnas, J. Villanen, C. Icheln, and P. Vainikainen, "From the radiation pattern measurements towards true performance evaluation of mobile terminal antennas," in *The 2nd European Conference on Antennas and Propagation (EuCAP)*, vol. 1, no. 6, Nov 2007, pp. 1–6.

[70] M. A. Garcia-Fernandez, J. P. Hidalgo, A. Torrecilla, and D. Sánchez-Hernández, "Evaluation of MIMO OTA parameters for LTE using a mode-stirred reverberation chamber," in *COST 2100, 12th MCM*, Bologna, Italy, Nov. 2010, TD(10)12073. [Online]. Available: www.cost2100.org

[71] C. Orlenius, C. L. Patané, A. Skårbratt, J. Åsberg, and M. Franzén, "Analysis of MIMO OTA measurements for LTE terminals performed in reverberation chamber," in *2012 6th European Conference on Antennas and Propagation (EuCAP)*, Prague, Czech, Mar. 2012, pp. 1934–1938.

[72] P.-S. Kildal, C. Orlenius, and J. Carlsson, "OTA testing in multipath of antennas and wireless devices with MIMO and OFDM," *Proceedings of IEEE*, vol. PP, May 2012, to be published, Early Access Article.

[73] C. Orlenius, M. Franzén, P.-S. Kildal, and U. Carlberg, "Investigation of heavily loaded reverberation chamber for testing of wideband wireless units," in *IEEE Antennas and Propagation Society International Symposium 2006*, Albuquerque, NM, Jul. 2006, pp. 3569–3572.

[74] P.-S. Kildal, C. Orlenius, and U. Carlberg, "MIMO LTE OTA measurements in reverberation chamber: Rich isotropic reference environment makes agreement with theoretical system model," in *2012 6th European Conference on Antennas and Propagation (EuCAP)*, Prague, Czech, Mar. 2012.

[75] P.-S. Kildal and C. Carlsson, "Detection of a polarization imbalance in reverberation chambers and how to remove it when measuring antenna efficiencies," *Microwave and Optical Technology Letters*, vol. 34, no. 2, pp. 145–149, Jul. 2002.

[76] N. Arsalane, M. Mouhamadou, C. Decroze, D. Carsenat, M. A. Garcia-Fernandez, and T. Monedière, "3GPP channel model emulation with analysis of MIMO-LTE performances in reverberation chamber," *International Journal of Antennas and Propagation*, vol. 2012, no. 239420, 2012. [Online]. Available: http://www.hindawi.com/journals/ijap/2012/239420/

[77] M. Franzén, C. Orlenius, D. Kurita, and Y. Okano, "Comparison of MIMO OTA performance characteristics as measured in reverberation chamber and spatial fading emulator," in *COST 2100, 10th MCM*, Athens, Greece, Feb. 2010, TD(10)10084. [Online]. Available: www.cost2100.org

[78] J. D. Sánchez-Heredia, P. Hallbjörner, and T. Bolin, "Throughput comparison with the same set of phones in multipath simulator and reverberation chamber," in *COST IC1004 1st MCM*, Lund, Sweden, Jun. 2011, TD(11)01022. [Online]. Available: www.ic1004.org

[79] D. A. Hill, M. T. Ma, A. R. Ondrejka, B. F. Riddle, M. L. Crawford, and R. T. Johnk, "Aperture excitation of electrically large, lossy cavities," *IEEE Trans. Electromagn. Compat.*, vol. 36, pp. 169–178, Aug. 1994.

[80] S. Prather, "Standardized calibration and test methodology for TRP / TIS measurement in reverberation chambers," in *COST 2100, 11th MCM*, Aalborg, Denmark, Jun. 2010, TD(10)11101. [Online]. Available: www.cost2100.org

[81] C. L. Patané and M. Franzén, "MIMO LTE round robin: Results, accuracy and repeatability," in *COST IC1004 1st MCM*, Lund, Sweden, Jun. 2011, TD(11)01029. [Online]. Available: www.ic1004.org

[82] Y. Jing, Z. Wen, H. Kong, S. Duffy, and M. Rumney, "Two-stage MIMO OTA method," in *COST 2100, 9th MCM*, Vienna, Austria, Sep. 2009, TD(09)924. [Online]. Available: www.cost2100.org

[83] ——, "Two-stage over the air (OTA) test method for MIMO device performance evaluation," in *IEEE International Symposium on Antennas and Propagation (APSURSI)*, Jul. 2011, pp. 71–74.

[84] Agilent. (2012, Mar.) R4-121980: Estimating receiver desensitization from UE SINR (RSRQ) measurements. [Online]. Available: http://www.3gpp.org

[85] W. L. Schroeder and Y. Feng, "Proposal for a built-in MIMO test function for E-UTRA user equipment and its application," in *COST 2100, 8th MCM*, Valencia, Spain, May 2009, TD(09)853. [Online]. Available: www.cost2100.org

[86] Agilent. (2012, Mar.) R4-121981: Definition of UE measurements in support of the two-stage MIMO OTA test method. [Online]. Available: http://www.3gpp.org

[87] J.-P. Nuutinen, P. Kyösti, and A. Byman, "Effect of channel model simplification on throughput in MIMO OTA," in *COST2100, 9th MCM*. Vienna, Austria: Elektrobit and ETS-Lindgren, Sep. 2009, TD(09)971. [Online]. Available: www.cost2100.org

[88] L. Manholm, "Discussion on channel conditions for MIMO OTA measurements," in *COST2100, 9th MCM*. Vienna, Austria: Ericsson, Sep. 2009, TD(09)978. [Online]. Available: www.cost2100.org

[89] H. Kong, Y. Jing, Z. Wen, S. Duffy, and M. Rumney, "MIMO OTA channel model comparison, analysis and recommendations," in *COST 2100, 10th MCM*, Athens, Greece, Feb. 2010, TD(10)10048. [Online]. Available: www.cost2100.org

[90] I. Szini, "Simplified SCME MIMO OTA test method," in *COST IC1004 1st MCM*, Lund, Sweden, Jun. 2011, TD(11)01006. [Online]. Available: www.ic1004.org

[91] ——, "Simplified SCME test method," in *COST IC1004 2nd MCM*, Lisbon, Portugal, Oct. 2011, TD(11)02010. [Online]. Available: www.ic1004.org

[92] C. L. Patané and M. Franzén, "MIMO LTE round robin: Analysis," in *COST IC1004 1st MCM*, Lund, Sweden, Jun. 2011, TD(11)01030. [Online]. Available: www.ic1004.org

[93] P. Kyösti and L. Hentilä, "Playback of measured radio channel data in MIMO OTA test set-up," in *COST IC1004 4th MCM*, Lyon, France, May 2012, TD(12)04048. [Online]. Available: www.ic1004.org

[94] T. Laitinen, P. Kyösti, J.-P. Nuutinen, and P. Vainikainen, "On the number of OTA antenna elements for plane-wave synthesis," in *Proceedings of the 4th European Conference on Antennas and Propagation (EuCAP '10)*, Barcelona, Spain, Apr. 2010, pp. 1–5.

[95] ——, "On the number of OTA antenna elements for plane-wave synthesis in a MIMO OTA test system involving circular antenna array," in *COST2100, 9th MCM*. Vienna, Austria: TKK and Elektrobit, Sep. 2009, TD(09)976. [Online]. Available: www.cost2100.org

[96] A. Khatun, T. Laitinen, V.-M. Kolmonen, and P. Vainikainen, "Dependence of error level on the number of probes in over-the-air multiprobe test systems," *International Journal of Antennas and Propagation*, vol. 2012, no. 624174, 2012. [Online]. Available: http://www.hindawi.com/journals/ijap/2012/624174/

[97] T. Imai, Y. Okano, K. Kitao, K. Saito, and S. Miura, "Theoretical analysis of adequate number of probe antennas in spatial channel emulator for MIMO performance evaluation of mobile terminals," in *COST 2100, 9th MCM*, Vienna, Austria, Sep. 2009, TD(09)931. [Online]. Available: www.cost2100.org

[98] Y. Okano, K. Kitao, and T. Imai, "Impact of number of probe antennas for MIMO OTA spatial channel emulator," in *Proceedings of the 4th European Conference on Antennas and Propagation (EuCAP '10)*, Barcelona, Spain, Apr. 2010, pp. 1–5.

[99] *Evolved Universal Terrestrial Radio Access (E-UTRA); Physical layer procedures (Release 8)*, 3GPP TS 36.213, Rev. 8.4.0, 2008.

[100] Y. Okano, "Impact of number of probe antennas for MIMO OTA spatial channel emulator," in *COST 2100, 9th MCM*, Vienna, Austria, Sep. 2009, TD(09)929. [Online]. Available: www.cost2100.org

[101] Y. Feng, W. L. Schroeder, C. von Gagern, A. Tankielun, and T. Kaiser, "Metrics and methods for evaluation of over-the-air performance of MIMO user equipment," *International Journal of Antennas and Propagation*, vol. 2012, no. 598620, 2012. [Online]. Available: http://www.hindawi.com/journals/ijap/2012/598620/

[102] Y. Feng, C. von Gagern, A. Tankielun, R. Acharkaoui, W. Richter, and W. L. Schroeder, "Test plan for DL 2×2 MIMO OTA testing - Part I: Concepts for straightforward characterization measurements and statistical metrics," in *COST IC1004 1st MCM*, Lund, Sweden, Jun. 2011, TD(11)01045. [Online]. Available: www.ic1004.org

[103] C. von Gagern, A. Tankielun, Y. Feng, W. L. Schroeder, R. Acharkaoui, and W. Richter, "Test plan for DL 2×2 MIMO OTA testing - Part II: Test plan description and examples," in *COST IC1004 1st MCM*, Lund, Sweden, Jun. 2011, TD(11)01044. [Online]. Available: www.ic1004.org

[104] E. Böhler, C. von Gagern, A. Tankielun, Y. Feng, and W. L. Schroeder, "Measurements of over-the-air performance of MIMO UE," in *33rd Annual Symposium of the Antenna Measurement Techniques Association, AMTA 2011*, Englewood, Colorado, U.S., Oct. 2011.

[105] A. Tankielun, J.-A. Antón, and R. Koller, "MIMO OTA measurements of LTE devices according to the Two-Channel Method," in *COST 2100, 12th MCM*, Bologna, Italy, Nov. 2010, TD(10)12047. [Online]. Available: www.cost2100.org

[106] W. L. Schroeder, Y. Feng, and M. Pesavento, "Discussion of some options and aspects in over-the-air (OTA) testing of multiple input – multiple output (MIMO) user equipment (UE)," in *COST 2100, 7th MCM*, Braunschweig, Feb. 2009, TD(09)740. [Online]. Available: www.cost2100.org

[107] C. von Gagern, "Cost-effective over-the-air performance measurements on MIMO devices," in *COST2100, 8th MCM*, Valencia, Spain, May 2009, TD(09)804. [Online]. Available: www.cost2100.org

[108] Y. Feng and W. L. Schroeder, "Discussion of low-effort MIMO OTA testing approaches & suggested applicable FOM," in *COST 2100, 9th MCM*, Vienna, Austria, Sep. 2009, TD(09)951. [Online]. Available: www.cost2100.org

[109] Y. Feng, J. Jonas, and W. L. Schroeder, "Discussion of statistical metrics for MIMO over-the-air (OTA) performance based on empirical results," in *Proceedings of the 5th European Conference on Antennas and Propagation (EuCAP '11)*, Rome, Italy, Apr. 2011, pp. 1233–1237.

[110] C. Orlenius and M. Franzén, "Statistical approach to MIMO OTA performance requirements," in *COST 2100, 10th MCM*, Athens, Greece, Feb. 2010, TD(10)10085. [Online]. Available: www.cost2100.org

[111] Y. Feng, A. Krewski, and W. L. Schroeder, "Step towards theoretical analysis and comparison of MIMO antenna metrics," in *COST 2100, 11th MCM*, Aalborg, Denmark, Jun. 2010, TD(10)11081. [Online]. Available: www.cost2100.org

[112] R. J. Pirkl and K. A. Remley, "MIMO channel capacity in 2D and 3D isotropic environments," *International Journal of Antennas and Propagation*, vol. 2012, no. 676405, 2012. [Online]. Available: http://www.hindawi.com/journals/ijap/2012/676405/

[113] Y. Jing, X. Zhao, H. Kong, M. Rumney, and S. Duffy, "Analysis of MIMO OTA performance using 2D and 3D channel models," in *COST IC1004 4th MCM*, Lyon, France, May 2012, TD(12)04036. [Online]. Available: www.ic1004.org

[114] C. Mehlführer, M. Wrulich, J. C. Ikuno, D. Bosanska, and M. Rupp, "Simulating the long term evolution physical layer," in *Proc. of the 17th European Signal Processing Conference (EUSIPCO 2009)*, Glasgow, Scotland, Aug. 2009. [Online]. Available: http://publik.tuwien.ac.at/files/PubDat_175708.pdf

[115] Y. Feng, A. Krewski, and W. Schroeder, "Towards a simulation tool for comparison of MIMO OTA measurement methods and metrics," in *COST 2100, 10th MCM*, Athens, Greece, Feb. 2010, TD(10)10058. [Online]. Available: www.cost2100.org

[116] *Spatial channel model for Multiple Input Multiple Output (MIMO) simulations (Release 7)*, 3GPP Technical Report TR 25.996, Rev. 7.0.0, Jun. 2007. [Online]. Available: http://www.3gpp.org

[117] L. Hentilä, P. Kyösti, M. Käske, M. Narandzic, and M. Alatossava. (2007, Dec.) MATLAB implementation of the WINNER phase II channel model ver1.1. [Online]. Available: https://www.ist-winner.org/phase_2_model.html

[118] *User Equipment (UE) conformance specification; Radio transmission and reception (Release 8)*, 3GPP TS 36.521, Rev. 8.0.1, Dec. 2008.

[119] Y. Feng, W. L. Schroeder, and T. Kaiser, "Straightforward MIMO OTA characterization and statistical metrics for LTE devices," in *2012 6th European Conference on Antennas and Propagation (EuCAP)*, Prague, Czech, Mar. 2012.

[120] *Test Plan for Mobile Station Over the Air Performance*, CTIA – The Wireless Association Std., Apr. 2005. [Online]. Available: www.ctia.org